On the understanding and applications of excited state p-electron delocalization

Rosenberg, Martin

Publication date:
2012

Document version
Early version, also known as pre-print

On the Understanding and Applications of Excited State π-Electron Delocalization

PhD Thesis

Martin Rosenberg
Department of Chemistry
Faculty of Science
University of Copenhagen
Denmark

2012

Typeset with LaTeX 2_ε using Times typefaces.

The PhD School of Science
Faculty of Science
University of Copenhagen
Denmark

Printed by Grafisk, University of Copenhagen

PhD Thesis
ISBN 978-87-91963-17-9

Preface

This thesis has been submitted to the Faculty of Science, University of Copenhagen, as a partial fulfillment of the requirements to obtain the PhD degree. The work presented here was carried out at the Department of Chemistry in the years 2008-2012 under the supervision of Kristine Kilså, University of Copenhagen.

Acknowledgements

I have spent a little more than three years, employed as a PhD student under the supervision of Kristine. I am sincerely grateful to Kristine, for giving me the opportunity, to be a part of her research group. It has been an interesting, challenging, and tough period of my life, that I would not have been without. I thank Kristine for a fruitful collaboration, during the years of my PhD studies.

During the first year of my PhD studies, I was fortunate to have the opportunity, to stay four full months in the research group, of Henrik Ottosson at Uppsala University, in Sweden. I will always remember this, as a challenging scientific experience that has developed my competences, within the field of computational chemistry. I am sincerely grateful to Henrik for letting me join his research group of friendly and inspiring colleagues, and for having faith in my scientific skills.

Special thanks go to Raül Crepso at the University of Valencia, in Spain, for letting me visit his research group for one month, and sharing with me, his expertise on computational chemistry.

I am grateful to the National Supercomputer Center (NSC) in Linköping, Sweden and the Uppsala Multidisciplinary Center for Advanced Computational Science (UPPMAX), for generous allotment of computer time. I am grateful to the Niels Bohr Foundation, the Oticon Foundation, and the Torkil Holm Foundation for financial support enabling the collaborations with Henrik and Raül. I also give thanks to Mikael Bols, Head of the Department of Chemistry, for approving an extended three month period of the PhD fellowship with payment.

For many years Theis I. Sølling and Steen Hammerum have had a significant influence on my education at the Department of Chemistry. My scientific discussions with Theis and Steen have without doubt made me a better chemist, which I am truly grateful for. A major thanks should be given to Johannes F. Petersen for volunteering to proofread the thesis.

The most important aspect of the time, I have spent as a PhD student, has not the scientific achievements. It has been the friendships that I have achieved. I would like to give a very special thank to Rasmus Y. Brogaard and Thomas S. Kuhlman, and all you from "B416", who over the years have contributing to a thriving social environment, which I have enjoyed ever since I started as a master student. Last but certainly, not least I would like to thank my girlfriend, Sanna, for being caring, understanding, and supportive during the final period of my PhD fellowship.

Martin Rosenberg
Copenhagen
February 2012

Abstract

The energetic aspects associated with cyclic delocalization of π-electrons in molecules, possessing a full circuit of conjugated π-bonds give rise to various characteristic chemical and physical properties of these molecules. It appears, that these energetic aspects, are highly dependent on the number of π-electrons, which constitute the circuit. Systems that have $4n$+2 π-electrons arranged in a cyclic array, are stabilized by delocalization of the π-electrons. In systems, where $4n$ π-electrons constitute the cyclic array, delocalization is avoided. Consequently, the chemical and physical properties of these two classes of compounds with cyclic arrangement of π-electrons are also depended on this. Thus, the understanding of such cyclic systems of π-electrons are therefore important, in order to account for this difference, and to know how to apply this knowledge. Electrophilic substitution- and pericyclic reactions are examples, of how the knowledge and understanding of cyclic interactions between π-electrons can be applied in synthesis. Interestingly, there exists a similar, but contrasting energetic relationship between the electronic ground state and excited state of these π-electrons systems. The systems with $4n$ π-electrons prefer to delocalize the π-electrons in the excited state, while in systems with $4n$+2 π-electrons the delocalization is not favored. In contrast to the wide applications of this knowledge for molecules in the ground state, applications of the aspects associated with cyclic delocalization of π-electrons, in excited states, are very scarce.

This thesis will describe cyclic delocalization of π-electrons in the excited state, and illustrate how this knowledge allows rationalization for the photochemical behavior and photophysical properties of systems with cyclic arrangement of π-electrons.

Computations serve as a valuable tool for the investigation of excited states properties. This tool is readily applied throughout this thesis, in order to examine excited state properties, which can not easily be probed experimentally. For example, it is illustrated, how the acid-base properties of a series of ionic cyclic polyenes, with a full circuit of conjugated π-electrons, are affected by the numbers of π-electrons. The properties are examined in both the ground- and triplet excited states. The results clearly illustrate, that these compounds possess contrasting acid-base properties in their ground- and triplet excited state, which reflect the different energetic aspects connected to π-electron delocalization, in the two states.

In the final part of the thesis, the knowledge of how π-electrons prefer to be delocalized in the ground- and excited states is used strategically for manipulation of excited state energies. Certain molecules are influenced by a $4n\pi$-electron density distribution in the excited state. The energetic aspects associated with this influence, are affected by the presence of substituents, which are positioned in either a favorable or non-favorable position for interaction with the $4n\pi$-electron density distribution. This was then used to design compounds that possess interesting excited state properties.

Resumé

Molekyler med et cyklisk arrangement af konjugerede π-bindinger besidder en række karakteristiske kemiske og fysiske egenskaber, som følge af de energetiske aspekter, knyttet til π-elektronfordelingen. Antallet af π-elektroner, som udgør det cykliske system er afgørende for hvilke energetiske aspekter, der gør sig gældende for molekylet. Et molekyle som besidder et cyklisk konjugeret system, bestående af $4n$+2 π-elektroner, opnår et stabiliserende bidrag til molekylets totale energi ved at fordele π-elektronerne ud i hele netværket. Det står i kontrast til molekyler, som besidder et cyklisk netværk af $4n$ π-elektroner. Disse molekyler opnår intet bidrag til deres totale energi, ved at fordele π-elektronerne i det fulde cykliske netværk. Det medfører, at de to systemers fysiske og kemiske egenskaber er forskellige. Forståelsen af vekselvirkningerne mellem π-elektroner i cykliske enheder er således vigtig, for at kunne gøre brug af de to systemers forskellige egenskaber. Sammenlignes molekylerne i deres laveste anslåede elektroniske tilstand, eksisterer der et lignende, men omvendt forhold. I den laveste anslåede tilstand for et molekyle, med et cyklisk arrangement af $4n$ π-elektroner, er det nu fordelagtigt af fordele π-elektronerne ud i det fulde netværk, mens det for molekyler med $4n$+2 π-elektroner er forbundet med et destabiliserende bidrag til systemet totale energi. Den viden kan anvendes til at forklare molekylernes egenskaber i deres anslåede tilstande.

Sigtet med afhandlingen er at opnå en større forståelse af vekselvirkningerne mellem π-elektroner i cykliske netværk i molekyler, der befinder sig i den laveste anslåede tilstand. På grundlag af den viden vil de fotokemiske egenskaber for disse molekyler blive forklaret. Kvantemekaniske beregninger er et værdifuldt redskab til at undersøge egenskaber for molekyler i anslåede tilstande. Redskabet er yderst bekvemt til at undersøge egenskaber, som er svære at undersøge eksperimentelt for molekyler, som befinder sig i anslåede tilstande. For eksempel er syre-base egenskaberne for ioniske polyener, med komplette cykliske netværk af π-elektroner undersøgt ved beregninger, med fokus på hvorledes antallet af π-elektroner i netværket påvirker disse egenskaber. Egenskaberne er undersøgt i grundtilstanden, såvel som i den laveste anslåede triplet tilstand. Det fremgår tydeligt af resultaterne, at der findes et modsætningsforhold mellem syre-base egenskaberne for de ioniske polyener i de to tilstande. Modsætningsforholdet reflekterer de energetiske aspekter, som er knyttet til π-elektron delokalisering i de to tilstande.

I den sidste del af afhandlingen udnyttes kendskabet til hvordan π-elektroner foretrækker, at organisere sig i molekylernes anslåede tilstand. Visse molekyler er, i deres anslåede tilstand, betydeligt influeret af elektronfordelinger svarende til et cyklisk $4n\pi$-elektron arangement. De energetiske aspekter, forbundet med den indflydelse, kan påvirkes ved strategisk placering af substituenter i molekylet, som kan vekselvirke enten konstruktivt eller ikke-konstruktivt med $4n\pi$-elektron systemet. Herved ændres energien af den anslåede tilstand, og den strategi er blevet anvendt til at designe forbindelser med interessante egenskaber i deres anslåede tilstand.

List of Papers

Joint efforts with collaborators lead to the manuscripts presented below. Titles marked with an asterisk contain work presented in this thesis.

Published or Submitted Manuscripts

* Rosenberg, M.; Dahlstrand, C.; Kilså, K.; Ottosson, H. "Excited State Aromaticity and Antiaromaticity - Opportunities for Photophysical and Photochemical Rationalizations", Submitted to *Chem. Rev.*, February 2012.

Minitti, M. P.; Zhang, Y.; Rosenberg, M.; Brogaard, R. Y.; Deb, S.; Sølling, T. I.; Weber, P. M. "The Far-UV Photochemical Bond Cleavage of *n*-Amyl Nitrite: Bypassing a Repulsive Surface", *J. Phys. Chem. A* **2012**, *116* (2), 810-819.

* Rosenberg, M.; Ottosson, H.; Kilså, K. "Influence of Excited State Aromaticity in the Lowest Excited States of Fulvene Derivatives", *Phys. Chem. Phys. Chem.* **2011**, *13* (28), 12912-12919.

Rosenberg, M.; Sølling, T. I.; Bisgaard, C. Z.; Weber, P. M.; Minitti, M. P.; Rusteika, N.; Deb, S. "Probing the Lifetimes of Internally Excited Amyl Nitrite Cations", *J. Phys. Chem. A* **2010**, *114*, (26), 7021-7025.

* Rosenberg, M.; Ottosson, H.; Kilså, K. "Proton and Hydride Affinities in Excited States: Magnitude Reversals in Proton and Hydride Affinities between the Lowest Singlet and Triplet States of Annulenyl and Benzannulenyl Anions and Cations", *J. Org. Chem.* **2010**, *75* (7), 2189-2196.

Rosenberg, M.; Sølling, T. I. "Computational Investigation of Photo Induced Processes in Alkyl Nitrites and the Product Alkoxy Radicals", *Chem. Phys. Lett.* **2010**, *484* (4-6), 113-118.

Manuscripts in Preparation

* Rosenberg, M.; Dahlstrand, C.; Ottosson, H.; Kilså, K. "Substituent Controlled Manipulation of Excited State Energies in 9*H*-Fluorenone Derivatives"

Rosenberg, M.; Göransson, E.; Ottosson, H.; Kilså, K. "Solvent Controlled Excitation Energies and Excited State Lifetimes of Fulvene Derivative: 2,3,4,5-tetrachloro-6,6-dicyanofulvene"

Tibbelin, J.; Wallner, A.; Heijkensköld, F.; Rosenberg, M.; Yamazaki, K.; Puglia, C.; Karlsson, L.; Feifel, R.; Pettersson, R.; Baumgartner, J.; Ottosson, H. "The 1,4-Disilacyclohexa-2,5-diene Cycle: A Molecular Building Block which Allows for Strong σ/π-Interaction"

Petersen, J. F.; Rosenberg, M.; Deo, C.; Scott, A.; Kilså, K.; Jockusch, S.; Turro, N. J.; Tomalia, D. A.; Christensen, J. B. "On the origin of fluorescence in PAMAM-dendrimers"

Dahlstrand, C.; Rosenberg, M.; Kilså, K.; Ottosson, H. "Exploration of the π-Electronic Structure of Singlet, Triplet, And Quintet States of Fulvenes and Fulvalenes Using the Electron Localization Function"

Outline

Chapter 1 Introduction, and motivation, to why the understanding of cyclic delocalization of π-electrons in the ground, as well as in the excited states is important.

Chapter 2 Theoretical description of conjugated π-electron systems and the energetic aspects associated with the delocalization of π-electrons. The validity of the theoretical predictions is subsequently discussed in relation to experimentally verified molecular properties. Finally, a brief discussion of the terms aromatic and antiaromatic is given.

Chapter 3 Expansion of the theoretical model for description of conjugated π-electron systems in the lowest excited singlet and triplet states. The validity of the theoretical model and its predictions, regarding the energetic aspects associated with delocalization of the π-electrons, is discussed and set in relation to experimentally and computationally obtained results.

Chapter 4 In this chapter, the impact of cyclic delocalization of π-electrons on photochemical reactivity is discussed on the basis of previously reported results. Presentation of the computational investigation of the acid-base properties of ionic cyclic polyenes in their ground state and triplet excited state.

Chapter 5 Illustration of the systematic trends in the energy difference between ground and excited state energies for cyclic polyenes with $4n$ and $4n$+2 π-electrons.

Chapter 6 This chapter gives a description of the structural and electronic aspects for tria-, penta, and heptafulvene. These aspects are discussed and compared in the ground state and in the lowest excited triplet state.

Chapter 7 Introduction to the concept of substituent controlled manipulation of excited state energies. The concept is illustrated for five differently substituted pentafulvene derivatives both experimentally and computationally.

Chapter 8 This chapter concerns experimentally and computationally investigations, which suggest that the concept of substituent controlled manipulation of excited state energies is expandable to molecules in close relation to pentafulvene.

Chapter 9 Final remarks and happy ending.

Contents

Chapter 1

The Cyclic Conjugation of π-Electrons

The energetic aspects, associated with cyclic π-electron delocalization in cyclic polyenes with a full circuit of conjugated π-bonds, have astonished chemists ever since benzene was isolated and discovered to possess unique chemical properties as compared to other olefinic compounds. In contrast to other olefinic compounds, which readily react with electrophilic species in addition reactions, benzene undergoes substitution reactions with electrophilic compounds, such as bromine (Scheme **A**, in Fig. 1.1). The need for a catalyst to initiate the electrophilic substitution reaction, and the re-formation of cyclic π-electron array subsequent to the electrophilic attack, indicates that the presence of the cyclic π-electron array is a thermodynamically stabilizing interaction. However, not all cyclic polyenes tend to be stabilized, by cyclic delocalization of the π-electrons, in the same way as benzene. For instance, cyclooctatetraene reacts readily with bromine, analogous to other olefinic compounds, without the presence of catalyst, and subsequently undergoes electrocyclic ring closure to a bicyclic diene product (Scheme **B**, in Fig. 1.1). [1–3]

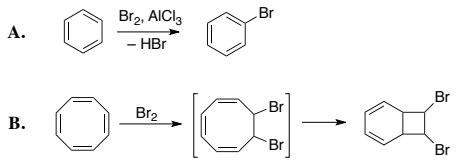

Figure 1.1: Reaction **A**. Bromination of benzene (electrophilic substitution). Reaction **B**. Bromination of cyclooctatetraene (electrophilic addition, and subsequent electrocyclic ring closure).

It appears that a general and interesting trend exists in the energetics associated with cyclic delocalization of π-electrons. In cyclic polyenes with $4n$ π-electrons in the cyclic array, like cyclooctatetraene, the cyclic delocalization of π-electrons, is a non-stabilizing interaction. The opposite is true for cyclic polyenes with $4n$+2 π-electrons in the cyclic array, like benzene, which are stabilized by cyclic delocalization of the π-electrons, and moreover, by a larger extent than corresponding linear polyenes.[4] This contrasting energetic aspect between $4n$ and $(4n+2)\pi$-electronic cyclic polyenes has been subject to several investigations and used to account for numerous chemical and physical properties of the cyclic polyenes and compounds in close relation to these.[5–13]

In the excited states of the cyclic polyenes the energetic aspects related to π-electron delocalization stand in contrast to the ground state aspects. In the lowest (π,π^*) excited singlet and triplet states cyclic delocalization of $4n$ π-electrons is connected with low energy points on the excited state potential energy surface, while the delocalization of $4n$+2 π-electron is a destabilizing interaction in the excited states.[4,14] In fact, this can be coupled to a range of photophysical and photochemical properties of cyclic polyenes.[15] Unfortunately, this has not drawn as much attention, as the coupling between the energetic aspects related to π-electron delocalization and the impact on ground state properties of cyclic polyenes. When π-electron interactions in cyclic conjugated π-bond arrays are understood in the ground- and excited state, this knowledge can serve as a valuable tool in the design of compounds with interesting excited state properties. This will be demonstrated in this thesis. However, before the power of π-electron delocalization can be utilized, it must be understood in the ground- and excited states, which will be the topics of the two following chapters.

Chapter 2

Interactions of π-Electrons in the Ground State

Before conjugated π-electron interactions are considered in the excited states, it is necessary to understand how conjugated π-electron interactions behave in the electronic ground state. To understand π-electron delocalization in conjugated π-electron systems, it is necessary to consider the energetic aspects associated with such systems. For this purpose, the Hückel molecular orbital (HMO) theoretical approach is a convenient tool.[16–20] Although HMO theory gives a drastically approximative description of π-electronic structure it is still used today for qualitative discussions of conjugated π-electron systems. This is because, this methodology allows for a simple and intuitive description of π-electron delocalization in molecules, and the energetics related to the π-electron delocalization can be evaluated easily. In HMO theory the energies are only related to the π-electron system. The energies are given in terms of the quantities α and β, which are the Coulomb- and resonance integrals, respectively. Both α and β are negative quantities.[20] Thus, HMO energies can be interpreted as the contribution, to the thermodynamic stability of a conjugated π-electron system, which arises from π-electron interactions. When comparing HMO energies, associated with linear and cyclic delocalization of π-electrons, an interesting trend arises. For instance, the energy of benzene can be calculated to be $6\alpha+8\beta$. In comparison, the HMO energy of the open-chain analogue, 1,3,5-hexatriene is $6\alpha+7\beta$.
If the three π-bonds are considered as being localized, the HMO energies of the two polyenes are identical and equal to the sum of the HMO energies for three separate C–C π-bonds, which is 6α+6β. From comparison of these three HMO energies it is obvious that both benzene and 1,3,5-hexatriene are stabilized by π-electron delocalization. Benzene, however, obtains a larger stabilization by π-electron delocalization as compared to 1,3,5-hexatriene.

In contrast, the opposite energetic relationship is found between cyclobutadiene and 1,2-butadiene, for which the HMO energies are 4α+4β and 4α+4.472β, respectively. These results indicate that 1,2-butadiene, the linear polyene, is the only one of the two polyenes that is stabilized by π-electron delocalization. Cyclobutadiene does not obtain stabilization by π-electron delocalization, but possess HMO energy equal to that of the two separate C–C π-bonds (4α+4β). These two examples illustrate a general trend. The number of interacting π-electrons governs whether or not a cyclic polyene is stabilized from cyclic delocalization of π-electrons. If the cyclic polyene is stabilized, the stabilization is more pronounced than the corresponding open-chain analogue. This trend can be generalized by the use of perturbation molecular orbital (PMO) approach.[4,21] The PMO approach is a variant of the HMO method, and is a convenient approach to describe energetic relations between cyclic and linear polyenes. Consider two radical fragments, each constituted of an odd number of C atoms, chosen in such a way, that they serve as building blocks for both a linear and cyclic polyene, containing the same number of π-electrons. For simplicity, one of the radical fragments can be chosen as the methyl radical and the second fragment can, for example, be either the propenyl or pentadienyl radical. The methyl and propenyl radicals can be merged into 1,2-butadiene or cyclobutadiene, and the methyl and pentadienyl radicals can be merged into 1,3,5-hexatriene or benzene, as shown in Fig. 2.1.

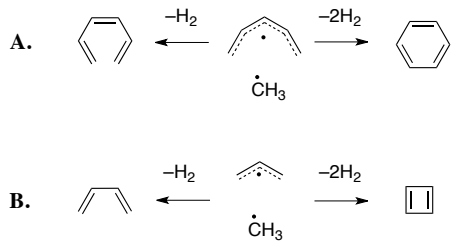

Figure 2.1: Illustration of the PMO construction of (**A**) 1,3,5-hexatriene or benzene from the pentadienyl and methyl radicals, and (**B**) the construction of 1,2-butadiene or cyclobutadiene from the propenyl and methyl radicals.

Each radical fragment is described by a set of π-molecular orbitals constructed from linear combination of the atomic 2p-orbitals of the C atoms. Upon merging, the pattern of the molecular π-orbitals is perturbed. This perturbed set of bonding and antibonding π-molecular orbitals, describes either the cyclic or linear polyene. The change in the π-orbital pattern, of the new system, can be analyzed to deduce how the energy is changed, when the two radical fragments are joined together.

Now, let us consider two polyenyl radical fragments, *A* and *B* that consist of an odd number of C atoms. The two polyenyl fragments are each described by a set of π-molecular orbitals constructed from linear combinations of the 2p-atomic orbitals at the C atoms in the fragment.

For convenience one of the radical fragments is chosen as the methyl radical, and the second radical fragment is constructed of $2k-1$ (an odd number) C atoms, for which k can be either a positive odd or even integer. If k is odd, then the resulting polyene possesses $4n+2$ π-electrons, while if k is even the resulting polyene possesses $4n$ π-electrons, with n being a positive integer. The first order perturbation energy for merging two radical fragments A and B to either a cyclic or linear polyene, is here defined as the π-electron delocalization energy and is expressed as:

$$E_\pi = 2\beta \sum_{x,y} a_{0,x} b_{0,y} \tag{2.1}$$

where β is the standard resonance integral between two adjacent C atoms.
The quantity, $a_{0,x}$, is the coefficient of the singly occupied molecular orbital at C atom x, in fragment A and $b_{0,y}$ is the coefficient at C atom y, in fragment B. Atoms x and y are the atoms, which are merged. If k is even, the singly occupied molecular orbital, of the radical fragment with $2k-1$ C atoms, will have opposite phases at the terminal C atoms (C_1 and C_{2k-1}) and equal phases if k is odd. For radical fragments with $2k-1$ C atoms the magnitude of the coefficients at the terminal positions, will be equal and can be calculated from $k^{-1/2}$.[4] The principle is illustrated in Fig. 2.2.

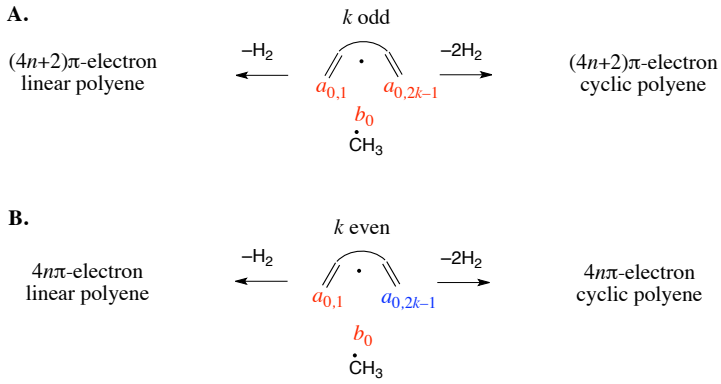

Figure 2.2: Illustration of the relationship between the phase of the singly occupied molecular orbital, at the terminal C atoms, of the radical fragments with the $2k-1$ C atoms. Red color represents a positive phase and blue color a negative phase. Part **A** illustrates the phase relation between the radical fragments with odd k, which can be combined with the methyl radical fragment to a linear or cyclic $(4n+2)\pi$-electron polyene. Part **B** illustrates the phase relation between the radical fragments with even k, which can be combined with the methyl radical fragment to a linear or cyclic $4n\pi$-electron polyene.

From Equation (2.1) the π-electron delocalization energies for ground state linear or cyclic polyenes become:

$$\text{Linear Polyenes} \quad E_\pi = 2\beta b_0(a_{0,1}) = 2\beta b_0 a_0 \tag{2.2}$$

$$\text{Cyclic Polyenes} \quad E_\pi = 2\beta b_0(a_{0,1} + a_{0,2k-1}) = 4\beta b_0 a_0, \quad k \text{ odd}, \ (4n{+}2)\pi \tag{2.3}$$

$$E_\pi = 2\beta b_0(a_{0,1} - a_{0,2k-1}) = 0, \quad k \text{ even}, \ 4n\pi \tag{2.4}$$

In the following, the three equations will be referred to as the "π-electron counting rules". The rules can also be shown to apply for polyenes with $4n$+2 or $4n$ π-electrons, consisting of an odd number of C atoms, *e.g.* the cycloheptatrienyl cation and anion, and in a limited extent to compounds containing more than one ring.[4]

Equation (2.2) shows that π-electron delocalization is always associated with a stabilizing contribution to the thermodynamic stability of linear polyenes. It can be deduced from Equation (2.3) that this is also the case for cyclic polyenes, if they contain $4n$+2 π-electrons, and the contribution is larger as compared to the corresponding open-chain analogues. In contrast, cyclic polyenes with frameworks of $4n$ π-electrons do not receive any additional stability by π-electron delocalization (Equation (2.4)). The π-electron delocalization energy of cyclic and linear polyenes are illustrated by an orbital interaction diagram in Fig. 2.3.

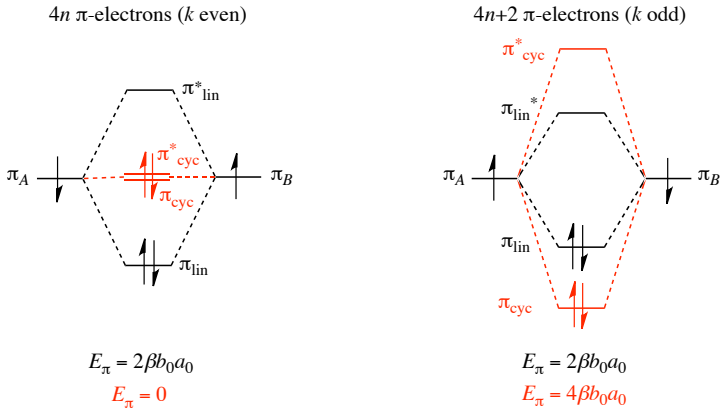

Figure 2.3: Illustration of the π-electron delocalization energy (E_π) gained by interaction between the singly occupied π-orbitals of radical fragments A and B (π_A and π_B, respectively). This orbital interaction gives rise to a perturbed set of bonding and antibonding π-orbitals for the linear (π_{lin} and π^*_{lin} respectively, black) and cyclic (π_{cyc} and π^*_{cyc}, respectively, red) polyenes containing $4n$ (left) and $4n$+2 (right) π-electrons. If either A or B is chosen as the methyl radical the singly occupied π-orbital would be a p-orbital. The difference between singly occupied orbitals and the bonding π-orbitals of the linear or cyclic fragment corresponds to the E_π.

From Equations (2.2)-(2.4) another interesting aspect can be drawn; the energy gained from π-electron delocalization decreases with increasing k.
Thus, larger ring systems will not experience any significant stabilization from delocalization of π-electrons. The contrasting energetic relationship between $4n\pi$- and $(4n+2)\pi$-electron cyclic and linear polyenes is demonstrated on the basis of a crude PMO treatment. Thus, the approximations included in this treatment renders results far from reality. It is therefore unknown whether the results obtained in Equations (2.2)-(2.4) are applicable for anything at all. However, chemical phenomena are very often rationalized on the basis of the qualitative results from Equations (2.2)-(2.4). To demonstrate why let us consider the examples shown in Fig. 2.4, on the following page.

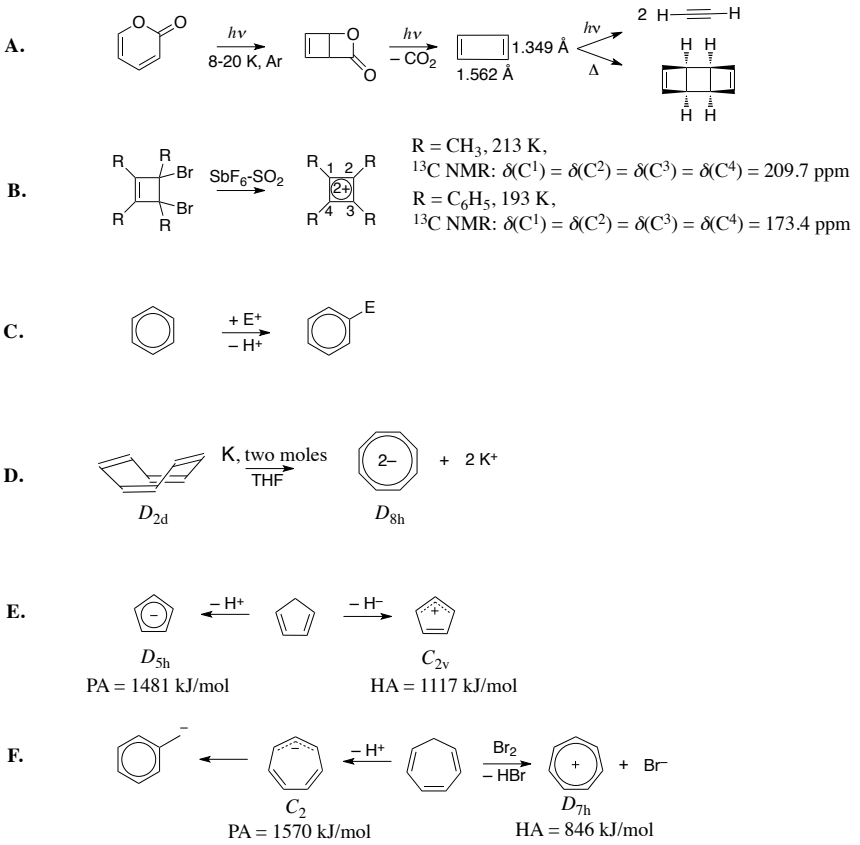

Figure 2.4: Summary of the examples that illustrate the reality of the qualititative content of the π-electron counting rules. Scheme **A**. Method for generation of cyclobutadiene.[22–24] Bond lengths of cyclobutadiene are calculated at the CASSCF level.[25] Scheme **B**. Generation of the tetraphenylcyclobutadiene and tetramethylcyclobutadiene dications.[26] Scheme **C**. Electrophilic substitution of benzene.[10,12] Scheme **D**. Illustration of the D_{2d} symmetric tub-shaped conformation of cyclooctatetraene and its reduction to its D_{8h} symmetric dianion.[27,28] Scheme **E**. Conversion of cyclopentadiene to its corresponding cation and anion.[29,30] Hydride and proton affinities (HA and PA, respectively) are taken from reference 29 and 30, and symmetries are taken from reference 30. Scheme **F**. Conversion of cycloheptatriene to its corresponding cation and anion.[30,31] Hydride and proton affinities (HA and PA, respectively), and symmetries are taken from reference 30.

In contrast to benzene, cyclobutadiene is found to be a highly unstable species and has only been observed at cryogenic conditions.[22–24] Cyclobutadiene can be generated as shown in Scheme **A**, in Fig. 2.4. But even at these conditions, this compound is short-lived. It has been reported to dimerize upon heating, or decompose into two acetylene molecules upon continued irradiation.[22] No experimental data are yet available on the bond lengths of non-substituted cyclobutadiene, but results from IR experiments in matrix isolated cyclobutadiene indicate that the molecular structure is not square, but closer to rectangular.[24,32,33]
This is supported by computational results, as for example, results of multireference coupled cluster calculations (MR-CCSD/DZP) suggest that the lowest energy conformation of cyclobutadiene is a D_{2h} symmetric rectangular structure with C–C bond lengths of 1.562 Å and 1.349 Å.[34] The large ring strain, of course, contributes to the instability of cyclobutadiene. However, in light of this, it may appear surprising that the tetraphenylcyclobutadienyl, and tetramethylcyclobutadienyl dications, which contain two π-electrons in cyclic arrangement, can be generated at -40 °C (213 K) and -60 °C (193 K), respectively (Scheme **B**, in Fig. 2.4).[26] Both of these compounds should indeed experience large ring strains, comparable to cyclobutadiene. Despite this, these compounds are stable enough to be investigated by NMR spectroscopy. The ^{13}C NMR studies indicate that the cyclobutadienyl dication moiety in these compounds are square (Scheme **B**, in Fig. 2.4).[26]

The structure of benzene has D_{6h} symmetry, and this compound is known to be rather resistant to chemical transformations. As previously mentioned, benzene undergoes electrophilic substitution, in contrast to other olefinic hydrocarbons, which undergo electrophilic addition. The substitution reaction involves re-formation of the cyclic 6π-electron array indicating that the cyclic interaction of the 6π-electron system is indeed energetically favorable (Scheme **C**, in Fig. 2.4).[10,12]

The monocyclic 8π-electron polyene, cyclooctatetraene, is proven to adopt a tub-shaped D_{2d} symmetric conformation with alternating single and double bonds.[35]
In the tub-shaped conformation the compound has C–C–C bond angles of 126.46°,[35] which are close to the ideal bond angles (120°) around an sp^2 hybridized C atom.
In the planar D_{4h} and D_{8h} symmetric conformations the C–C–C bond angles would, according to results from calculations (CASSCF/6-31G(d)), be increased to 135°.[36]

Despite the more unfavorable C–C–C bond angles in the D_{8h} symmetric conformation, this conformation is adopted, when the compound is reduced to the dianion, a 10π-electron system. This reduction can readily be done with two moles of potassium metal in oxygen free tetrahydrofuran (THF) solution (Scheme **D**, in Fig. 2.4).[27,28]
Finally, the contrasting reactivities of cyclopentadiene and cycloheptatriene (Scheme **E** and **F**, respectively, in Fig. 2.4) illustrate that the number of π-electrons in cyclic polyenes is important for thermochemical stability. Cyclopentadiene has proven to be an unusual acidic hydrocarbon in solution ($pK_a = 18$)[37,38] while cycloheptatriene is not easily deprotonated ($pK_a = 36$).[39–41]

The proton affinities for the cyclopentadiene and cycloheptatriene anions are 1481 and 1570 kJ/mol,[29] respectively, which show that even in the gas phase, cyclopentadiene is still the more acidic species. Conversely, recent computational studies show that the hydride affinities of the cyclopentadiene and cycloheptatriene cations (in their lowest energy singlet states) are 1117 and 846 kJ/mol, respectively.[30] This indicates that the formation of cyclopentadiene, is much more exothermic in comparison to the formation of cycloheptatriene, from the cyclopentadienyl and cycloheptatrienyl cations respectively. Moreover, the cycloheptatriene cation is easily generated by oxidation of cycloheptatriene with bromine,[31] and the cycloheptatrienyl cation is commercially available as the tetrafluoroborate salt.

In summary, the examples in Scheme **B**, **C**, **E**, and **F** in Fig. 2.4, illustrate that cyclic polyenes containing $4n$+2 π-electrons prefer delocalization of the π-electrons. This can be considered afford a substantial contribution to the thermodynamic stability of this class of cyclic polyenes. On the other hand, the examples also illustrate that cyclic delocalization of π-electrons (Fig. 2.4, Scheme **A**, **D**, **E**, and **F**) is not preferred in cyclic polyenes with $4n$ π-electrons. Thus, for this class of cyclic polyenes, the π-electron delocalization does not seem to have any stabilizing effect at all. All in all, the qualitative content derived from Equations (2.2)-(2.4) is supported in reality.

2.1 Aromatic and Anti-aromatic Compounds

The abnormality of cyclic polyenes, in comparison to the linear polyenes, have long astonished chemists. Commonly, the cyclic polyenes are classified as *aromatic* and *anti-aromatic* compounds, depending on whether the cyclic polyene has $4n$+2 or $4n$ π-electrons, respectively in the cyclic array.[5–13] These terms are somewhat unfortunate and confusing, as the term *aromatic* evoke the subjective content of the word, originally used to characterize the distinct smell of benzene. However, the term *aromatic* has persisted throughout history and has later been accompanied by the term *anti-aromatic*, distinguishing between the $(4n+2)\pi$- and $4n\pi$-electron annulenes.[42,43]

The next obvious question that arises from this classification of cyclic polyenes is: "What are the characteristic properties of aromatic and anti-aromatic molecules?" Unfortunately, this question cannot by easily answered. However, the tendency to delocalization of the π-electrons in aromatic molecules, or the tendency, for anti-aromatic molecules, not to delocalize the π-electrons, have a range of consequences for the physical and chemical properties of the two classes of cyclic polyenes. These consequences are often set-in inseparable relation to the *aromaticity* of the aromatic compounds and the *anti-aromaticity* of the anti-aromatic compounds.[5–13]
In short, these 'property' terms often appear in the literature as 'measures' for how aromatic or anti-aromatic the cyclic polyenes are. Unfortunately, aromaticity and anti-aromaticity are not easily quantifiable and more importantly, they have never been proven experimentally to exist.

It has been argued that aromaticity and anti-aromaticity are measurable through structural,[44] magnetic,[45] energetic,[46] electronic,[47] and reactivity-based probes.[6,48]
However, these probes are not always equally affected by aromatic or anti-aromatic compounds and therefore, they can only be considered as projections of the somewhat invented properties of aromaticity and anti-aromaticity. Thus, quantification of aromatic and anti-aromatic compounds, through aromaticity and anti-aromaticiy, is difficult to handle and evaluate, and must be treated with great care!
Such a quantification is in my personal opinion not recommended, as it very often leads to confusion, by virtue of the many different and diffuse interpretations of the terms aromaticity and anti-aromaticity throughout the chemical society. Thus, to avoid confusion the terms aromaticity and anti-aromaticity will not be used in this thesis.

Chapter 3

π-Electron Delocalization in the Excited States

When π-electron delocalization is considered in the lowest excited states it appears that the associated energetic aspects are reversed. In a first approximation, the lowest (π,π^*) excited state of linear and cyclic polyenes can be described, *via* the PMO model, as a state with single electron occupation of the perturbed bonding and antibonding π-orbitals in Fig. 2.3. At this level the antibonding π^*-orbital is destabilized to the same extent as the bonding π-orbital is stabilized. Thus, this level of approximation leads to no change in energy when compared to the two radical fragments, *i.e.* no additional stability is gained by π-electron delocalization in any of the excited state polyenes. However, the simple PMO treatment gives an insufficient description of the excited states as it underestimates the "antibondingness" of the antibonding π-orbitals.[4] If the PMO model is slightly modified it can be used to evaluate the energetics associated with π-electron delocalization in the lowest excited states.
This modification of the PMO model was presented by Baird, who focused attention on the energetic aspects associated with π-electron delocalization in the lowest (π,π^*) excited triplet states of linear and cyclic polyenes.[14,49] Again, two radical fragments consisting of an odd number ($2k-1$) of C atoms are considered to merge, to either a linear or cyclic polyene, as shown in Fig. 2.2.

The expression that describes the π-electron delocalization energy in the triplet excited state ($E_\pi(\pi,\pi^*)$) polyenes are shown in Equation (3.1).[14,49]

$$E_\pi(\pi,\pi^*) = -\frac{\frac{3}{2}\alpha S^2\left(\sum_{x,y} a_{0,x}b_{0,y}\right)^2}{1 - S^2\left(\sum_{x,y} a_{0,x}b_{0,y}\right)^2} \tag{3.1}$$

In contrast to Equation (2.1) this expression includes the overlap integral, S, between the atoms, x and y that are merged, which is set to zero in the derivation of Equation (2.1).[21] The quantities α, $b_{0,y}$, and $a_{0,x}$ are of the same meaning as described in Chapter 2. The negative sign of Equation (3.1) indicates that the π-electron delocalization energy in a triplet state polyene will be zero, or act as a destabilizing contribution to the thermodynamical stability of the triplet state polyene, depending on whether $\sum_{x,y} a_{0,x}b_{0,y}$ is zero or non-zero, respectively (*vide infra*). The inclusion of overlap integrals affects the energetic splitting of the interacting singly occupied π-orbitals as illustrated in Fig. 3.1. In reference 14 the $E_\pi(\pi,\pi^*)$ for a triplet state cyclic polyene is evaluated and compared to $E_\pi(\pi,\pi^*)$ for the most stable conformation of the corresponding triplet state open-chain polyene. This conformation has one of the bonds twisted by 90°, and consequently the singly occupied π-orbitals, of each radical fragment are arranged perpendicular to each other and therefore S becomes zero. Thus, in this conformation the π-electron delocalization energy is zero, which makes the comparison between the cyclic and linear triplet state polyenes particular easy.[14,49]

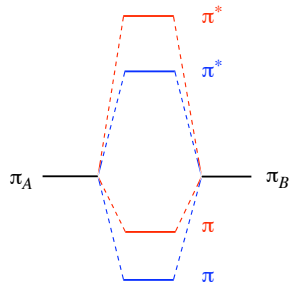

Figure 3.1: Interaction between the singly occupied π-orbitals (electrons are not shown for clarity) of two radical fragments A and B (π_A and π_B, respectively), with neglect of overlap integrals (blue, $S = 0$) and the inclusion of overlaps (red, $S > 0$).

However, it is in my personal opinion, an unfortunate choice of reference conformation for the linear polyene. When the π-electron delocalization energy is compared, for the triplet state linear and cyclic polyenes, they should experience the same interactions, and this is not the case for the planar cyclic polyene and the twisted linear polyene. In this thesis, the π-electron delocalization energies, of the triplet state linear and cyclic polyenes, are compared in their planar conformations in contrast to reference 14. By the same approach as described previously, a set of π-electron counting rules can be derived for the triplet excited state polyenes. In fact, these rules are valid for the lowest (π,π^*) excited singlet state as well, as these states are not distinguished in PMO theory. The π-electron counting rules for the lowest (π,π^*) excited singlet and triplet states are:

$$\text{Linear Polyenes} \quad E_\pi(\pi,\pi^*) = -\frac{\frac{3}{2}\alpha(Sa_0b_0)^2}{1-(Sa_0b_0)^2} \tag{3.2}$$

$$\text{Cyclic Polyenes} \quad E_\pi(\pi,\pi^*) = -\frac{6\alpha(Sa_0b_0)^2}{1-4(Sa_0b_0)^2}, \quad k \text{ odd, } (4n{+}2)\pi \tag{3.3}$$

$$E_\pi(\pi,\pi^*) = 0, \qquad k \text{ even, } 4n\pi \tag{3.4}$$

Equation (3.2) is always negative, thus excited state linear polyenes experience destabilization from π-electron delocalization. The excited state cyclic polyenes with $4n$ π-electrons experience no additional stability by π-electron delocalization, while excited state cyclic polyenes with $4n$+2 π-electrons are destabilized by π-electron delocalization. By comparing Equations (3.2) and (3.3) the (not so elegant) energetic relationship between the cyclic and linear polyenes with $4n$+2 π-electrons, shown in Equation (3.5), can be derived.

$$\frac{E_\pi^{\text{cyc}}(\pi,\pi^*)}{E_\pi^{\text{lin}}(\pi,\pi^*)} = \frac{4-4(Sa_0b_0)^2}{1-4(Sa_0b_0)^2} \tag{3.5}$$

Equation (3.5) shows that an excited state cyclic polyene is more destabilized than the corresponding open-chain excited state polyene, as the nominator is always larger than the denominator. On the other hand, the excited state cyclic polyenes with $4n$ π-electrons are neither stabilized nor destabilized, by cyclic delocalization of the π-electrons, but when compared to the corresponding linear polyene they can be considered as stabilized by cyclic delocalization of the π-electrons. Thus, in principle the terms aromatic and anti-aromatic can be extended to characterize molecules in the lowest excited triplet and singlet states, which achieve either more or less thermodynamic stability by cyclic delocalization of their π-electrons as compared to their open-chain analogues. However, this terminology, in the excited states, is unfortunately misleading. In the ground state the term aromatic implies that ($4n$+2)π-electron cyclic polyenes are stabilized by cyclic delocalization of π-electrons *and* are more stabilized with reference to the corresponding linear polyene.

In the excited state the term only implies that cyclic delocalization, of $4n$ π-electrons, can be considered as a stabilization, only if it is in reference to the corresponding linear polyene, but in fact neither destabilization nor stabilization arise from π-electron delocalization according to the PMO model.

The PMO model gives a crude description of the lowest (π,π^*) excited singlet and triplet states of the linear polyenes. For example, the ground state and the lowest (π,π^*) excited triplet and singlet states of the $4n\pi$-electron cyclic polyenes are degenerate at this level. This picture is different and more complicated, when more sophisticated molecular orbital descriptions are employed. It is therefore definitely not certain that the energetic trends derived in the approximative PMO picture are meaningful or real at all. Thus, it is appropriate to examine whether the qualitative content of the excited state π-electron counting rules, can be traced to have any considerable impact on the excited state properties of cyclic polyenes.

3.1 Impact of Cyclic π-Electron Delocalization on Excited State Molecular Structures

One of the excited state properties that is affected by an enhanced or reduced degree of cyclic delocalization of π-electrons in the excited state, is the molecular structure. In this section, focus will be put on how the structure of cyclobutadiene, benzene, and cyclooctatetraene will change in the lowest (π,π^*) excited singlet and triplet states in comparison to the ground state structures. The ground state and excited state structures of cyclobutadiene, benzene, and cyclooctatetraene have been examined by several groups. A large collection of the reports on the structures of these compounds can be found in a recent review by Gellini and Salvi.[50]

First, let us consider how the structure changes of cyclobutadiene and cyclooctatetraene, in the lowest excited states in comparison to the ground state. As mentioned previously, the minimum energy structure of ground state cyclobutadiene has been calculated to be the rectangular D_{2h} conformation, with alternating single and double bonds.[32,34,51,52] The ground state is ^1A_g symmetric with the π-electron configuration illustrated in the π-orbital diagram in Fig. 3.2. The two lowest excited states for D_{2h} symmetric cyclobutadiene have been calculated to be triplet and singlet (π,π^*) states of $^3B_{1g}$ and $^1B_{1g}$ symmetry, respectively (donated $^1(\pi,\pi^*)$, and $^3(\pi,\pi^*)$ states, respectively).[34,51,52] The electron configuration of these two excited states are illustrated by the molecular π-orbital diagram in Fig. 3.2. In both of these states the structure of cyclobutadiene converges diabatically towards a square D_{4h} symmetric minimum energy conformation, which is calculated to be non-vertically located 0.57 eV and 2.12 eV above the ground state of the rectangular conformation by Eckert-Maksić *et al.* (MR-AQCC/SA-4-CASSCF/aug-cc-pVTZ).[52]

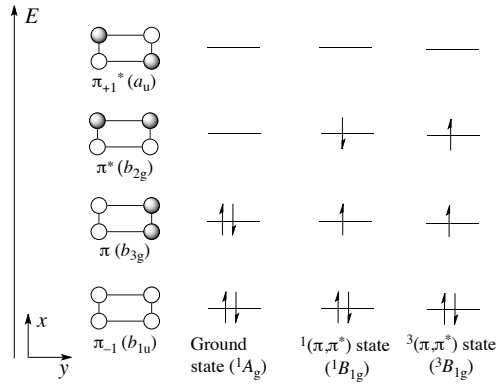

Figure 3.2: Schematic representations of the four π-orbitals for D_{2h} symmetric cyclobutadiene and their relative energetic positions. Orbital symmetries are given in parentheses. The three molecular orbital diagrams illustrate the π-electron configuration of the ground state, first excited singlet ($^1(\pi,\pi^*)$) and triplet states ($^3(\pi,\pi^*)$)

Estimated from Figure 2 in reference 52 the vertical excitation energies from the ground state of D_{2h} symmetric conformation of cyclobutadiene to the $^3(\pi,\pi^*)$ and $^1(\pi,\pi^*)$ states are 1.5 eV and 3.3 eV, respectively.[25] Thus, in the $^1(\pi,\pi^*)$ and $^3(\pi,\pi^*)$ states the energy of the molecule is lowered 0.93 eV and 1.18 eV by changing its structure from the D_{2h} to the D_{4h} symmetric conformation.

The excited states of cyclooctatetraene have been investigated computationally by Garavelli *et al.* and Frutos *et al.*[53,54] The results of their calculations suggest the lowest vertical excited states, of the tub-shaped D_{2d} symmetric conformation of cyclooctatetraene are the singlet and triplet (π,π^*) excited states of A_2 symmetry (donated $^1(\pi,\pi^*)$ and $^3(\pi,\pi^*)$, respectively). The π-electron configuration of these two states are equivalent, except for the electron spin, and can be represented with the π-orbital diagram in black in Fig. 3.3, on the following page.
According to the computational results the molecule adopts a planar D_{8h} symmetric conformation in both of these states.[53,54] The D_{8h} symmetric conformation is also lowest in energy in the lowest excited (π,π^*) triplet state, as revealed by several computational investigations.[25,55–59] The minimum energy D_{8h} symmetric structure in this triplet state was confirmed by photoelectron spectroscopy experiments.[60]
According to the calculated results by Garavelli *et al.* the $^1(\pi,\pi^*)$ state is lowered 2.24 eV in energy upon relaxation from the D_{2d} to the D_{8h} symmetric structure (CASPT2/6-31G(d)),[53] whereas according to the results of Frutos *et al.* the $^3(\pi,\pi^*)$ state is lowered 2.04 eV in energy upon the same geometrical relaxation.[54]

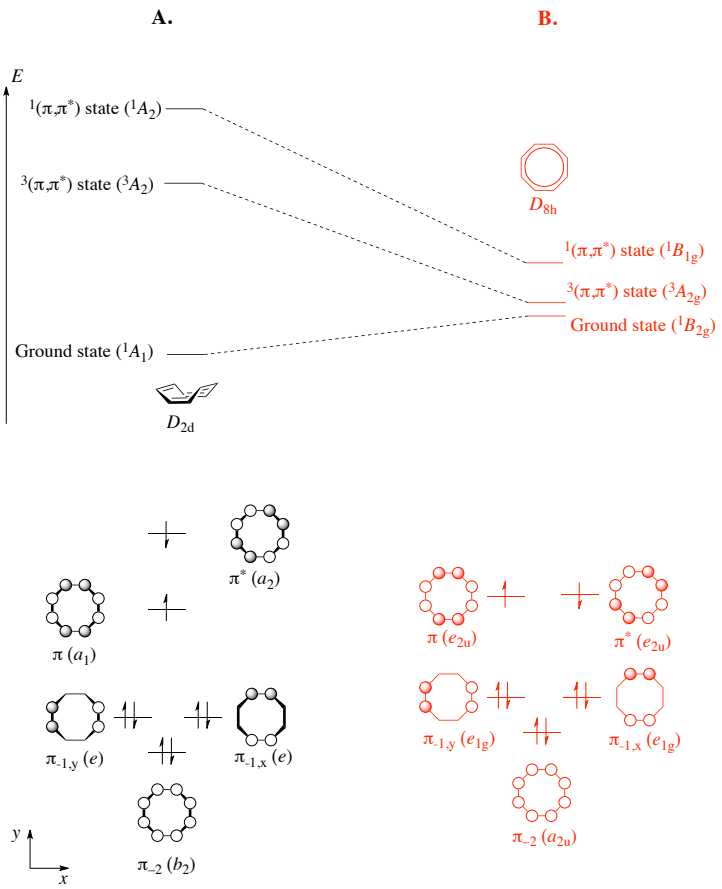

Figure 3.3: **A**, black: Schematic illustration of the relative energetic positions of the ground state and the first excited triplet ($^3(\pi,\pi^*)$) and singlet ($^1(\pi,\pi^*)$) states in the D_{2d} symmetric tub-shaped conformation. Symmetries of the three states within the D_{2d} point group are given in parentheses. The black π-orbital diagram shows the five lowest π-orbitals of D_{2d} symmetric cyclooctatetraene, and the dominant electron configuration in the $^1(\pi,\pi^*)$ state is represented. **B**, red: Schematic illustration of the relative energetic positions of the ground state, and the $^3(\pi,\pi^*)$ and $^1(\pi,\pi^*)$ states in the planar D_{8h} symmetric conformation. Symmetries within the D_{8h} point group of the three states are given in parentheses. The red π-orbital diagram represents the dominant electron configuration in the $^1(\pi,\pi^*)$ state. The $^3(\pi,\pi^*)$ state has the same electron configuration, with both electrons having the same spin. The black π-orbital diagram shows the five lowest π-orbitals of D_{8h} symmetric cyclooctatetraene, and the dominant electron configuration in the $^1(\pi,\pi^*)$ state is represented. The content of this figure is based on the computational results from references 53 and 54.

Thus, as for cyclobutadiene the energy of cyclooctatetraene is substantially lowered in the $^1(\pi,\pi^*)$ and $^3(\pi,\pi^*)$ excited states upon relaxation to the D_{8h} conformation. In this context, it is also worth mentioning that the 4π-electron cyclopentadienyl cation has proven experimentally to be a triplet ground state compound,[61] which adopts a D_{5h} symmetric conformation in this state.[62–64]

The examples above indicate that the cyclic delocalized arrangement of $4n$ π-electrons, are located at low energy points on the $^1(\pi,\pi^*)$ and $^3(\pi,\pi^*)$ state potential energy surfaces. In the cyclopentadienyl cation the cyclic delocalized arrangement of the π-electrons is associated with such low energy in the triplet state, that it becomes the ground state. It is therefore reasonable to consider cyclic delocalized arrangements of $4n$ π-electrons to be favorable in the lowest (π,π^*) excited singlet and triplet states. It would be obvious to expect that the structure of benzene would change in the lowest (π,π^*) excited singlet and triplet state as π-electron delocalization, according to the excited state π-electron counting rules, is unfavorable in contrast to in the ground state. However, before considering the structure of benzene in these excited states, an important aspect has to be considered. In the ground state of benzene the six π-electrons occupy the three lowest π-orbitals as shown in Fig. 3.4. There is four possible excitations from the highest occupied π-orbitals (π_x and π_y, in Fig. 3.4) to the lowest unoccupied π-orbitals (π_x^* and π_y^*, in Fig. 3.4). This will give rise to four excited states, which are degenerate if electron correlation is not considered. When electron correlation is considered this degeneracy is lifted as shown in Fig. 3.4. Consequently, three energetically distinct excited states appear, where one of them is a degenerate excited state.

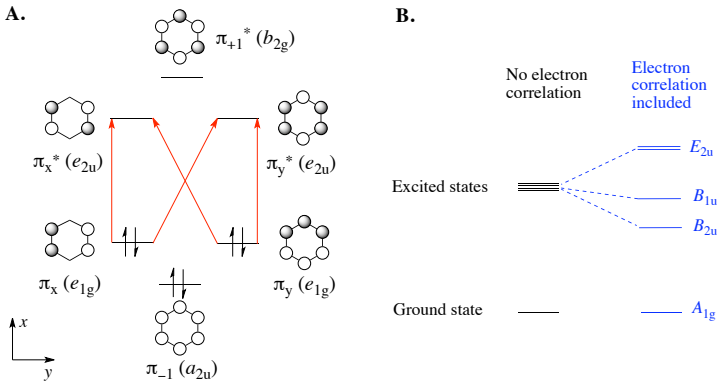

Figure 3.4: Illustration of (**A**) the electron configuration of benzene in the ground state, and the four possible excitations from the highest occupied π-orbitals, π_x and π_y, to the lowest unoccupied π-orbitals, π_x^* and π_y^* shown in red. Part **B** illustrates the energetic location of the four excited states, without (black) and with (blue) electron correlation taken into account.

Each of these states cannot be easily described by a single electron configuration as those illustrated in the orbital diagrams in Fig. 3.2 and Fig. 3.3. In fact, it can be argued that each of the excited states correspond to the 'lowest (π,π^*) excited state' described in the PMO model, with single electron occupation of the highest occupied π-orbital, and the lowest unoccupied π^*-orbital. Thus, for benzene each of the four excited states, illustrated in Fig. 3.4, have to be considered in light of the π-electron counting rules for excited states. However, for simplicity only the $^1B_{2u}$, $^1B_{1u}$, and $^3B_{1u}$ states are considered here. It has been calculated and verified experimentally, that benzene retains the D_{6h} symmetric conformation in the $^1B_{2u}$ excited state.[65–67] However, it has been argued that the π-electron framework of benzene is less bound in this excited state, as the b_{2u}vibrational mode, illustrated in Fig. 3.5, is increased in this state as compared to the ground state.[68,69] This argument is supported by the experimental fact that the C–C bonds are significantly elongated in this state going from 1.397 Å in the ground state to 1.435 Å in the $^1B_{2u}$ excited state.[65]

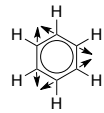

Figure 3.5: The b_{2u} vibrational mode for benzene. For this mode the frequency is exalted in the $^1B_{2u}$ excited state, which can be interpreted as a consequence of the less bounded π-electron framework.

The lowest (π,π^*) excited triplet state is $^3B_{1u}$ symmetric and in this state benzene undergoes geometrical distortion to a D_{2h} symmetric conformation. This conformation can be either quinoidal or antiquinoidal as shown in Fig. 3.6.[70–72] The geometrical distortion away from the D_{6h} symmetric structure in this triplet state has been verified by low temperature ESR experiments.[73–75] The relevant data reported on the structures in the latter three excited states are summarized in Fig. 3.6.

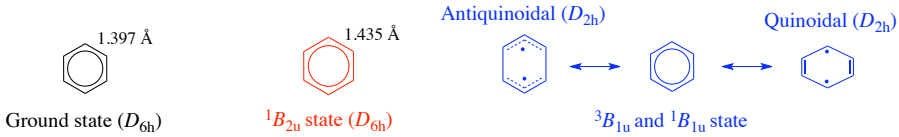

Figure 3.6: Illustration of the (black) D_{6h} symmetric ground state equilibrium structure, (red) D_{6h} symmetric $^1B_{2u}$ state minimum energy conformation, and (blue) D_{2h} symmetric antiquinodal and quinodal minimum energy conformations in the $^1B_{1u}$ and $^3B_{1u}$ states.

In summary, the examples reflect that the qualitative content of the excited state π-electron counting rules is valid and that cyclic delocalization of $4n$ π-electrons can be considered as favorable in the lowest (π,π^*) excited singlet and triplet state, while cyclic delocalization of $4n+2$ π-electrons is less favorable when compared to the ground state. The energetics associated with π-electron delocalization in the lowest excited states can be used to rationalize photochemical reactivity. This will be the focus in the following chapter.

Chapter 4

Implications of Cyclic Delocalization of π-Electrons on Photochemistry

The energetic aspects of cyclic delocalization of π-electrons, in the excited states, have been shown to have considerable impact on photochemical reactions. Probably the most famous examples are the photo-induced pericyclic reactions. These proceed preferentially *via* transition states that include reorganization of $4n$ π-electrons, and do not proceed *via* transition states that involve reorganization of $4n$+2 π-electrons. The qualitative results of the excited state π-electron counting rules are also reflected in other types of photochemical reactions. Compounds which have the possibility to achieve either $4n\pi$- or $(4n+2)\pi$-electron arrays, by chemical transformations, show interestingly contrasting reactivity in the ground state and lowest excited singlet state (S_1 state). Such contrasting reactivity was investigated intensively by Wan and co-workers for various compounds.[76–90]

Photochemical reactions such as photosolvolysis have been found to be driven by generation of precursors with cyclic frameworks of $4n$ π-electrons.[76,77,80,91–93] In the case of conversion of 9*H*-fluoren-9-ol to 9-methoxy-9*H*-fluorene it was found, that only very harsh conditions would yield a reaction in the ground state, while the photochemically initiated reaction proceeded under mild conditions with a reaction quantum yield of 20 % (Scheme **A**, in Fig. 4.1).[76,77] Interestingly, neither diphenylmethanol with no central ring, nor 5*H*-suberen-5-ol with a larger central ring underwent photolysis (Scheme **B** and **C**, in Fig. 4.1). This led Wan and co-workers to the conclusion that formation of a $4n\pi$-electron cation species in the excited state was a prerequisite for the reaction, and the presence of the intermediate cationic species was later confirmed experimentally.[91,93]

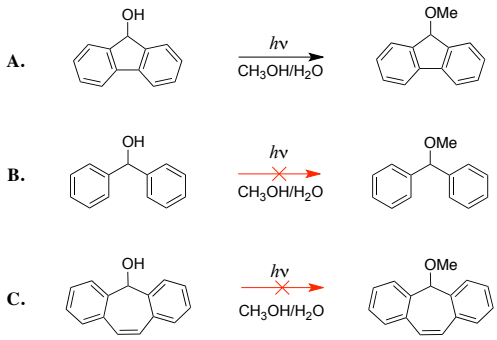

Figure 4.1: Photosolvolysis of (**A**) 9*H*-fluoren-9-ol, (**B**) diphenylmethanol, and (**C**) 5*H*-suberen-5-ol. Results from references 76 and 77.

Photodecarboxylations of a series of benzannelated acetic acids in aqueous solution showed a different, although similar tendency (Fig. 4.2).[79,83] Photodecarboxylation of 5*H*-suberene-5-carboxylic acid yielded 50 % product (Scheme **C**, in Fig. 4.2), while photolysis of 9*H*-fluorene-9-carboxylic acid and diphenylacetic acid (Scheme **A** and Scheme **B**, respectively, in Fig. 4.2) resulted in low yields (less than 3 % and 6 %, respectively) of the decarboxylated product. The formation of deutorated product in D_2O, revealed that the decarboxylation involves the formation of an anionic species. The yields of the reactions indicate that the generation of such an anion is favorable if it possesses $4n$ π-electrons, and this was concluded by the authors.

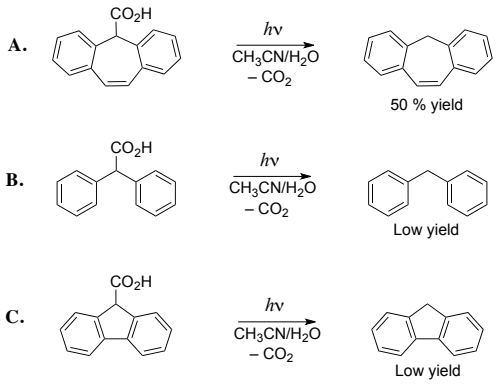

Figure 4.2: Photodecarboxylation of (**A**) 5*H*-suberene-5-carboxylic acid, (**B**) diphenylacetic acid, and (**C**) 9*H*-fluorene-9-carboxylic acid. Results from references 79 and 83.

The last series of experiments show that compounds that can form $4n\pi$-electron arrays by deprotonation, are very acidic in the S_1 state, in stark contrast to their non-existent acidity in the ground state. Moreover, compounds which form $(4n+2)\pi$-electron arrays by deprotonizion are, in contrast to the ground state, not acidic in their S_1 states.[78,81,82,84–90] The ground and S_1 state acidity of 9*H*-fluorene and 5*H*-suberene (Reactions **A** and **B**, in Fig. 4.3)[78,84] are illustrative for this trend.
Deuterium exchange was shown to occur in the 9-positions of 9*H*-fluorene in a 50 % D_2O/CH_3CN mixture. The amount of deuterium labeled 9*H*-fluorene molecules were significantly reduced, when the mixture was irradiated. In contrast, no observable deuterium exchange in the 5-position(s) of 5*H*-suberene was observed in a similar D_2O/CH_3CN mixture. When the mixture was irradiated the amount of deuterium labeled 5*H*-suberene was increased. Thus, 9*H*-fluorene is acidic in the ground state, but not in the S_1 state, while 5*H*-suberene is non-acidic in the ground state but acidic in the S_1 state (Fig. 4.3).

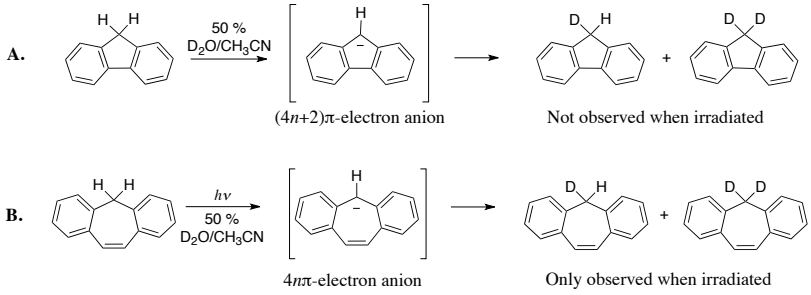

Figure 4.3: Reaction **A**: Deuterium exchange in the 9-position of 9*H*-fluorene in 50 % D_2O/CH_3CN mixture indicates that deprotonization proceed *via* the fluorene anion in the ground state. When the reaction mixture is irradiated, no deuterium exchange is observed. Results from references 78 and 84. Reaction **B**: No deuterium exchange is observed in 50 % D_2O/CH_3CN mixture, but exchange is observed in the 5-position(s) of 5*H*-suberene, when the mixture is irradiated. Results from references 78 and 84.

In summary, the examples in Fig. 4.1, Fig. 4.2, and Fig. 4.3 show that, in analogy to the ground state, photochemical reactivity can be rationalized on the basis of favorable and non-favorable cyclic interactions of π-electrons.

If the conclusions drawn by Wan and co-workers are considered from another point of view, it would be expected that compounds with cyclic arrays of $4n$ π-electrons would be less reactive in the excited state in comparison to the ground state, and *vice versa* for compounds with cyclic arrays of $4n+2$ π-electrons. Other experimental results suggest that this can indeed be argued to be the case.

These experimental results indicate that the acidity of unsaturated ionic cyclic hydrocarbons with $4n+2$ π-electrons in a cyclic array (ionic $(4n+2)\pi$-electron cyclic polyenes) are increased upon irradiation, which the reactions shown in Fig. 4.4 illustrate. The cyclooctatetraene dianion and cyclononatetraene anion have been shown to be resistant to protonation by 1-hexyne in THF in the absence of light (Reaction **A** and **B**, in Fig. 4.4).[94,95] When the reaction mixtures were irradiated the protonation of the two compounds by 1-hexyne were verified to proceed. The cyclopentadienyl anion would be expected to exhibit similar contrasting acidic behavior in the ground and excited states. The photoacidity of this compound has been investigated in *tert*-butanol (Reaction **C**, in Fig. 4.4).[96] This compound was neither protonated by *tert*-butanol in the presence or absence of irradiation. Instead the dimeric product [1,1'-bi(cyclopentane)]-2,2'-diene was generated upon irradiation (Reaction **C**, in Fig. 4.4). Van Tamelan *et al.* suggested that the excited cyclopentadienyl anion first undergoes hydrogen abstraction from *tert*-butanol, then protonation of the intermediate radical anion by *tert*-butanol, and finally dimerization to yield [1,1'-bi(cyclopentane)]-2,2'-diene.[96] This illustrates the competing reaction pathways to the photoacidic reaction, which should be considered on the excited state potential energy surface.

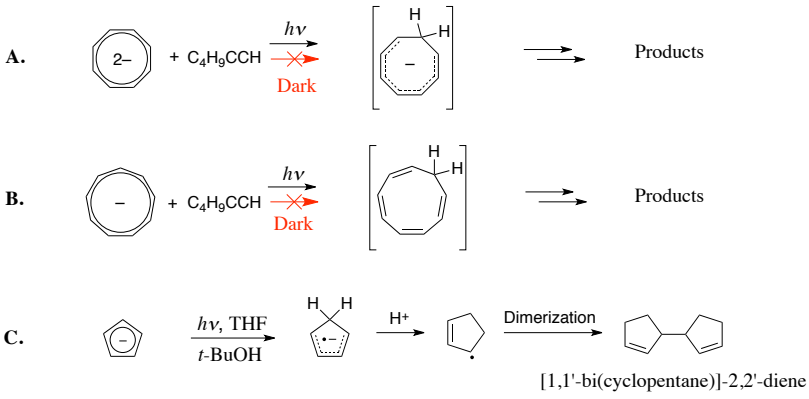

Figure 4.4: Reaction **A**. Excited state protonation of the cyclooctatetraene dianion. Results from reference 94. Reaction **B**. Excited state protonation of the cyclononatetraene anion. Results from reference 95. Reaction **C**. Photochemical behavior of the cyclopentadienyl anion. Results from reference 96.

4.1 Reactivity of Cyclic Polyenes in the Lowest (π,π^*) Triplet State

The impact of cyclic π-electron delocalization on photochemical reactivity, in the triplet excited state, has not drawn as much attention as in the singlet excited states. This encouraged us to examine the reactivity of cyclic polyenes in their lowest (π,π^*) excited triplet state, and compare this to the ground state reactivity of the compounds. Therefore, in a computational investigation we investigated eight proton and eight hydride addition reactions, for a series of ionic cyclic polyenes in the ground state and lowest excited triplet state. The results of this investigation were published in *The Journal of Organic Chemistry* in 2010.[30] In the following subsections, a summary of the published results will be presented.

4.1.1 Proton and Hydride Affinities of Ionic Cyclic Polyenes

Illustrated in Fig. 4.5 are the ensemble of proton (**A**, in blue) and hydride (**B**, in red) addition reactions, which were investigated computationally in the energetically lowest closed-shell singlet state (S_0 state) and the lowest energy triplet state (T_1 state). In order to assess how cyclic π-electron delocalization affects these reactions in the T_1 state, the gas phase proton and hydride affinities were calculated for the various compounds in the T_1 state. These energies were compared against those of the same species in the S_0 state. In short, the structures of the compounds in Fig. 4.5 were optimized to their minimum energy conformation at the (U)B3LYP/6-311+G(d,p) level. This method was chosen, as it has been used earlier for structural optimization of some of the ionic cyclic polyenes shown in Fig. 4.5, in their S_0 and T_1 states in another investigation.[56] The heats of formation (ΔH_f) at 298 K, for the compounds were calculated using the composite G3(MP2) method, using the (U)B3LYP/6-311+G(d,p) calculated structures (G3(MP2)//B3LYP/6-311+G(d,p)). The calculated heats of formation were then used to calculate the gas phase proton affinities (PA's) and hydride affinities (HA's) according to these equations:

$$\mathrm{PA} = \Delta H_f(\mathrm{M}^-) + \Delta H_f(H^+) - \Delta H_f(\mathrm{MH}) \tag{4.1}$$

$$\mathrm{HA} = \Delta H_f(\mathrm{M}^+) + \Delta H_f(H^-) - \Delta H_f(\mathrm{MH}) \tag{4.2}$$

Here, $\mathrm{M}^{-/+}$ refers to an anion/cation in either the lowest energy singlet or triplet state and MH is the reduced/oxidized neutral counterpart in either the S_0 or T_1 state, respectively. The heats of formation of the proton and the hydride ions were set to the literature values of 1530 and 145 kJ/mol, respectively.[97,98] Equation 4.1 is the IUPAC definition of proton affinity, and Equation 4.2 is Göbbert's and Wenthold's definiton of hydride affinity.[98]

The proton and hydride affinities are the negative reaction enthalpies of the proton and hydride addition reactions, respectively. Thus, the (positive) magnitude of the proton or hydride affinity indicates how exothermic the proton or hydride addition reaction is.

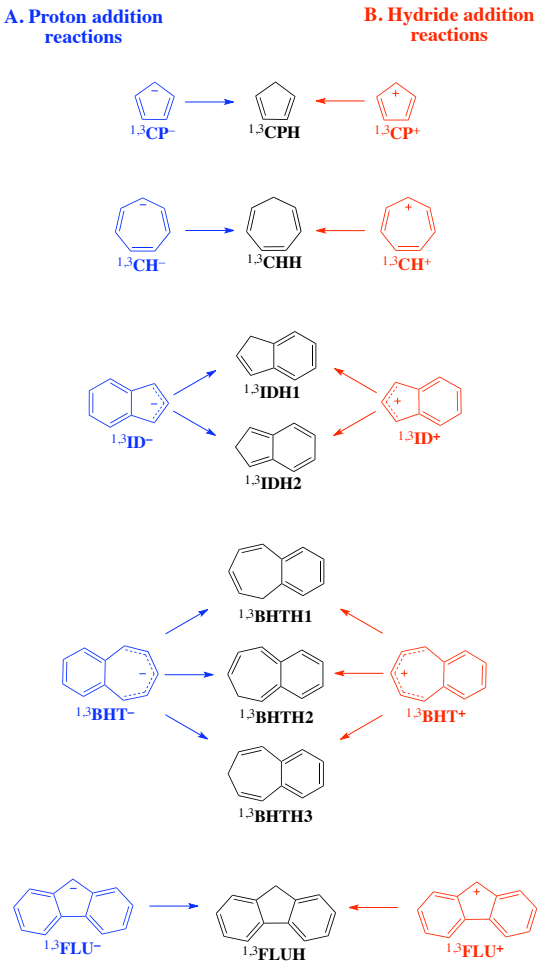

Figure 4.5: Investigated compounds (with the abbreviations used in the following text) and their proton (**A**, in blue) and hydride (**B**, in red) addition reactions. The superscript numbers 1 and 3, preceding the compound abbreviation refer, to the compound in the S_0 and T_1 state, respectively.

In the following, the ionic cyclic polyenes, which are S_0 state $(4n+2)\pi$-electron or T_1 state $4n\pi$-electron species, will be referred to as being of aromatic-character (A-character). Ionic cyclic polyenes, which are S_0 state $4n\pi$-electron or T_1 state $(4n+2)\pi$-electron species, will be referred to as anti-aromatic-character compounds (AA-character).

In order to assess if the energy associated with cyclic delocalization of π-electrons affects the calculated proton/hydride affinity of a particular anion/cation in its T_1 state, the S_0 state proton/hydride affinity is used for comparison. Although the formation of two different hydrocarbon isomers may be energetically preferred for the larger benzofused polyene anions and cations in the S_0 and T_1 state, the assessment of how π-electron delocalization influences on proton and hydride affinities in the T_1 state *vs.* S_0 state must relate to formation of the same particular isomer in both states.

4.1.2 Proton Affinities of Cyclic Polyene Anions

First, the results regarding the proton addition reactions in Fig. 4.5 are presented. The heats of formation and proton affinities of the cyclopentadienyl (**CP**$^-$), cycloheptatrienyl (**CH**$^-$), indenyl (**ID**$^-$), benzocycloheptatrienyl (**BHT**$^-$), and fluorenyl (**FLU**$^-$) anions, with respect to their protonated isomers were calculated in the S_0 and T_1 states. For **FLU**$^-$ only the proton affinity with respect to 9*H*-fluorene was calculated.

The calculated heats of formation and proton affinities of the anionic compounds are shown in Table 4.1. The calculated heats of formation for the neutral product compounds are given in Table 4.2. In Table 4.1, are also tabulated the difference in proton affinity of a particular anion in its state of AA-character, relative to its state of A-character (ΔPA(AA$-$A)). A positive value of ΔPA(AA$-$A) indicates that the proton addition reaction is more exothermic in the AA-character state, as compared to the reaction in the A-character state, and *vice versa* for a negative ΔPA(AA$-$A).

The values in parentheses are experimentally determined heats of formation and proton affinities, these values are in reasonable agreement with the calculated ones. By comparing the heats of formation for the S_0 and T_1 states, it is evident that the S_0 state compounds are lowest in energy, *i.e.* the S_0 states are the ground state for all compounds.

Before an analysis of the proton affinities for the anions in the T_1 state *vs.* those in the ground state, is given it should be mentioned that the small value of ΔPA(AA$-$A) for **CP**$^-$ actually should not be considered in this study. The T_1 state for this compound is a (π,3s) Rydberg state, while the T_1 states of the remaining compounds are (π,π^*) states. The second lowest excited triplet state of **CP**$^-$ was revealed to be a (π,3p) Rydberg state, and no further attempts to locate the lowest excited (π,π^*) triplet state for **CP**$^-$ were performed. However, the result indicate that the lowest excited (π,π^*) triplet state must possess a much larger heat of formation, than the calculated value given for ^{3}**CP**$^-$ in Table 4.1.

Consequently, the proton affinity that would be comparable, to the other triplet state compounds, would also become larger than the 11 kJ/mol given in Table 4.1, which would enhance ΔPA(AA$-$A) for $\mathbf{CP}^-$.

Table 4.1: Calculated heats of formation (ΔH_f), proton affinities (PA), and differences in proton affinities between AA- and A-character states (ΔPA(AA$-$A)).

Compound[a]	Character	ΔH_f (kJ/mol)[b]	PA (kJ/mol)[c]	ΔPA(AA$-$A) (kJ/mol)
$^1\mathbf{CP}^-$	A	75	1477 (1481)[d]	
$^3\mathbf{CP}^-$	AA	337	1488	11
$^1\mathbf{CH}^-$	AA	224	1579 (1570)[d]	
$^3\mathbf{CH}^-$	A	231	1395	184
$^1\mathbf{ID}^-(\mathbf{1})$	A	84	1466 (1472)[e]	
$^3\mathbf{ID}^-(\mathbf{1})$	AA	333	1430	-36
$^1\mathbf{ID}^-(\mathbf{2})$	A	84	1381	
$^3\mathbf{ID}^-(\mathbf{2})$	AA	333	1496	115
$^1\mathbf{BHT}^-(\mathbf{1})$	AA	198	1531	
$^3\mathbf{BHT}^-(\mathbf{1})$	A	253	1356	175
$^1\mathbf{BHT}^-(\mathbf{2})$	AA	198	1454	
$^3\mathbf{BHT}^-(\mathbf{2})$	A	253	1383	81
$^1\mathbf{BHT}^-(\mathbf{3})$	AA	198	1520	
$^3\mathbf{BHT}^-(\mathbf{3})$	A	253	1327	193
$^1\mathbf{FLU}^-$	A	103	1466 (1466)[e]	
$^3\mathbf{FLU}^-$	AA	313	1372	-94

[a] Numbers in parentheses indicate, which isomer of the neutral hydrocarbon is formed upon protonation. [b] G3(MP2)//(U)B3LYP/6-311+G(d,p), 298 K. [c] Numbers in parentheses are experimentally determined values. [d] Reference 29. [e] Reference 99.

Table 4.2: Calculated heats of formation (ΔH_f) of the neutral hydrocarbons.

Compound	ΔH_f (kJ/mol)[a]	Compound	ΔH_f (kJ/mol)[a]
^{1}**CPH**	128 (133)[b]	^{3}**CPH**	379
^{1}**CHH**	175 (187)[c]	^{3}**CHH**	366
^{1}**IDH1**	148 (161)[d]	^{3}**IDH1**	433
^{1}**IDH2**	233	^{3}**IDH2**	367
^{1}**BHTH1**	197	^{3}**BHTH1**	427
^{1}**BHTH2**	274	^{3}**BHTH2**	400
^{1}**BHTH3**	208	^{3}**BHTH3**	456
^{1}**FLUH**	168 (175)[e]	^{3}**FLUH**	472

[a] G3(MP2)//(U)B3LYP/6-311+G(d,p), 298 K; numbers in parentheses are experimentally determined values. [b] Reference 100. [c] Reference 101. [d] Reference 102. [e] Reference 103.

The average proton affinity corresponding to the seven protonation reactions, not including ^{3}**CP**$^-$, in the T_1 state (1394 kJ/mol) is lower than the average proton affinity for the eight reactions including ^{1}**CP**$^-$, in the S_0 state (1484 kJ/mol). The lower proton affinities of the anions in their T_1 states than in their S_0 states, should stem from the fact that the T_1 state is an electronically excited state, in which an orbital with more antibonding character is occupied. A proton added to an anion in this state will therefore in general be less strongly bound, than when added to an anion in its electronic S_0 state.

In regard to the proton affinities in the S_0 states, the anions, which have ground states of A-character, have lower average PA (1447 kJ/mol) than the anions, which have S_0 states of AA-character (1521 kJ/mol), a result of the stabilization gained from π-electron delocalization in the S_0 state A-character anions. The same relationship, between the magnitudes of the average proton affinities, is found in the T_1 states, because the anions with T_1 states of A-character have significantly lower average proton affinity (1365 kJ/mol) than those with T_1 states of AA-character (1433 kJ/mol, ^{3}**CP**$^-$ not included). The calculated proton affinities show that all, except two of the protonation reactions, yield higher proton affinities in their AA-character state than in their A-character state. Another noteworthy aspect is that for three of the four protonation reactions of anions, with S_0 states of AA-character, the ΔPA(AA$-$A) values are particularly large (175-193 kJ/mol).

This illustrates that the compounds are easier to protonate in their A-character states as compared to their AA-character states.

The two negative ΔPA(AA−A) values can, in part, be explained by the fact that the proton affinities of the T_1 states are generally lower than those of the S_0 states, as observed above. A second contributing factor to the negative ΔPA(AA−A) values is the ability of the larger benzofused anions to attain local cyclic arrangement of delocalized π-electrons in the AA-character state. For **ID**$^-$, and similarly for **FLU**$^-$, the negative ΔPA(AA−A) can also be rationalized, by comparing the calculated bond lengths of ^{1}**ID**$^-$ and ^{3}**ID**$^-$ with those of ^{1}**IDH1** and ^{3}**IDH1**, shown in Fig. 4.6, in order to obtain knowledge of possible contributions from resonance structures.

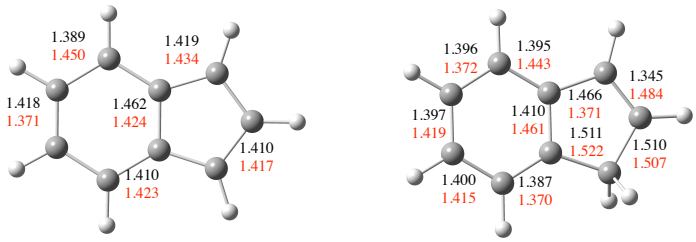

Figure 4.6: Calculated C–C bond lengths (Å) for ^{1}**ID**$^-$ (left, black) and ^{3}**ID**$^-$ (left, red), ^{1}**IDH1** (right, black), and ^{3}**IDH1** (right, red).

In regard to ^{1}**ID**$^-$, it is best described as a 10π-electron ring involving the peripheral C–C bonds. This is supported by the maximal bond length variation of merely 0.030 Å, in the external C–C bond periphery. On the other hand, ^{3}**ID**$^-$ has a large maximum bond length variation in the peripheral bonds of 0.079 Å.
Yet, the variation within the five-membered ring is only 0.017 Å. The average C–C bond length of this ring (1.425 Å) is only slightly longer than the C–C bond length, of the D_{5h} symmetric cyclopentadienyl anion in its ground state (1.415 Å). Based on the geometry, anion ^{3}**ID**$^-$ should therefore, to a substantial degree, be represented by a resonance structure, with a five-membered ring with 6π-electrons delocalized as illustrated in Fig. 4.7. Consequently, **ID**$^-$ is influenced, by a favorable local closed-shell cyclic delocalized arrangements of $4n$+2 π-electrons in both the S_0 and T_1 states.

As the protonation of **ID**$^-$ leading to isomer **IDH1** corresponds to a negative ΔPA(AA−A), one also needs to regard the geometries of this neutral hydrocarbon in the S_0 and T_1 states. The C–C bond lengths (Fig. 4.6), suggest that ^{1}**IDH1** and ^{3}**IDH1** are well represented by the resonance structures shown in Fig. 4.7. Thus, when **ID**$^-$ is protonated in its A-character ground state it preferentially yields ^{1}**IDH1**.

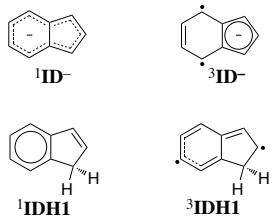

Figure 4.7: Important resonance structure representations of ^{1}**ID**$^-$, ^{3}**ID**$^-$, ^{1}**IDH1**, and ^{3}**IDH1** based on the calculated bond lengths.

In this protonation reaction, both the anionic reactant and the neutral product are influenced by a favorable cyclic delocalized arrangement of π-electrons.
However, in the T_1 state, ^{3}**ID**$^-$ is stabilized, by closed-shell cyclic arrangement of 6π-electrons, and this array is destroyed upon protonation to yield ^{3}**IDH1**, which is not stabilized by any favorable cyclic arrangements of π-electrons. As a result, the proton affinity of **ID**$^-$ will be low in the T_1 state, which is of AA-character, and the ΔPA(AA$-$A) becomes negative. Indeed, this reveals that when considering the polycyclic anionic compounds, one must consider that they can adjust their geometries in both states, in order to adopt the most favorable π-electron arrangement in one or several of their rings, depending on what is optimal for each particular state.

One should also note the differences between the proton affinity of the T_1 and S_0 states, for protonation at the various sites of the anions (Table 4.1). For example, protonation of **ID**$^-$ in the S_0 state will preferentially give **IDH1** because this IDH*n* isomer (*n* = 1 or 2) has the lowest heat of formation, and the protonation reaction also corresponds to the highest proton affinity. In the T_1 state, on the other hand, the **IDH2** isomer has the smallest heat of formation and its formation is complimented, by the largest proton affinity. Whereas **IDH1** is stabilized by the 6π-electron system in the S_0 state, and **IDH2** is not, the opposite applies for the two isomers in the T_1 state (Table 4.2). To a significant extent, ^{3}**IDH2** is well described, by a resonance structure composed of a closed-shell singlet 6π-electron ring, and due to this, the proton affinity for this reaction should be high. The ^{3}**IDH1** is, as concluded above, not represented by a resonance structure containing a cyclic array of π-electrons (Fig. 4.7). Similar differences are found for the three possible protonation reactions of **BHT**$^-$ in the S_0 state *vs.* the T_1 state.

4.1.3 Hydride Affinities of Cyclic Polyene Cations

With regard to the hydride affinities it should first be remarked that several aspects resemble those of the proton affinities, and therefore this section is more brief. The calculated heats of formation, hydride affinities , and differences in hydride affinities between AA- and A-character states (ΔHA(AA$-$A)) are tabulated in Table 4.3. All the triplet states were calculated to be (π,π^*) states.

Table 4.3: Calculated heats of formation (ΔH_f), hydride affinities (HA), and differences in hydride affinities between AA- and A-character states (ΔHA(AA$-$A)).

Compound[a]	Character	ΔH_f (kJ/mol)[b]	HA (kJ/mol)	ΔHA(AA$-$A) (kJ/mol)
^{1}**CP**$^+$	AA	1102	1117	
^{3}**CP**$^+$	A	1076	843	274
^{1}**CH**$^+$	A	876	846	
^{3}**CH**$^+$	AA	1206	985	139
^{1}**ID**$^+$(**1**)	AA	1002	999	
^{3}**ID**$^+$(**1**)	A	1058	770	229
^{1}**ID**$^+$(**2**)	AA	1002	913	
^{3}**ID**$^+$(**2**)	A	1058	837	76
^{1}**BHT**$^+$(**1**)	A	900	849	
^{3}**BHT**$^+$(**1**)	AA	1125	843	-6
^{1}**BHT**$^+$(**2**)	A	900	771	
^{3}**BHT**$^+$(**2**)	AA	1125	870	99
^{1}**BHT**$^+$(**3**)	A	900	838	
^{3}**BHT**$^+$(**3**)	AA	1125	814	-24
^{1}**FLU**$^+$	AA	979	956	
^{3}**FLU**$^+$	A	1037	710	246

[a] Numbers in parentheses indicate, which isomer of the neutral hydrocarbon is formed upon protonation. [b] G3(MP2)//(U)B3LYP/6-311+G(d,p), 298 K.

The cations have singlet ground states apart from the cyclopentadienyl cation, ^{3}**CP**$^+$, which has a triplet multiplicity ground state, in correspondence with the experimental findings by Saunders *et al.*[61] However, for simplicity the terms S_0 and T_1 states will also in this subsection refer to the lowest energy closed-shell singlet state and lowest energy triplet state, respectively. Similar as for the proton affinities, the hydride affinities of the cations are in general higher in the ground state than in the T_1 state (average hydride affinities are 911 and 834 kJ/mol for the S_0 and T_1 states, respectively), a fact that needs to be taken into consideration, when regarding the ΔHA(AA$-$A) values, in particular when the AA-character state is a T_1 state.
The lower average hydride affinities in the T_1 state, in comparison to the S_0 state, should stem from weakened bonding character, in the T_1 state, as this is an electronically excited state.

In the S_0 state, the cations of A-character have lower average hydride affinity than the ones of AA-character (826 *vs.* 996 kJ/mol, respectively), and the same relationship is found in the T_1 state because the hydride affinities of the A-character compounds in the T_1 state are, in average lower (790 kJ/mol) than those of the AA-character compounds (879 kJ/mol).

With regard to the ΔHA(AA$-$A) values only two of the eight protonation reactions considered have negative values, these being the protonations of **BHT**$^+$ leading to **BHTH1** and **BHTH3**, respectively. However, similar as for ^{3}**ID**$^-$ it can be concluded that ^{3}**BHT**$^+$, to a significant extent, is represented by a resonance structure, with a closed-shell seven-membered ring, with six delocalized π-electrons, as shown in Fig. 4.8, and that ^{3}**BHTH1** and ^{3}**BHTH3** are not favorable T_1 state structures while ^{3}**BHTH2** is. For the other cations, the ΔHA(AA$-$A) range is 76 to 274 kJ/mol, with the highest values for cations where the S_0 state is of AA-character, and the T_1 state is of A-character. This is similar to the trend observed in the ΔPA(AA$-$A), and reflects that the T_1 state compounds possess lower average hydride affinities, for both the A- and AA-character systems, and from the fact that larger polycyclic cations are able to redistribute their electron density in a favorable manner in the AA-character state.

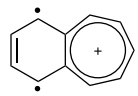

Figure 4.8: Important resonance structure of ^{3}**BHT**$^+$.

In conclusion, this computational investigation illustrated that the qualitative content of the π-electron counting rules (Equations (3.2)-(3.4)), for excited states, can indeed be used, to rationalize the acid-base chemistry involving cyclic polyenyl anions and cations in their T_1 states, in a similar way as the ground state π-electron counting rules (Equations (2.2)-(2.4)) can be used, to explain acid-base chemistry involving cyclic polyenyl anions and cations in the ground state. The trend that appears is shown in Fig. 4.9. However, the results also importantly reveal that when π-electron delocalization is considered for large fused ring systems, the possibility for formation of local smaller π-electron arrays must be taken into account.
This illustrates that competing stabilizing effects are always present and these must be taken into account, when chemical behavior is considered in the light of cyclic delocalization of π-electrons.

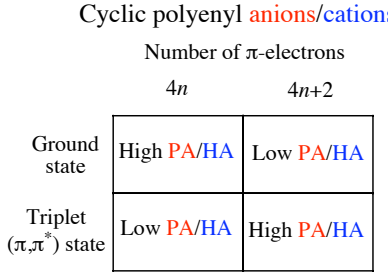

Figure 4.9: Relationship between the relative magnitudes of the proton and hydride affinities (PA and HA, respectively) of polyenyl anions and cations and the electronic state as well as π-electrons.

Chapter 5

Excited State Energies and Cyclic Delocalization of π-Electrons

Another interesting trend can be coupled to the energetic aspects associated with π-electron delocalization in the ground and excited states of cyclic polyenes. This trend is revealed, when the difference in energy, between the lowest energy closed-shell singlet state and lowest energy (π,π^*) triplet states, for the ionic cyclic polyenes, discussed in sec. 4.1 are compared. These energy differences (ΔE_{ST}) are listed in Table 5.1.

Table 5.1: Energy differences, given in eV, between the lowest energy closed-shell singlet state and the lowest energy triplet state (ΔE_{ST}) for the ionic cyclic polyenes in Fig. 4.5.

Anionic compounds[a]	ΔE_{ST} (eV)[b]	Cationic compounds[a]	ΔE_{ST} (eV)[b]
CP$^-$	[c]	**CP**$^+$	−0.25
CH$^-$	0.07	**CH**$^+$	3.42
ID$^-$	2.58	**ID**$^+$	0.58
BHT$^-$	0.57	**BHT**$^+$	2.33
FLU$^-$	2.18	**FLU**$^+$	0.60

[a] Abbreviations for the compounds correspond to those in Fig. 4.5. [b] ΔE_{ST} = ΔH_f(lowest energy triplet state) − ΔH_f(lowest energy closed-shell singlet state). Values from Table 4.1 and Table 4.3. [c] Not included, as the lowest energy triplet state is not of (π,π^*) character.

The ionic cyclic polyenes that possess an array of $4n$ π-electrons, in the external C−C bond periphery, *i.e.* **CP**$^+$, **CH**$^-$, **ID**$^+$, **BHT**$^-$, and **FLU**$^+$, have significantly lower ΔE_{ST} values, in comparison to the compounds that possess $4n$+2 π-electrons in the outer C−C bond periphery of the cyclic polyene, *i.e.* **CP**$^-$, **CH**$^+$, **ID**$^-$, **BHT**$^+$, and **FLU**$^-$. The average ΔE_{ST}, for the $4n\pi$-electron containing cyclic polyenes, is 0.31 eV. For the $(4n+2)\pi$-electron containing cyclic polyenes the average value is 2.63 eV. A similar trend is also found, when comparing cyclobutadiene, benzene, and cyclooctatetraene.

The difference between the lowest energy points on the $^3(\pi,\pi^*)$ state and ground state potential energy surfaces, that corresponds to ΔE_{ST}, are 0.57 eV, 3.65 eV, and 0.78 eV for cyclobutadiene, benzene, and cyclooctatetraene, respectively.[52,54,104] Although, these energy differences are obtained computationally, using different methods for cyclobutadiene and cyclooctatetraene, and the energy is experimentally determined for benzene, they clearly follow the same trend as the energy differences in Table 5.1, *i.e.* small energy differences for cyclobutadiene and cyclooctatetraene, and a comparatively larger energy difference for benzene. Interestingly, this trend is also found, when comparing the energy difference between the lowest energy points on the $^1(\pi,\pi^*)$ state and ground state potential energy surfaces (ΔE_{SS}), for cyclobutadiene (ΔE_{SS} = 2.12 eV),[52] benzene (ΔE_{SS} = 4.59 eV),[104] and cyclooctatetraene (ΔE_{SS} = 1.76 eV).[53] The ΔE_{ST} and ΔE_{SS} values for cyclobutadiene, benzene, and cyclooctatetraene are listed in Table 5.2. In Table 5.2 are also listed the vertical transition energies; between the ground state and $^1(\pi,\pi^*)$ state ($\Delta E_{SS,v}$), and between the ground and the $^3(\pi,\pi^*)$ state ($\Delta E_{ST,v}$), for the three compounds. These also follow the trend mentioned above. Fig. 5.1 can serve as convenient support, when considering the numbers in Table 5.2.

In summary, it appears that compounds with cyclic arrays of $4n$ π-electrons, in general possess low excitation energies to the lowest (π,π^*) excited singlet and triplet states. Subsequent to excitation, the structures of the $4n\pi$-electron cyclic polyenes, converge towards low energy points on the excited state potential energy surface, which correspond to conformations where π-electron delocalization is preferred, as discussed in sec. 3.1. The opposite tendency is found, for the cyclic polyenes containing $4n$+2 π-electrons, which in general possess higher excitation energies.
The knowledge of how π-electron delocalization affects the ground and excited state energies can be strategically used, in the design of compounds with interesting optical properties. In the last chapters of this thesis this strategic utilization will be demonstrated.

Table 5.2: Energy differences between the lowest points on the ground state and the lowest (π,π^*) excited singlet and triplet states potential energy surfaces (ΔE_{SS} and ΔE_{ST}, respectively), and vertical transition energies between the ground state and the lowest (π,π^*) excited singlet and triplet states ($\Delta E_{SS,v}$ and $\Delta E_{ST,v}$, respectively). For benzene the $^1(\pi,\pi^*)$ and $^3(\pi,\pi^*)$ states corresponds to the $^1B_{2u}$ and $^3B_{1u}$ states, respectively. For cyclobutadiene and cyclooctatetraene the $^1(\pi,\pi^*)$ and $^3(\pi,\pi^*)$ states refer to those discussed in sec. 3.1.

Compound	$\Delta E_{SS,v}$ (eV)	$\Delta E_{ST,v}$ (eV)	ΔE_{SS} (eV)	ΔE_{ST} (eV)
Cyclobutadiene	3.3[a]	1.5[a]	2.12[b]	0.57[b]
Benzene	4.76[c]	3.95[c]	4.59[c]	3.65[c]
Cyclooctatetraene	4.43[d]	3.05[d]	1.76[e]	0.78[f]

[a] MR/AQCC/SA-4-CASSCF/aug-cc-pVTZ, estimated from Figure 2 in reference 52. [b] MR/AQCC/SA-4-CASSCF/aug-cc-pVTZ, data from reference 52. [c] Experimental data in hexane or cyclohexane solution, data from reference 104. [d] Results of electron-impact energy loss spectroscopy, data from reference 105. [e] CASPT2/6-31G(d), data from reference 53. [f] CASPT2/C,N,O[4s3p1d]/H[2s1p] + 2s2p2d (Rydberg functions) ANO-type basis set , data from reference 54.

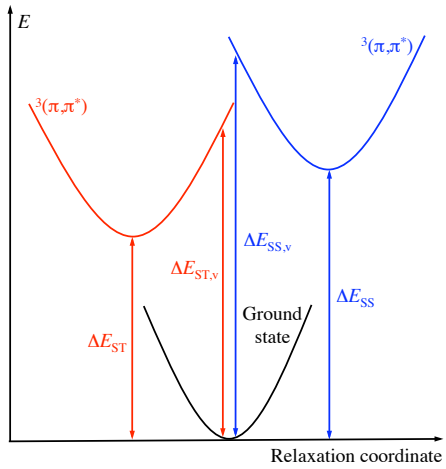

Figure 5.1: Illustrative explanation of the energy differences presented in Table 5.2.

Chapter 6

Fulvenes - Cyclic Polyenes in Disguise

A class of compounds, which are particularly interesting, in the context of cyclic delocalization of π-electrons, in both the ground and excited states, are the fulvenes. The fulvenes can be categorized as isomers of monocyclic polyenes, with the empirical formula C_kH_k ($k \leq 4$), which have a single exocyclic methylene group cross-linked to an odd-numbered ring moiety. This class of compounds can be viewed as camouflaged cyclic polyenes, as they can be represented by dipolar resonance structures, with either $4n$- or $4n$+2 π-electrons distributed in the ring moiety.
This is illustrated in Fig. 6.1 for triafulvene, pentafulvene, and heptafulvene.

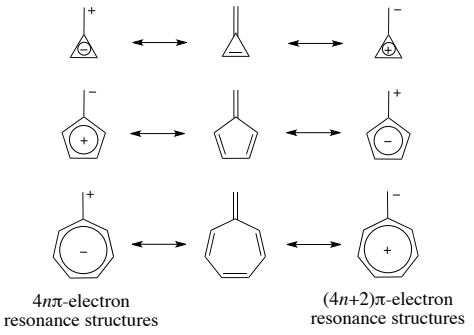

Figure 6.1: Triafulvene (top), pentafulvene (middle), and heptafulvene (bottom) represented by their $4n$- and $(4n+2)\pi$-electron dipolar resonance structures (left and right, respectively).

In the following, the electron density distributions, that are representative for the dipolar $4n\pi$- or $(4n{+}2)\pi$-electron resonance structures in Fig. 6.1, will be referred to as $4n\pi$- or $(4n{+}2)\pi$-electron density distributions. The fulvenes shown in Fig. 6.1 have all been prepared, but they are all reactive compounds and require special conditions for investigation.[106–111] The experimental determination of the structures of tria-, penta-, and heptafulvene, suggest that the compounds have C_{2v} symmetry, and alternating C−C single- and double bonds.[109,111–114] However, the direction of the dipole moments, for the three compounds, suggest that they are influenced, by the $(4n{+}2)\pi$-electron density distributions.[109–111,115,116] The experimentally determined magnitudes of the dipole moments are 1.90 D, 0.42 D, and 0.48 D for tria-, penta-, and heptafulvene, respectively. The dipole moments for tria- and heptafulvene are directed from a negatively charged C atom, to a positive charge in their ring moiety. The dipole moment of pentafulvene has opposite direction in comparison to the two other fulvenes. The dipolarity of the fulvenes changes significantly, when the exocyclic position(s) is substituted, as illustrated in Fig. 6.2.

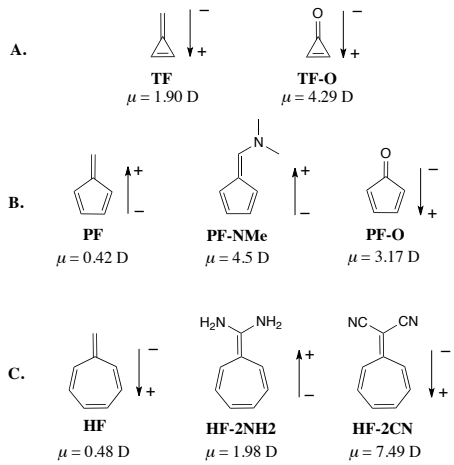

Figure 6.2: Illustration of how exocyclic substituents affect the dipolarities of (**A**) triafulvene, (**B**) pentafulvene, and (**C**) heptafulvene. The dipole moments presented correspond to: **TF**: Experimentally determined value, taken from reference 109, **TF-O**: Experimentally determined value, taken from reference 117, **PF**: Experimentally determined value, taken from reference 110, **PF-NMe**: Experimentally determined value, taken from reference 118, **PF-O**: Calculated value (CASPT2), taken from reference 119, **HF**: Experimentally determined value, taken from reference 111, **HF-2NH2**: Calculated value (OLYP/6-311G(d,)), taken from reference 120, **HF-2CN**: Experimentally determined value, taken from reference 121.

In addition to the changes in dipolarity, the stabilities of the unstable parent fulvenes are also changed, when exocyclic substituents are introduced. For example, tria- and heptafulvene derivatives, with π-electron withdrawing group(s) or atoms substituted in or at the exocyclic position(s), can readily be isolated.[122–127] On the other hand, reports on derivatives, with π-electron donating groups in these positions are scarce. To my knowledge, there are no experimental reports on triafulvene derivatives, with π-electron donating groups in the exocyclic positions. Only a few reports exist on heptafulvene derivatives, substituted with π-electron donating groups in the exocyclic positions.[128–130]
The tetramethylated derivative of **HF-2NH$_2$** (8,8-bis(dimethylamino)heptafulvene) was reported to be very easily oxidized,[129,130] and this compound reacts with molecular oxygen, upon formation of *N*,*N*-dimethylbenzamide.[128] The derivatives of pentafulvene, with π-electron donating groups in the exocyclic positions, are more easily prepared, in comparison to the derivatives, with π-electron withdrawing groups in these positions.[118,131–138] For example, cyclopentadienone (**PF-O**) dimerizes rapidly, and is not observed in its monomeric form at ambient conditions.[133] Thus, when the dipolarities of the fulvenes are changed, by the presence of substituents, which enhance the influence of the $(4n+2)\pi$-electron density distribution, the fulvenes obtain enhanced stability, as it would be expected, from the qualitative content of the ground state π-electron counting rules. Contrastingly, but also in accordance with the qualitative content of the π-electron counting rules, no stabilizing contribution appears to be present, when the exocyclic substituents contribute to an enhanced influence of the $4n\pi$-electron density distribution.

It is worth mentioning, that computational results, by Stępień *et al.*, support that properly substituted penta- and heptafulvenes experience enhanced influence of cyclic delocalization of $4n+2$ π-electrons in their ring moieties. The results suggest that the C−C bond lengths in the ring moieties are more equidistant, when π-electron donating group(s) are substituted in the exocyclic positions of pentafulvene, and when electron withdrawing groups are substituted in the exocyclic position(s) of heptafulvene, when comparing to the parent fulvenes.[139,140] Moreover, their results showed, that the opposite tendency appears for the C−C bond lengths, in the ring moiety of exocyclically substituted penta- and heptafulvenes, which possess substituents that enhance the influence of the $4n\pi$-electron density distribution. Thus, for these substituted penta- and heptafulvenes, the cyclic delocalization of π-electrons seems to be unimportant.

6.1 The Lowest Excited States of Fulvenes

In light of the excited state π-electron counting rules, it is reasonable to expect that a $4n\pi$-electron density distribution, may have a predominating influence on the excited states. The excited states of the three fulvene molecules have been investigated, both experimentally and computationally.[106,108,118,131,141–145] The lowest energy transitions for tria-, penta-, and heptafulvene appear in the absorption spectra as broad banded and weak intensity absorption envelopes, with maximum intensities at 4.01 eV (*n*-pentane), 3.45 eV (gas phase), and 2.90 eV (*n*-hexane), respectively.[106,108,118] These transitions are assigned to be $^1A_1 \rightarrow {}^1B_2$ transitions for all of the fulvenes.[108,118,131,141,142] This transition is calculated to involve promotion of an electron, from the highest occupied π-orbital (π, in Fig. 6.3) to the lowest unoccupied π-orbital (π^*, in Fig. 6.3).[108,141–145] Focus will be put on this type of transition, as it is interesting in the context of the qualitative content of the excited state π-electron counting rules.

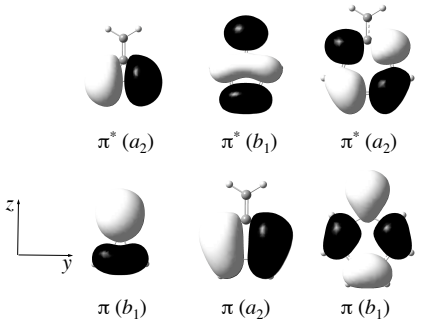

Figure 6.3: Illustration of the highest occupied and lowest unoccupied π-orbitals (π and π^*, respectively) of the planar C_{2v} symmetric tria-, penta-, and heptafulvene. Orbital symmetries are given in parentheses. The orbitals are calculated at the OLYP/cc-pVTZ level.

6.1.1 The B_2 Excited State π-Electron Density

From inspection of the π- and π^*-orbitals, in Fig. 6.3, it can be deduced that the π-electron density is effectively reorganized, from the exocyclic C atom to the ring moieties for tria- and heptafulvene, upon excitation to the $^1B_2$ state. The opposite is observed for pentafulvene, *i.e.* the π-electron density is reorganized from the ring to the exocyclic region, when excited to the $^1B_2$ state.

Computations, performed at the OLYP/cc-pVTZ level, were performed during this PhD project, to clarify how the electron density distribution changes, when the fulvenes are excited to their $^1B_2$ states. The combination, of functional and basis set, was chosen because it had been used previously in an investigation of the dipolarities of fulvene molecules.[120] The structural optimizations of three fulvene molecules resulted in parameters, which corresponded well, with experimental data for tria- and pentafulvene, as well as the magnitudes and directions of the dipole moments. For heptafulvene, the deviation, from experimental data is slightly more pronounced. The calculated C−C bond lengths, and magnitudes of the dipole moments, together with their directions, are shown in Fig. 6.4. The change in electron density distribution of the fulvenes, upon excitation to the $^1B_2$ state, was investigated through population analysis of the calculated excited state electron densities, obtained from TD-OLYP/cc-pVTZ//OLYP/cc-pVTZ calculations. The results of these calculations are illustrated in Fig. 6.4 and suggest that the dipolarities of the three fulvenes are reversed, in comparison to their ground state dipolarities, as expected from the simple inspection of the π and π^* orbitals. It is reasonable to assign this dipolarity reversal, to be caused mainly by reorganizations in the π-electron density, as the $^1B_2$ state has (π,π^*) electron configuration. Thus, according to these results the $4n\pi$-electron density distribution indeed becomes predominant, when the fulvenes are excited to their $^1B_2$ states.

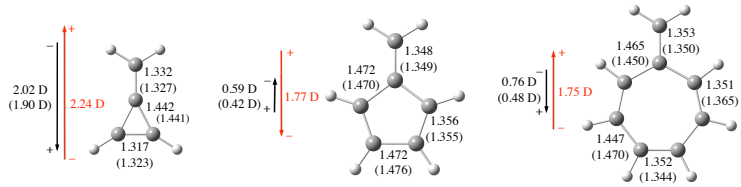

Figure 6.4: Calculated C−C bond lengths, and magnitudes and direction of the dipole moments for tria-, penta-, and heptafulvene in the ground state (OLYP/cc-pVTZ). The directions and magnitudes of the dipole moments, in the Franck-Condon $^1B_2$ state were calculated, using the excited state electron density from the results from TD-OLYP/cc-pVTZ//OLYP/cc-pVTZ calculations (in red). Values in parentheses are experimentally determined values. Triafulvene: Bond lengths and dipole moment from reference 109. Pentafulvene: Bond lengths and dipole moment from reference 110. Heptafulvene: Bond lengths and dipole moment from reference 111.

Computational results, performed by others, show that excitation of pentafulvene to the $^1B_2$ state is followed by ultrafast internal conversion to the ground state, through a conical intersection seam between the $^1B_2$, and ground state potential energy surfaces.[146–149] These results support that no fluorescence is observed from pentafulvene.[150] The lowest point on the $^1B_2$ state potential energy surface is located at the conical intersection seam and corresponds to a structure, where the exocyclic methylene group is perpendicular to the molecular plane.[144,147,149] Interestingly, for this excited state conformation of pentafulvene, the magnitude of the dipole moment is calculated to be 0.67 D, with a direction opposite to the ground state dipole moment.[144] Although the reversal of the dipole moment agrees with our results, their calculated value 0.67 D deviates much from the calculated value of 1.77 D presented here (Fig. 6.4). These values differ, as they are calculated using different methods and different geometries on the excited state potential energy surface and therefore different electron density distributions. To my knowledge, no investigations that focus on the $^1B_2$ excited state electron density distributions of tria- and heptafulvene exist.

The lowest excited triplet states (T_1 states), for the three fulvenes have been computationally investigated by Möllerstedt *et al.* It was found, that the dipolarity of the T_1 state fulvenes are opposite, when compared to the ground states.[116] Möllerstedt *et al.* describes these states as (π,π^*) states, but do not specify the symmetry of the T_1 states. However, calculations at the UOLYP/cc-pVTZ level have been performed here, and these results are consistent with those reported by Möllerstedt *et al.*, and show that the T_1 states have the same electron configuration as the $^1B_2$ states.

In summary, the singlet and triplet B_2 states for the three fulvenes appears, to be predominately influenced, by electron density distributions corresponding to the $4n\pi$-electron resonance structures, in contrast to the ground state, but in accordance with what was expected from the excited state π-electron counting rules.

Chapter 7

Manipulation of Excited State Energies of Pentafulvenes

The influence of the oppositely polarized π-electron density distributions, in the ground state and the lowest excited singlet and triplet B_2 states, serve as a convenient tool to control excited state energies of these compounds in a systematic way. Ottosson *et al.* presented the idea of tuning the energy gap between the lowest energy points on the ground and T_1 state potential energy surfaces (ΔE_{ST}) for pentafulvene, by strategic positioning of substituents.[120] In the work by Ottosson *et al.* it was illustrated, that substitution of electron donating groups in the exocyclic positions increase the ΔE_{ST}, in comparison to the parent pentafulvene, while electron withdrawing groups have the opposite effect. Here, it must be noted, that this tendency only applies, if the T_1 states of the substituted pentafulvenes correlate with the $^3B_2$ state of pentafulvene. The general idea is that substituents, which are positioned to provide a favorable interaction with the $(4n+2)\pi$-electron density distribution lower the ground state energy and increases the energy of the T_1 state. Conversely, if the substituents are positioned to provide a favorable interaction with the $4n\pi$-electron density distribution, the ground state energy will be increased and the energy of the T_1 state will be decreased. This idea is illustrated in Fig. 7.1, and through computational results, Ottosson *et al.* proved this tunability idea to be consistent, for a set of different exocyclically substituted pentafulvenes, and experimentally for a smaller selection of pentafulvenes. More recently, but yet unpublished, computational results performed in the group of Ottosson, have shown that substitution, on the cyclopentadienyl ring moiety of pentafulvene, also has a systematic effect on the ΔE_{ST} gap.[151] In this case, electron donating groups, substituted at the ring, decrease ΔE_{ST} in comparison to the parent pentafulvene, while electron withdrawing groups enhance ΔE_{ST} (Fig. 7.1, on the following page).

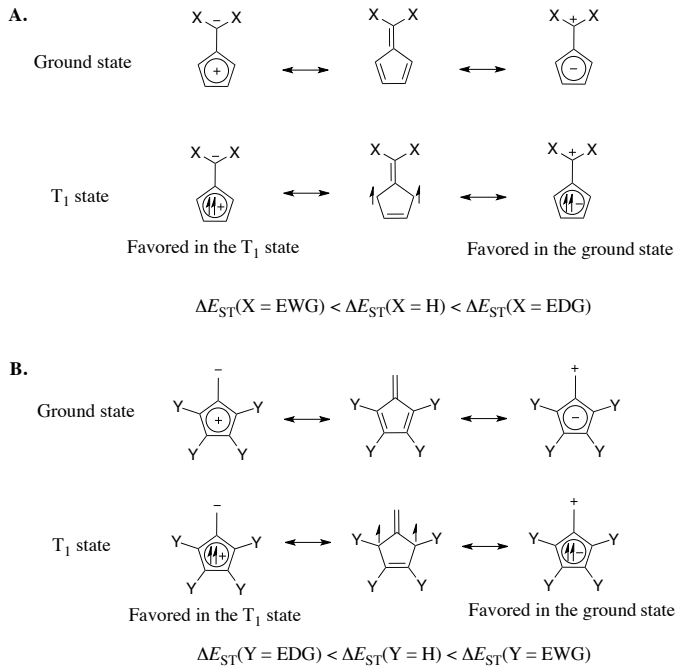

Figure 7.1: Illustration of the ΔE_{ST} tunability idea. Electron donating groups (EDG) increase the ΔE_{ST} in comparison to the parent pentafulvene, when placed in the exocyclic positions (**A**), and decrease ΔE_{ST} when placed at the ring (**B**). Electron withdrawing groups (EWG) decrease the ΔE_{ST} in comparison to pentafulvene, when placed in the exocyclic positions (**A**), and increase ΔE_{ST} when placed at the ring (**B**).

The idea was also proved to be consistent for a set heptafulvenes, with different exocyclic substituents. However, as it would be expected, the opposite tendency was found for heptafulvene derivatives, *i.e.* electron donating groups decrease ΔE_{ST}, and electron withdrawing groups increase ΔE_{ST}.[120]

7.1 Substituent Controlled Manipulation of the Pentafulvene Excited State Energy

As previously mentioned, the $^1B_2$ state of pentafulvene is also predominately influenced, by the $4n\pi$-electron density distribution, and one may therefore expect, that substituents also affect the energy difference between the ground and $^1B_2$ states, as shown in Fig. 7.1. To clarify this, a small series of differently substituted pentafulvenes were investigated computationally and experimentally, in order to examine the π-electron density distribution in their singlet excited states, and how substituents influence this. The results were published in *Physical Chemistry Chemical Physics* in 2011.[152]

The investigation involved a small series of symmetrically substituted pentafulvene derivatives. These were selected based, on their stability and their easy characterization by spectroscopy. Subsequent to publication an additional pentafulvene derivative was synthesized and investigated experimentally. In this presentation of the published results, the pentafulvenes will be divided into two classes, which are discussed separately. The compounds are shown in Fig. 7.2. The two classes are defined as the ground state stabilized pentafulvenes, **PF1**-**PF3**, and the excited state stabilized pentafulvenes, **PF4** and **PF5**. The ground state stabilized pentafulvenes possess substituents, which interact constructively with the $(4n+2)\pi$-electron density distribution. The excited state stabilized pentafulvenes possess substituents, which enhance the influence of the $4n\pi$-electron electron density distribution.

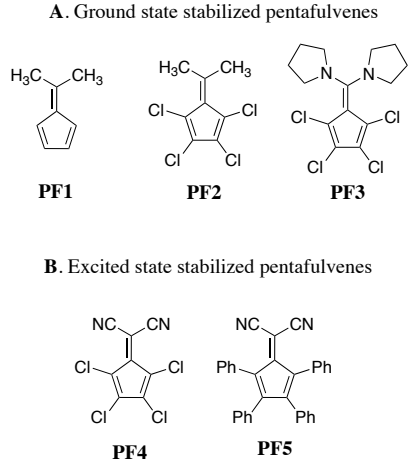

Figure 7.2: Illustration of the (**A**) ground state stabilized pentafulvenes **PF1**, **PF2**, and **PF3** and (**B**) the excited state stabilized pentafulvenes **PF4** and **PF5**.

7.1.1 The Excited State Dipolarity of the Ground State Stabilized Pentafulvenes

The absorption spectra of the ground state stabilized pentafulvenes, **PF1**-**PF3**, are shown in Fig. 7.3, and they agree with the spectra published earlier.[120] The corresponding spectral data are listed in Table 7.1. For comparison, the spectral data for the parent pentafulvene is also listed.[118,131] The compound **PF1** was purchased from Sigma-Aldrich and used as received. The compounds **PF2** and **PF3** were synthesized as previously described,[120] by the collaborating group of Henrik Ottosson at Uppsala University.

Similar spectral features appear, in the absorption spectra of **PF1**-**PF3**, as those described for pentafulvene, although the spectra of **PF1**-**PF3** are recorded in CH_3CN. To investigate whether states of similar electron configurations are involved in the transitions presented in Table 7.1, TD-DFT calculations were employed to calculate the vertical excitation energies, oscillator strengths, spatial symmetries, and major electron configurations of the excited states of **PF1**-**PF3**. The computational results are presented in Table 7.2. The π-orbitals involved in the calculated transitions are depicted in Fig. 7.4. Calculations, related to this investigation, were performed with the Gaussian 03 suite of programs.[153] The B3LYP/6-311+G(d) method was chosen for geometry optimizations and the TD-B3LYP/6-311+G(d) method for the calculation of vertical excitation energies. This choice was made, as the B3LYP/6-311+G(d,p) and TD-B3LYP/6-311+G(d,p) methods have proven to yield geometries and vertical excitation energies, in accordance with experimental data for fulvenic molecules.[154] However, due to the lack of hydrogen atoms in **PF4** (results are discussed in sec. 7.1.3), the polarization functions, at the hydrogen atoms, were excluded for all compounds, to achieve comparable results. The calculated structures were in good agreement with previously calculated structures.[120] All compounds were optimized to minima on the potential energy surfaces. This was verified through frequency calculations, revealing no imaginary frequencies. To simulate the non-specific solvent interactions of CH_3CN, the B3LYP/6-311+G(d) optimized structures were used for re-optimization, at the same level of theory, using the polarizable continuum model (PCM).[155–157] The PCM/B3LYP/6-311+G(d) optimized structures were then used to calculate vertical excitation energies, at the PCM/TD-B3LYP/6-311+G(d) level using non-equilibrium linear response solvation.

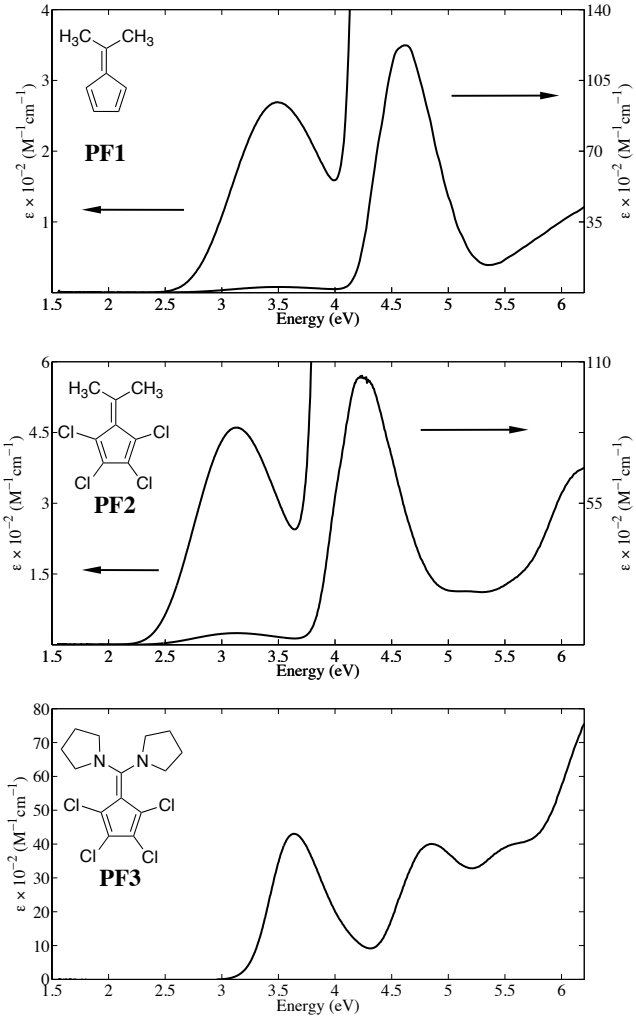

Figure 7.3: Absorption spectra of **PF1**, **PF2**, and **PF3** recorded in CH_3CN. The corresponding spectral data are listed in Table 7.1. Note the different scalings of the vertical axis.

Table 7.1: Experimentally determined excitation energies (ΔE_{exp}, in eV) for the two lowest energy transitions ($S_0 \rightarrow S_1$ and $S_0 \rightarrow S_2$, respectively) determined from the absorption maxima in the absorption spectra in Fig. 7.3 and the corresponding molar excitation coefficients (ϵ_{max}, in $M^{-1}cm^{-1}$) for the ground state stabilized pentafulvenes **PF1**, **PF2**, and **PF3**. Data for pentafulvene (**PF**) is also listed, but oscillator strengths (*f*) are listed, instead of ϵ_{max} and are presented in *italics*.

Compound	Transition	ΔE_{exp} (eV)	ϵ_{max} ($M^{-1}cm^{-1}$)
PF[a]	$S_0 \rightarrow S_1$	3.44	*0.008*
	$S_0 \rightarrow S_2$	5.28	*0.34*
PF1	$S_0 \rightarrow S_1$	3.50	260
	$S_0 \rightarrow S_2$	4.64	12150
PF2	$S_0 \rightarrow S_1$	3.14	460
	$S_0 \rightarrow S_2$	4.25	10270
PF3	$S_0 \rightarrow S_1$	3.63	4160
	$S_0 \rightarrow S_2$	4.84	4000

[a] Gas phase data from reference 114.

First, it should be emphasized, that the calculated vertical excitation energies in Table 7.2 are given by three significant figures, in contrast to the published work, where four significant figures are given.[152] It is my revised opinion, posterior of publication, that the accuracy of the calculated results, in the published work, does not allow for four significant figures. For consistency throughout this thesis energies are converted to eV, in contrast to the the published work, where energies are given in cm^{-1}. The calculated vertical excitation energies, for the transitions mentioned above, are overall in good agreement, with the experimental excitation energies for the $S_0 \rightarrow S_1$ and $S_0 \rightarrow S_2$ transition energies, for **PF1**-**P3** in Table 7.1. Although the calculated $S_0 \rightarrow S_2$ transition energy of **PF3** deviates by 25 % from the experimental value, the remaining calculated energies only deviate by less than 8 %, when compared to the experimental values. The calculated relative magnitudes, between the calculated oscillator strengths, also agree with the observed intensity relationship, between the $S_0 \rightarrow S_1$ and $S_0 \rightarrow S_2$ transitions. The $S_0 \rightarrow S_1$ and $S_0 \rightarrow S_2$ transitions for the three compounds are therefore assigned to involve the states, which were calculated to be involved in these transitions.

The calculated results in Table 7.2 show that the lowest energy transition, for all of the compounds, mainly involves promotion of an electron from the π-orbitals to π^*-orbitals, depicted in Fig. 7.4, on the following page. These correlate with the π-orbitals, involved in the $^1A_1 \rightarrow {}^1B_2$ transition of pentafulvene (Fig. 6.3).

To gain information, on how the electron density distributions of **PF1**-**PF3** change upon excitation to the S_1 states, solvatochromic studies of $S_0 \rightarrow S_1$ transitions for the fulvene derivatives were performed. The compounds appeared to be non-emissive, and therefore only solvatochromic studies of the absorption spectra were performed.

Table 7.2: Calculated vertical excitation energies (ΔE_{cal}, in eV) and the corresponding oscillator strengths (f) for **PF1**-**PF3**. The character of the transition (Character) is determined by inspection of the calculated orbitals that are mainly involved in the excitation. Point group symmetries of the compounds are given in parentheses, posterior the number of the compound.

Compound	ΔE_{cal} (ΔE_{exp})^{a,b}	Transition (Character)^c	f ($\times 10^3$)^a
PF1 (C_{2v})	3.38 (3.50)	$S_0(^1A_1) \rightarrow S_1(^1B_2)$ ($\pi \rightarrow \pi^*$, 87 %)	13.5
	4.76 (4.64)	$S_0(^1A_1) \rightarrow S_2(^1A_1)$ ($\pi_{-1} \rightarrow \pi^*$, 75 %)	600
PF2 (C_2)	2.96 (3.14)	$S_0(^1A) \rightarrow S_1(^1B)$ ($\pi \rightarrow \pi^*$, 87 %)	29.2
	4.28 (4.25)	$S_0(^1A) \rightarrow S_2(^1A)$ ($\pi_{-1} \rightarrow \pi^*$, 76 %)	550
PF3 (C_2)	3.39 (3.62)	$S_0(^1A) \rightarrow S_1(^1B)$ ($\pi \rightarrow \pi^*$, 95 %)	11.9
	3.64 (4.84)	$S_0(^1A) \rightarrow S_2(^1A)$ ($\pi_{-1} \rightarrow \pi^*$, 91 %)	223

[a] PCM/TD-B3LYP/6-311+G(d)//PCM/B3LYP/6-311+G(d). [b] Experimental determined values (ΔE_{exp}) from Table 7.1. [c] The contributions given in percentage are calculated from the two times the square of the largest expansion coefficient in the excited state Kohn-Sham solution. Configurations that contribute less than 10 % are not listed.

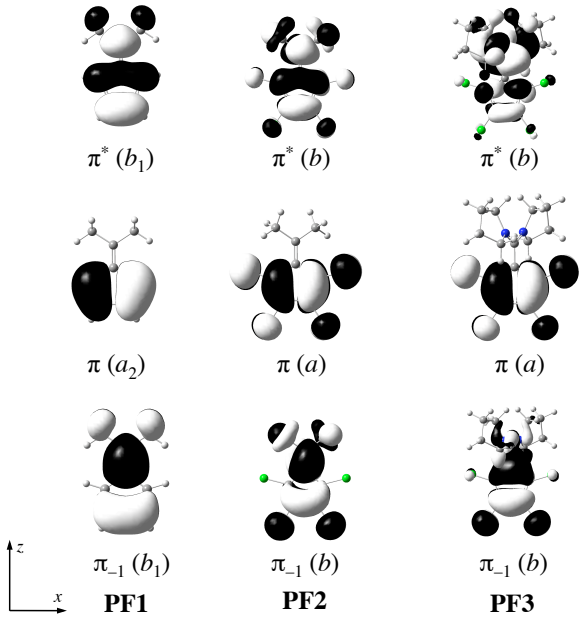

Figure 7.4: Calculated π-orbitals involved in the two lowest energy transitions for **PF1**, **PF2**, and **PF3** in a reaction field, simulating a CH_3CN dielectric continuum environment (PCM/TD-B3LYP/6-311+G(d)//PCM/B3LYP/6-311+G(d)).

Information about the difference in electron density distribution, between the ground and a Franck-Condon (FC) excited state can be obtained, by interpreting the solvatochromic behavior of the transition energy in the absorption spectrum, using a simple dielectric continuum model.[158–160]

For a given molecule the vertical transition energy, from a ground state (g) with a permanent dipole moment $\vec{\mu_g}$ to a FC excited state (e) with the permanent dipole moment $\vec{\mu_e}$ will change, in comparison to the gas phase as a consequence of the surrounding solvent environment. In the approach utilized, the solvent is described by its dielectric constant (ϵ) and refractive index (n). The molecule is characterized simply by its permanent dipole moment ($\vec{\mu_g}$) in a spherical cavity of radius a. The polar molecule generates an electric field, which the solvent molecules then respond to.

This "orientation reaction field" ($\vec{R}$) can be expressed as:

$$\vec{R} = \frac{(f(\epsilon) - f(n^2))}{4\pi\epsilon_0 a^3}\vec{\mu}_g \tag{7.1}$$

In which ϵ_0 is the vacuum permittivity, and $f(\epsilon)$ and $f(n^2)$ are Onsager's polarity functions defined as:[161]

$$f(\epsilon) = \frac{2(\epsilon - 1)}{2\epsilon + 1} \tag{7.2}$$

$$f(n^2) = \frac{2(n^2 - 1)}{2n^2 + 1} \tag{7.3}$$

It can be shown that the solvatochromic shift, of a vertical transition energy (ΔE_{ge}) relative to the gas phase transition energy, can be expressed as:[162]

$$\Delta E_{ge} = \Delta E^0_{ge} - \frac{1}{4\pi\epsilon_0 a^3}(\vec{\mu}_e(\vec{\mu}_e - \vec{\mu}_g)(f(\epsilon) - f(n^2)) - 2(\vec{\mu}_g^2 - \vec{\mu}_e^2)f(n^2)) \tag{7.4}$$

Here, ΔE^0_{ge} is the gas phase transition energy, and the second term describes energy arising from the dipole-dipole interactions between the molecule and the solvent. The third term describes the energy arising from dipole-induced dipole interactions.[158,159] The expression can be simplified, if it is assumed that the dipole-induced dipole interactions are constant in different solvents. As ΔE_{ge} is proportional to $f(\epsilon) - f(n^2)$ and the relative magnitude of the dipole moments in the ground and excited states, can be deduced from a plot of ΔE_{ge} as function of $f(\epsilon) - f(n^2)$. If such a plot shows reasonable linear dependencies, then the sign of the slope, α, of the linear regression expression is $\vec{\mu}_e(\vec{\mu}_e - \vec{\mu}_g)a^{-3}$. If the slope is negative, then the FC excited state dipole moment is larger than the ground state dipole moment, and *vice versa* if the slope is positive. This model is of course an extreme simplification, of the molecule's interaction with the solvent, and it does not take into account specific solvent interactions such as for example hydrogen bonding.

The energetic position of the $S_0 \rightarrow S_1$ absorption maximum (ΔE_{exp}), for **PF1**-**PF3** in solvents of different polarities, are shown in Table 7.3, on the following page. Solvent polarity is difficult to quantify, but different measures exist.[163,164] Solvent polarity is, in this thesis, chosen to be quantified by the E_T^N values, which are dimensionless normalized $E_T(30)$ values.[163] The closer an E_T^N value for a given solvent is to unity, the more polar the solvent is. The solvents in Table 7.3 were chosen as they span a rather broad variety in both E_T^N and $f(\epsilon)$–$f(n^2)$ values.

Table 7.3: Solvents and their $f(\epsilon)-f(n^2)$ and E_T^N values. The $S_0 \rightarrow S_1$ transition energies (ΔE_{exp}) for the compounds **PF1**, **PF2**, and **PF3** are given in eV.

Solvent	$f(\epsilon)-f(n^2)$*	$E_T^{N\dagger}$	ΔE_{exp}(**PF1**) (eV)	ΔE_{exp}(**PF2**) (eV)	ΔE_{exp}(**PF3**) (eV)
Cyclohexane	-4.13×10^{-3}	0.006	3.44	3.07	3.35
n-Heptane	4.55×10^{-4}	0.012	3.44	3.07	3.37
Toluene	2.65×10^{-2}	0.099	3.44	3.08	3.44
$CHCl_3$	0.293	0.259	3.46	3.08	3.47
Ethyl Acetate	0.390	0.228	3.47	3.11	3.53
THF	0.420	0.207	3.46	3.11	3.53
CH_2Cl_2	0.434	0.309	3.46	3.10	3.55
Acetone	0.568	0.355	3.48	3.12	3.59
CH_3CN	0.609	0.460	3.50	3.14	3.63

* n and ϵ values are taken from reference 164. † Data from reference 164.

In Fig. 7.5 the relationships between ΔE_{exp} and $f(\epsilon)-f(n^2)$ for **PF1**-**PF3** are shown. It is evident that a linear relationship exists for all three pentafulvene compounds. The linear regression analysis gave slopes, α, of 7.506×10^{-2} eV, 9.649×10^{-2} eV, and 0.3856 eV, for **PF1**, **PF2**, and **PF3**, respectively. The positive values of the slopes indicate, as mentioned, that the dipolar character, of all three compounds, is reduced in the FC excited state. To extract further information about the excited state dipole moments, for the three compounds, values of the ground state dipole moments are needed. Unfortunately, only the experimental value for **PF1** has been determined. The ground state dipole moments of **PF1**-**PF3** have previously been calculated as 1.99 D, 3.60 D, and 8.92 D, respectively, at the OLYP/TZ2P level for **PF1** and at the UOLYP/cc-pVTZ level for **PF2** and **PF3** by Ottosson *et al.*[120] These values were therefore chosen to be representative for the ground state dipole moments. However, for consistency the ground state dipole moment of **PF1** was also calculated at the OLYP/cc-pVTZ level, which resulted in a minor change from 1.99 D to 1.90 D. The calculated ground state dipole moments of **PF1**-**PF3** all have the same direction, with the negative charges located at the five-membered ring and the positive charge at the exocyclic C atom of the pentafulvene moiety. Spherical cavity radii, for **PF1**-**PF3** were calculated from the SCF electron density, for the OLYP/cc-pVTZ optimized structures. The values of the cavity radii (a) were calculated to be 4.31 Å, 4.91 Å and 5.37 Å for **PF1**, **PF2**, and **PF3**, respectively. The radii given are 0.5 Å larger than the computed radii following the recommendations in Gaussian 03.[165] From these values the S_1 state dipole moments (μ_e) can be determined to be -3.18 D, -1.48 D, and -1.80 D for **PF1**, **PF2**, **PF3**, respectively (Table 7.4), *i.e.*, indicating a reversal of the dipole moment direction in the FC S_1 state for all three compounds.

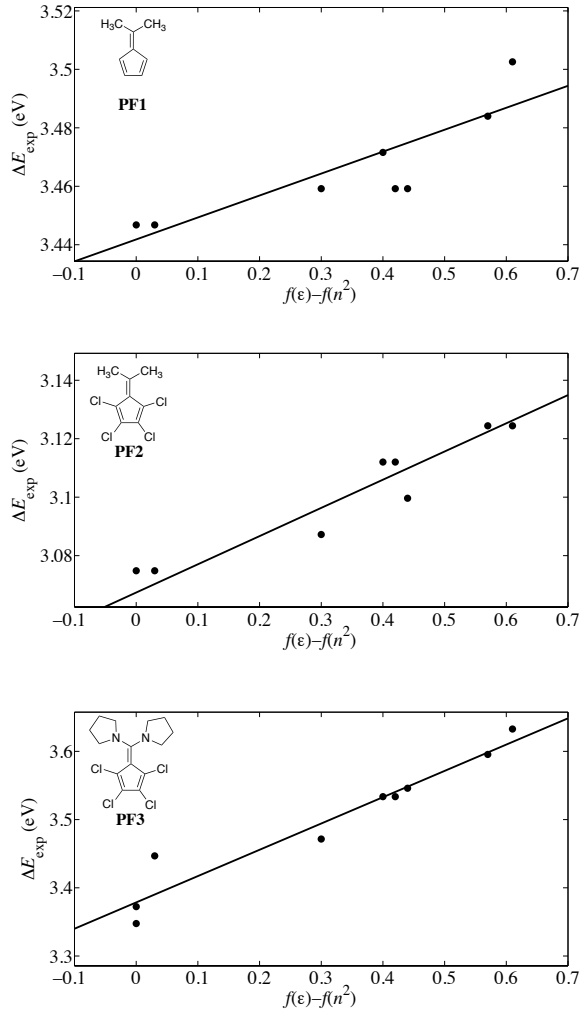

Figure 7.5: Plots of the measured $S_0 \rightarrow S_1$ transition energies (ΔE_{exp}) for **PF1**-**PF3** in the solvents listed in Table 7.3 as function of the solvents' corresponding $f(\epsilon)-f(n^2)$ values. Note the different scalings of the vertical axis. The squared correlation coefficients (R^2) for the linear regressions are 0.8457, 0.9208, and 0.9392 for **PF1**, **PF2**, and **PF3**, respectively.

Table 7.4: Slopes, (α) for the fitted linear regressions presented in Fig. 7.5 given in eV, calculated cavity radii (a) in Å, calculated ground dipole moments, (μ_g), in D and determined dipole moments in the FC S_1 state, (μ_e) in D.

Compound	α (eV)	a (Å)	μ_g (D)[i,j]	μ_e (D)[j]
PF1	605.4	4.31	1.90 (1.49)[k]	−3.17
PF2	778.2	4.91	3.60	−1.48
PF3	3110	5.37	8.92	−1.80

[i] (U)OLYP/cc-pVTZ. [j] A positive dipole moment implies a dipole directed from the ring system to the exocyclic position, and *vice versa* for a negative dipole moment. [k] Experimental value in parentheses from reference 131.

Consequently, the dipolar electron density distributions with a negative charge located at the exocyclic carbon atom, and a positive charge at the ring are important in the FC S_1 states of **PF1**-**PF3**, despite the presence of substituents that are not in position for a favorable interaction, with such an electron density distribution. The differences in electron density distributions are illustrated, with different resonance structures of **PF1**-**PF3** in Fig. 7.6.

It is appropriate to comment on the calculated dipole moments used in the interpretation. The calculated dipole moments reflect the dipolarity of the electron density distribution for the compounds in the gas phase. However, when the compounds are in solution their structures are different from the gas phase structures, as the molecule equilibrates differently, in the presence of the surrounding solvent. By virtue of this, the dipole moments of the pentafulvene derivatives are also different. This is evident from the dipole moments of **PF1**-**PF3** calculated for the optimized structures at the PCM/OLYP/cc-pVTZ level. In presence of a reaction field representing CH_3CN, the magnitudes of the ground state dipole moments are calculated to be 2.61, 5.10, and 14.88 D for **PF1**, **PF2**, and **PF3**, respectively. The direction of these dipole moments are unchanged, when compared to the gas phase. Using these values for the magnitude of the ground state dipole moments, the excited state dipole moments are evaluated to be −1.08, 1.51, and 8.45 D for **PF1**, **PF2**, and **PF3**, respectively. Thus, in CH_3CN the excited state dipole moments for **PF1**-**PF3** are reduced, but only reversed for **PF1**, in comparison to the ground state dipole moments. In this case the dipolar π-electron density distributions, shown for the FC S_1 state structures in Fig. 7.6, cannot be claimed to be important. However, the difference, in magnitudes between the ground and excited state dipole moments, remain independent of the surrounding environment. Although the magnitude and direction of the excited state dipole moments, would be different in CH_3CN, when solution compared to gas phase, this should be considered as an effect forced by the surrounding solvent.

Therefore, to evaluate what dipolar characters the molecule itself prefers in the ground and excited state, the gas phase values have to be compared.

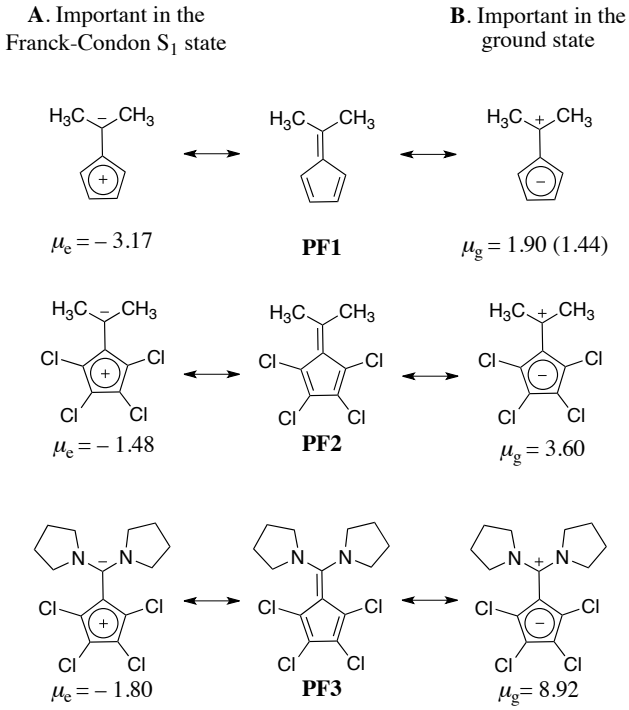

Figure 7.6: Illustration of the oppositely polarized electron density distributions that predominately influence the ground state compounds (**A**) and FC S_1 state compounds (**B**). The ground state dipole moments are OLYP/cc-pVTZ calculated values given in Table 7.4. The value in parentheses of **PF1** is the experimental determined value from reference 131.

7.1.2 Substituent Effects in the Ground State Stabilized Pentafulvenes

By comparing **PF2** to **PF1** (Fig. 7.6) it is seen that the incorporation of Cl atoms, on the 6,6-dimethylfulvene moiety, results in an enhancement of the ground state dipole moment. This is interpreted as a consequence of the σ-inductive electron withdrawing effect of the Cl atoms. In the following it is assumed that the σ-electrons have minor influence on the change in dipolarity of the compounds upon excitation, because the excitation to the S_1 state involves the π-electrons. Thus, mainly π-polarization effects are responsible for the change in the electron density distribution upon excitation. The magnitude of the difference, between the ground and FC S_1 state dipole moments ($|\Delta\mu_{ge}|$), follow the trend: $|\Delta\mu_{ge}(\mathbf{PF3})| > |\Delta\mu_{ge}(\mathbf{PF2})| \approx |\Delta\mu_{ge}(\mathbf{PF1})|$. As $|\Delta\mu_{ge}(\mathbf{PF1})|$ and $|\Delta\mu_{ge}(\mathbf{PF2})|$ are essentially equal (5.07 D *vs.* 5.08 D), it can be deduced that π-electron donation, of the lone-pair electrons on the Cl atoms (n(Cl)) to the ring, has minor effect on the the change in electron density distribution upon excitation. However, the excitation energy, for the $S_0 \rightarrow S_1$ transition of **PF2**, is less than that of **PF1**. This can be explained by an interaction between n(Cl) and the π-electrons in the fulvene moiety. As the ring moiety is electron abundant in the ground state, this interaction will destabilize the ground state, while stabilizing the FC S_1 state, as the ring is electron deficient in this state. This lowers the energy gap between the ground and the FC S_1 state in **PF2**, when compared to **PF1** as observed experimentally.

The incorporation of N atoms at the exocyclic positions (**PF3**) has a huge effect on the magnitude of the ground state dipole moment, when compared to **PF2** (8.92 D for **PF3** *vs.* 3.60 D for **PF2**). This further enhancement of the ground state dipole moment is assigned to be a consequence of the π-donating effect of the lone-pair electrons at the N atoms (n(N)) towards the ring, which act more stabilizing in the ground state than the methyl groups in **PF1** and **PF2**. However, when **PF3** is excited to the S_1 state, the dipolarity in electron density is reversed in the fulvene moiety, and π-donation towards the ring is no longer possible. Thus, the large change in dipole moment ($|\Delta\mu_{ge}(\mathbf{PF3})|$ = 10.72 D) is a consequence of the loss of the N atoms ability to donate π-electron density towards the ring in the S_1 state. Moreover, the interaction between n(N) and the negative charge distribution on the exocyclic C atom acts destabilizing on the S_1 state. Additionally, as for **PF2**, the interaction between the π-electrons and n(Cl) will stabilize the FC S_1 state and destabilize the ground state. However, as the n(Cl) and n(N) occupies 3p and 2p type orbitals, respectively, it can be argued that the interaction, between lone-pair electrons and the π-electrons at the fulvene moiety, is most pronounced for the N atoms. The excitation energy of **PF3** should therefore increase, when compared to **PF1** and **PF2**, and this is indeed observed. However, in *n*-heptane, cyclohexane, and toluene the excitation energy of **PF3** is similar to that of **PF1** (Table 7.1). The ground state of **PF3** is the most dipolar state; it is assumed that this state is influenced the most by solvent polarity.

Thus, in non-polar solvents the ground state of **PF3** is destabilized, resulting in excitation energies comparable with those of **PF1**. Similarly, the σ-inductive effect, of the substituents, influence the magnitude of the FC S_1 state dipole moments. Comparison of the magnitudes of the FC S_1 state dipole moments yield: $|\Delta\mu_{ge}$**(PF3)**$| > |\Delta\mu_{ge}$**(PF2)**$|$. For **PF1** there is no opposing σ-inductive effect present, in the FC S_1 state, and therefore $|\Delta\mu_{ge}$**(PF1)**$|$ achieves the largest value. The difference between $|\Delta\mu_{ge}$**(PF3)**$|$ and $|\Delta\mu_{ge}$**(PF2)**$|$ (1.80 D *vs.* 1.48 D) can be explained by the presence of nitrogen atoms in **PF3**, which are σ-withdrawing, and thus enhance the FC S_1 state dipole moment of **PF3** in comparison to **PF2**.

In conclusion, examination of the FC S_1 state dipole moments, of the three different ground state stabilized pentafulvenes using solvatochromy and calculated ground state dipole moments, revealed that the dipolarities of the compounds are reversed in this state. The oppositely polarized electron density distributions, which dominate the ground and S_1 states for **PF1**-**PF3** respectively, indicate that the cyclic delocalized arrangement of $4n$ π-electrons is favorable in the S_1 state. This supports that the π-electron counting rules for a ground state species are reversed in the S_1 state when compared to the ground state. The order of the $S_0 \rightarrow S_1$ transition energies shows that the substituents indeed affect these in a predictable way, in analogy to the manner that the ΔE_{ST}'s are affected (Fig. 7.1).

7.1.3 The Excited State Stabilized Pentafulvenes

The excited state stabilized pentafulvenes, **PF4** and **PF5**, were also investigated similarly to the ground state stabilized compounds. The two compounds were also prepared in the collaborating group of Ottosson, according to the procedures described in the litterature.[120,166] The absorption spectra recorded in CH_3CN are shown in Fig. 7.7 and the corresponding spectral data are presented in Table 7.5. The absorption spectrum for **PF4** and those of **PF1**-**PF3** are qualitatively similar, except for the splitting of the $S_0 \rightarrow S_2$ absorption envelope for **PF4**. The $S_0 \rightarrow S_1$ absorption envelope, in the spectrum for **PF5** overlaps with the $S_0 \rightarrow S_2$ absorption envelope, but the similarity between the $S_0 \rightarrow S_1$ absorption envelopes for **PF4** and **PF5** is obvious.

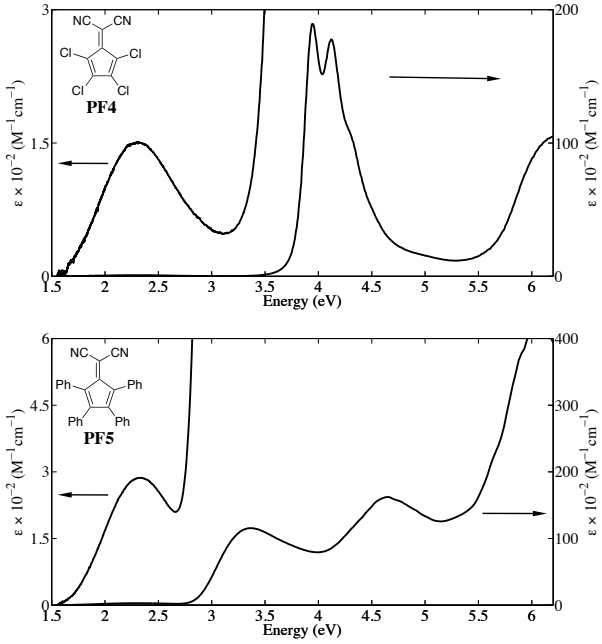

Figure 7.7: Absorption spectra of **PF4** and **PF5** recorded in CH_3CN. The corresponding spectral data are listed in Table 7.5.

Table 7.5: Experimental excitation energies (ΔE_{exp}, in eV) for the two lowest energy transitions ($S_0 \rightarrow S_1$ and $S_0 \rightarrow S_2$, respectively), determined from the absorption maxima in the absorption spectra in Fig. 7.7, and the corresponding molar excitation coefficients (ϵ_{max}, in $M^{-1}cm^{-1}$), for the excited state stabilized pentafulvenes **PF4** and **PF5**.

Compound	Transition	ΔE_{exp} (eV)	ϵ_{max} ($M^{-1}cm^{-1}$)
PF4	$S_0 \rightarrow S_1$	2.32	150
	$S_0 \rightarrow S_2$	3.94	18820
PF5	$S_0 \rightarrow S_1$	2.33	287
	$S_0 \rightarrow S_2$	3.36	11600

However, the remaining spectrum of **PF5** is not readily comparable to that of **PF4**. The $S_0 \rightarrow S_1$ transitions for **PF4** and **PF5** are essentially located at the same energy, and on basis of the qualitative similarities to the $S_0 \rightarrow S_1$ transitions for **PF1**-**PF3** the $S_0 \rightarrow S_1$ transitions for **PF4** and **PF5** are assigned to be transitions that correlate with those of **PF1**-**PF3**. This assignment is supported by computational results. The two lowest excitation energies were calculated, for **PF4**, as described for the ground state stabilized pentafulvenes, and the results are shown in Table 7.6, on the following page.

Table 7.6: Calculated vertical excitation energies (ΔE_{cal}, in eV), and the corresponding oscillator strengths (f) for **PF4**. The experimental determined energies (ΔE_{exp}, in eV), are given in parentheses. The character of the transition (Character) is determined from inspection of the calculated orbitals that are mostly involved in the excitation. The compound is calculated within the C_{2v} point group.

Compound	ΔE_{cal} (ΔE_{exp}) (eV)[a]	Transition (Character)[b]	f ($\times 10^3$)[a]
PF4 (C_{2v})	1.75 (2.32)	$^1A_1 \rightarrow {}^1B_2$ ($\pi \rightarrow \pi^*$, 86 %)	1.7
	3.61 (3.94)	$^1A_1 \rightarrow {}^1A_1$ ($\pi_{-1} \rightarrow \pi^*$, 75 %)	643

[a] PCM/TD-B3LYP/6-311+G(d)//PCM/B3LYP/6-311+G(d). [b] The contribution percentage given are calculated from the two times the square of the value for the largest expansion coefficient in the excited state Kohn-Sham solution. Configurations that contribute less than 10 % are not listed.

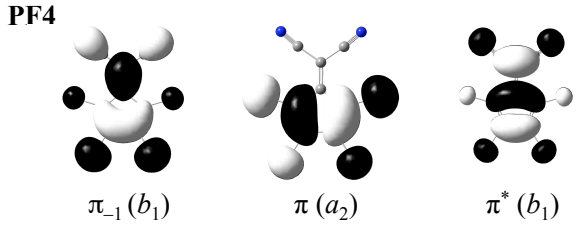

Figure 7.8: Calculated π-orbitals involved in the two lowest energy transitions for **PF4** in a CH_3CN environment (PCM/TD-B3LYP/6-311+G(d)//PCM/B3LYP/6-311+G(d)).

Calculation of the excitation energies of **PF5** has not yet been performed. The calculated excitation energies for **PF4** are lower in energy, as compared to the experimental values, but it is noteworthy that the calculated oscillator strengths, reflect the intensity relationship found in the experimental spectrum. The π-orbitals involved in the two calculated transitions are shown in Fig. 7.8, and they clearly correlate with those of the **PF** and **PF1**-**PF3**. Interestingly, the $S_0 \rightarrow S_1$ transition energies are significantly lower, for **PF4** and **PF5** than those of **PF1**-**PF3**.

In light of the results in the last section, this finding supports that the $4n\pi$-electron density distribution is important in the S_1 state. The π-electron withdrawing cyano groups stabilize this π-electron density distribution, and this would lower the excitation energies for **PF4** and **PF5**, as compared to **PF1**-**PF3**, and this is indeed what is observed. However, **PF4** and **PF5** do not exhibit any correlation, between the excitation energy and $f(\epsilon)-f(n^2)$. This indicates that the dielectric continuum model is not sufficient to describe the interactions between solvent and the excited state stabilized pentafulvenes. Therefore, information about the direction and magnitude of the dipole moment, in the S_1 state of **P4** and **P5**, cannot be extracted from the experimental results, by the use of this model. This may indicate that specific interactions with the solvents are present for these two compounds, but it could also be that the change in magnitude of the dipole moment upon excitation is not significant enough, to be probed by this methodology. This could very well be the case, as according to results from B3LYP/6-311+G(d), calculations, the ground state dipole moments, of **PF4** and **PF5**, are 4.28 D and 6.99 D, respectively, directed by a negative charge at the exocyclic region and a positive charge in the pentadienyl ring. Thus, the two compounds already possess π-electron density distributions, which are favorable in the S_1 state, and presumably only a minor change in dipolarity will occur when the compounds are excited to their S_1 states.

For future investigations it would be desirable to synthesize 6,6-dicyanopentafulvenes with π-electron donating groups at the cyclopentadienyl ring moiety, to reveal if the $^1A_1 \rightarrow {}^1B_2$ transition energy can be lowered even further. For example, the synthetic strategy similar to that of Potter and Hughes could be adopted,[167] as shown in the proposed synthetic scheme in Fig. 7.9. This approach is a convenient strategy, as a variety of symmetrical 1,3-diphenylacetone derivatives can be prepared by the recent reported method by Romer.[168]

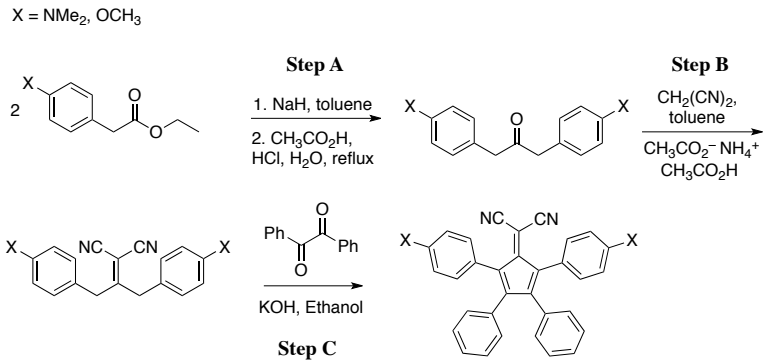

Figure 7.9: Proposed synthetic scheme of 6,6-dicyanopentafulvenes with π-electron donating substituents in the 1,4-positions. **Step A**. Adopted from reference 168. **Step B**. Adopted from reference 169. **Step C**. Adopted from reference 167.

Recently, the excited state stabilized pentafulvene **PF6**, shown in Fig. 7.10, was prepared by Jayamurugan *et al.*[170,171] The absorption spectrum of **PF6** shows that this compound absorbs at even lower energies (< 1.24 eV), than **PF4** and **PF5**. However, in this compound it is unknown whether the pentafulvene moiety acts as the main chromophore, and thus, whether the low energy absorption property is a result of energetic tuning of a transition, which correlates to the $^1A_1 \rightarrow {}^1B_2$ transition of the parent penta-fulvene, or if the chromophore is different. Thus, this compound deserves further attention in future investigations.

PF6

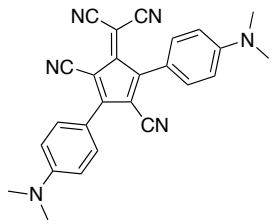

Figure 7.10: Illustration of **PF6** recently prepared by Jayamurugan *et al.*

Chapter 8

Expanding the Concept of Substituent Controlled Manipulation of Excited State Energies

It is interesting to investigate, whether the idea of substituent controlled manipulation of excited state energies, can be applied for compounds, closely related to pentafulvene. One class of compounds, which are interesting in this context, are compounds, that can be viewed, as camouflaged fluorenyl cation and anions, as shown in Fig. 8.1.

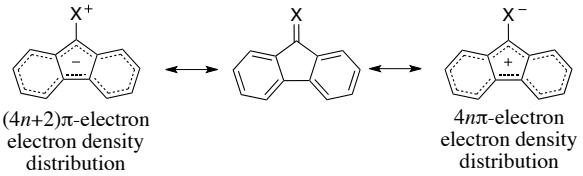

Figure 8.1: Illustration of a compound, that may be influenced by either a $(4n+2)\pi$-electron density distribution (left) or a $4n\pi$-electron density distribution (right) depending on the nature of X.

Why such compounds are particularly interesting, is the contrasting reactivity of 9*H*-fluorene derivatives, in the ground and excited states, observed by Wan and co-workers. As mentioned in Chapter 4, the experimental results illustrate that; the formation of the fluorenyl cation, which possess a cyclic array of $4n$ π-electrons, is favorable in the excited state; the formation of the fluorenyl anion, with a $4n$+2 π-electron array, is favorable in the ground state.

In this chapter focus is put on dibenzofused derivatives of 6,6-dicyanopentafulvene (**1**). The parent dibenzofused derivative of **1** is 2-(9*H*-fluoren-9-ylidene)malononitrile (**2**), which is shown in Fig. 8.2. It is interesting whether **2** is influenced by the $4n\pi$-electron density distributions, as shown Fig. 8.1, in the excited state. It is also interesting how the compounds relate to the pentafulvene derivative, **2**, Fig. 8.2. An investigation of this aspect is presented in this chapter.

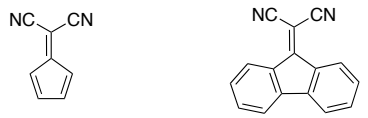

1 **2**

Figure 8.2: Structures of 6,6-dicyanopentafulvene (**1**), and (**2**) 2-(9*H*-fluoren-9-ylidene)malononitrile.

8.1 The Ground State Structures

As a starting point, the ground state structures of **1** and **2** are examined computationally. The B3LYP functional was used for the optimization, as in sec. 7.1, but the 6-311G(d,p) basis set was used instead of the 6-311+G(d) basis set. The smaller basis set was chosen, to reduce the computational costs associated with the larger size of the derivatives of **2**, which were also investigated (*vide infra*). Both compounds were optimized to C_{2v} symmetric conformations, and the calculated bond lengths and dipole moment magnitudes are shown in Fig. 8.3 The calculated dipole moments of **1** and **2** are in reasonable agreement with those calculated earlier at the CASSCF and OLYP/6-311G(d) levels.[120] However, although the two compounds have the same polarity in the ground state, inspection of the calculated bond lengths reveal that their π-electron density distributions appear to be different. The calculated bond lengths of **1** suggest, that this compound possess localized double bonds, and should be interpreted as an electron deficient diene. Such an interpretation is reasonable, as this compounds has been reported to undergo dimerization, in a Diels-Alder reaction, rapidly.[166] The calculated bond lengths, in the two benzene rings of **2**, are all fairly similar, to the bond lengths of benzene (1.399 Å). In comparison, the bond connecting the two benzene rings is significantly longer (1.470 Å).

The ground state structure of **2** can therefore be interpreted, as the resonance structure that represents two separate benzene rings, connected by a single C−C bond, and through the dicyanomethylene group, as shown in Fig. 8.4. This interpretation, is supported by the fact, that **2** is a stable crystalline compound, that does not dimerize.

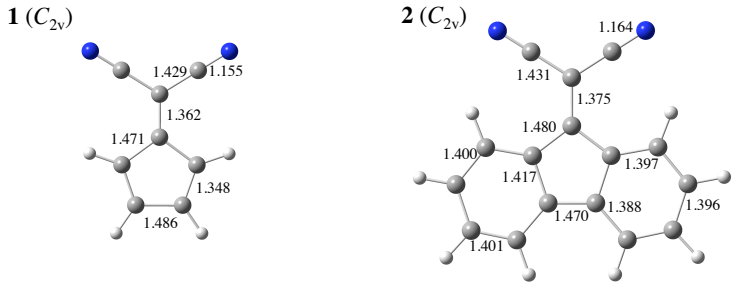

Figure 8.3: Calculated C−C bond lengths (in Å) and dipole moment magnitudes (in D) for **1** and **2** in their ground state equilibrium conformations (B3LYP/6-311G(d,p)). C−H bond lengths are omitted for clarity. Point group symmetries are given in parentheses. The dipole moments are directed, from a negative charge in the exocyclic region, to a positive charge in the ring moieties. The values in parentheses for **1** and **2**, are values calculated, at the CASSCF level and OLYP/6-311G(d) levels, respectively. [120]

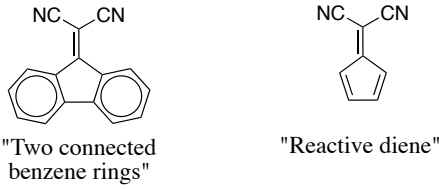

Figure 8.4: Resonance structures, which best represent, how the π-electron densities are distributed in the ground state compounds in Fig. 8.2.

8.2 The Correlation between the Excited States

Although the calculated results suggest that the compounds are influenced, by quite different π-electron density distributions in the ground state, it appears that the compounds are closely related in their excited states, when taking into account computational results presented later in this section. The vertical excitation energies, for two compounds, were calculated using the TD-DFT methodology. In this chapter, all calculations were performed, with the more recent Gaussian 09 suite of programs.[172] The vertical excitation energies, to the two lowest excited singlet states, were calculated for the optimized structures of **1** and **2**. This was done using the TD-M062X/6-311+G(2d,p) method. The M062X functional was chosen, as it has shown to perform well, for calculations of excitation energies.[173] The 6-311+G(2d,p) basis set was chosen, as it shows excellent performance for calculations of excited state energies, in comparison to the 6-311++G(3df,3pd) basis set.[174] The computational results are listed in Table 8.1.

Table 8.1: Calculated lowest two vertical excitation energies (ΔE_{cal}, in eV) for **1** and **2**, and the corresponding oscillator strengths (f). Character of the transition, and the contribution from this type of excitation, is given in parentheses.

Compound	Transition (Character)[b]	ΔE_{cal} (eV)[a]	f ($\times 10^3$)[a]
1 (C_{2v})	$S_0(^1A_1) \rightarrow S_1(^1B_2)$ ($\pi_{\mathbf{1}} \rightarrow \pi^*_{\mathbf{1}}$, 100 %)	2.62	0.8
	$S_0(^1A_1) \rightarrow S_2(^1A_1)$ ($\pi_{\mathbf{1}}$' $\rightarrow \pi^*_{\mathbf{1}}$, 99 %)	4.47	561
2 (C_{2v})	$S_0(^1A_1) \rightarrow S_1(^1B_2)$ ($\pi_{\mathbf{2}} \rightarrow \pi^*_{\mathbf{2}}$, 97 %)	2.96	0.4
	$S_0(^1A_1) \rightarrow S_2(^1A_1)$ ($\pi_{\mathbf{2}}$' $\rightarrow \pi^*_{\mathbf{2}}$, 97 %)	3.89	444

[a] TD-M062X/6-311+G(2d,p)//B3LYP/6-311G(d,p). [b] The contribution percentages are calculated, as two times the square of the value of the largest expansion coefficient for the excited state Kohn-Sham solution.

The character of the transitions are assigned, by inspection of the orbitals, which are mainly involved in the excitations. These orbitals are depicted in Fig. 8.5, and the π-orbitals involved in the $^1A_1 \rightarrow {}^1B_2$ transitions, correlate to those involved in the lowest energy $^1A_1 \rightarrow {}^1B_2$ transition for pentafulvene (Fig. 6.3). Thus, it is reasonable to expect that the $^1B_2$ excited state of **2**, may have similarities to the $^1B_2$ state of pentafulvene.

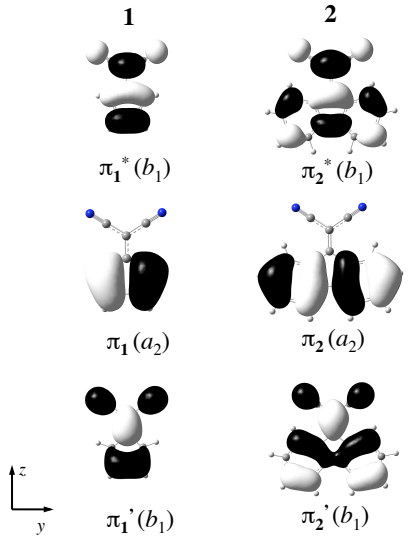

Figure 8.5: Orbitals, which are calculated to be directly involved in the $S_0 \rightarrow S_1$ and $S_0 \rightarrow S_2$ transitions of **1** and **2** given in Table 8.1. Orbital symmetries are given in parentheses.

Despite the close similarity between the $^1A_1 \rightarrow {}^1B_2$ transitions, for **1** and **2**, it is at this point unknown, how the π-electron density distributions, should be interpreted in the $^1B_2$ state of **2**, and how it compares to the $^1B_2$ states of the pentafulvene compound. To investigate this aspect, the structure of **2** was optimized, at the TD-B3LYP/6-311G(d,p) level, along the potential energy surface of the $^1B_2$ state with the ($\pi_{\mathbf{2}}$,$\pi_{\mathbf{2}}^*$) electron configuration. The method for this calculation was chosen, as it allows for comparison, with the ground state optimized structure.

The computational results showed that the $^1B_2$ state structure of **2** remains planar, and C_{2v} symmetric in this state. The excited state optimized structure was verified, as a true minimum energy structure through a numerically frequency calculation, at the same level of theory. The calculated bond lengths, for the $^1B_2$ state equilibrium structure of **2**, are shown in Fig. 8.6. The calculated bond lengths, for the ground state compound, are shown for comparison.

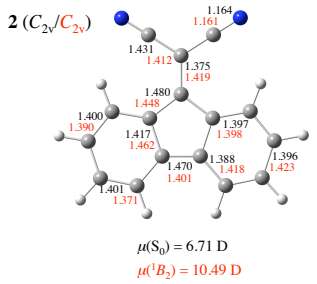

Figure 8.6: Calculated C−C bond lengths (in Å) of **2** for the ground state (black) and the $^1B_2$ state (red) equilibrium geometries ((TD)-B3LYP/6-311G(d,p)). C−H bond lengths are not given for clarity. The calculated magnitudes of the dipole moments, in the ground state ($\mu(S_0)$, black) and $^1B_2$ state ($\mu(^1B_2)$, red) are also given.

Attempts to optimize **1** along the $^1B_2$ excited state surfaces, gave unreliable results, using the TD-DFT approach. The results suggested, that several configurations contributed significantly, in the description of the optimized excited state structure. Thus, optimization of this compound, in the $^1B_2$ state, requires multiconfigurational methods, but such computations were not performed. However, based on the discussion in Chapter 6, it is assumed that the $4n\pi$-electron density distribution is important in the $^1B_2$ states, of the pentafulvene. This is supported, by comparing the calculated magnitude difference, between the dipole moments in the ground and FC $^1B_2$ states of **1**. The magnitude of the dipole moment in the FC $^1B_2$ states of **1** was deduced, from an electron population analysis, using the excited state electron density obtained from a calculation, of the vertical $^1B_2$ excited state energy, at the TD-B3LYP/6-311G(d,p)//B3LYP/6-311G(d,p) level. The magnitude of the dipole moment was calculated to be enhanced, from 5.10 D to 12.1 D, when **1** is excited from the ground state to the FC $^1B_2$ state.

When comparing the calculated ground and $^1B_2$ state structure of **2**, in Fig. 8.6, the largest bond length differences are found, in the five-membered ring moiety. When the structure of **2** is optimized, to the $^1B_2$ state electron density distribution, the fused C−C bonds are elongated by 0.045 Å, and the two C−C bonds connecting the two benzene rings, through the dicyanomethylene group, are shortened by 0.032 Å. The C−C bond, that directly connects the two benzene rings is shortened by 0.069 Å. Furthermore, the exocyclic C−C(CN)$_2$ bond, is elongated by 0.044 Å. The magnitudes of the dipole moment, in the $^1B_2$ state optimized structure, was calculated to be 10.49 D. This indicates, that the dipolarity of this compound is larger in the $^1B_2$ state, when compared to the ground state.

The calculated bond lengths and dipole moment, for the $^1B_2$ state structure of **2** suggests, that **2** can be interpreted, to a significant extent, as the resonance structure that represent a negative charge located, at the exocyclic region, and a positive charge delocalized over the external periphery of the fluorene moiety, as shown in Fig. 8.7. Thus, in analogy to the pentafulvene derivatives, the $^1B_2$ state of **2** appears, to be influenced by a $4n\pi$-electron density distribution.

The calculated results suggest, that **2** is indeed an interesting compound, in the context of substituent controlled manipulation of excited state energies, but in order to examine, whether the calculated results can be trusted, **2** were investigated experimentally.

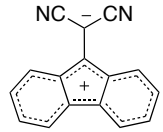

Figure 8.7: Proposed resonance structure representation of **2**, which best describes the π-electron density distribution in the $^1B_2$ state.

8.3 The Absorption Spectrum of 2

In order to investigate **2** experimentally, the absorption spectrum of this compound was recorded in toluene, CH_2Cl_2, and CH_3CN solutions. The spectra are shown in Fig. 8.8.

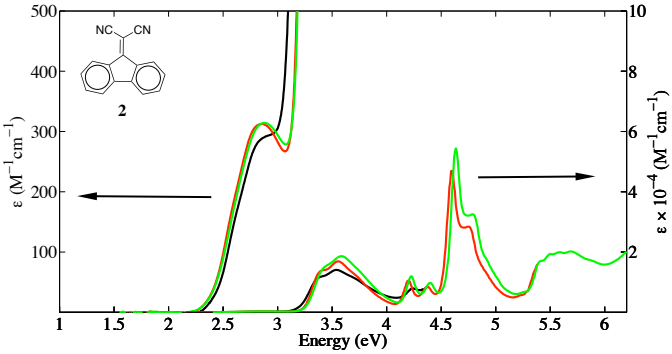

Figure 8.8: Absorption spectra of **2** in toluene (black), CH_2Cl_2 (red), and CH_3CN (green) solutions.

The compound was synthesized by PhD student Christian Dahlstrand from Uppsala University, according to the procedure previously described by Wang and Cheng.[175] The three solvents were chosen, because the compound was soluble herein, and due to the different polarity of the solvents, according to their $f(\epsilon)-f(n^2)$ and E_T^N values (values can be found in Table 7.3). The spectra of **2**, agrees with the spectral data, previously reported by Mukherjee.[176] However, for the purpose of the present investigation, only the lowest energy part of the spectrum, will be focused on. As illustrated in the previous chapters, calculations serve, as a handy tool to examine the character, of the transitions that correspond to the bands in an absorption spectrum. In order to compare the experimental absorption data of **2**, with calculated data, the structure of **2** was calculated, at the PCM/B3LYP/6-311G(d,p)) level, simulating non-specific dipolar solvent interactions with toluene, CH_2Cl_2, and CH_3CN, respectively. The two lowest excitation energies were then calculated, for the equilibrium structures of **2**, at the PCM/TD-M062X/6-311+G(2d,p) level. The results are presented in Table 8.2.

In general, the calculated results in Table 8.2, are in excellent agreement with the experimental spectra. The calculated values for the lowest energy transitions are slightly lower (2.87, 2.81, and 2.80 eV in toluene, CH_2Cl_2, and CH_3CN, respectively), but very close to the experimental transition energies (2.90, 2.86, and 2.87 eV in toluene, CH_2Cl_2, and CH_3CN, respectively), which are deduced from the maximum of the lowest energy absorption envelope, which appears as a shoulder to the remaining spectrum. The observed low intensity of this absorption band (ϵ_{max} = 300, 310, and 310 $M^{-1}cm^{-1}$ in toluene, CH_2Cl_2, and CH_3CN, respectively) supports the low oscillator strengths, which were calculated for this transition. In the absorption spectrum, the second lowest energy absorption envelope is broad, moderately intense, and has a maximum intensity, at 3.54, 3.55, and 3.58 eV in toluene, CH_2Cl_2, and CH_3CN, respectively.

Table 8.2: Calculated lowest two vertical excitation energies (ΔE_{cal}, in eV) for **2**, and the corresponding oscillator strengths (f). The character of the transition (Character), and the contribution of this type of excitation is given in parentheses.

Compound	Solvent	Transition (Character)[b]	ΔE_{cal} (eV)[a]	f ($\times 10^3$)[a]
2 (C_{2v})	Toluene	$S_0(^1A_1) \rightarrow S_1(^1B_2)$ ($\pi_{\mathbf{2}} \rightarrow \pi^*_{\mathbf{2}}$, 97 %)	2.87 (2.90)[c]	0.3
		$S_0(^1A_1) \rightarrow S_2(^1A_1)$ ($\pi_{\mathbf{2}}' \rightarrow \pi^*_{\mathbf{2}}$, 98 %)	3.75 (3.54)[c]	578.2
	CH_2Cl_2	$S_0(^1A_1) \rightarrow S_1(^1B_2)$ ($\pi_{\mathbf{2}} \rightarrow \pi^*_{\mathbf{2}}$, 97 %)	2.81 (2.86)[c]	0.1
		$S_0(^1A_1) \rightarrow S_2(^1A_1)$ ($\pi_{\mathbf{2}}' \rightarrow \pi^*_{\mathbf{2}}$, 98 %)	3.74 (3.55)[c]	558.2
	CH_3CN	$S_0(^1A_1) \rightarrow S_1(^1B_2)$ ($\pi_{\mathbf{2}} \rightarrow \pi^*_{\mathbf{2}}$, 97 %)	2.80 (2.87)[c]	0.1
		$S_0(^1A_1) \rightarrow S_2(^1A_1)$ ($\pi_{\mathbf{2}}' \rightarrow \pi^*_{\mathbf{2}}$, 98 %)	3.75 (3.58)[c]	538.4

[a] PCM/TD-M062X/6-311+G(2d,p)//PCM/B3LYP/6-311G(d,p). [b] The contribution percentages are calculated, as two times the square of the value of the largest expansion coefficient for the excited state Kohn-Sham solution. [c] Values in parentheses are experimental values, determined at the maximum intensity of the corresponding the lowest energy absorption envelopes in Fig. 8.8.

Inspection of this absorption envelope reveals, that it consists of three peaks with equidistant energy difference in-between these (approximately 0.14 eV or 1100 cm^{-1}). The calculated results predict the $S_0 \rightarrow S_2$ transition, to be located at 3.75, 3.74, and 3.75 eV in toluene, CH_2Cl_2, and CH_3CN, respectively. These values are less than 6 %, from the energy of the maximum intensity, for the second lowest energy absorption envelope. The calculated oscillator strength were supported by the intensity of this absorption envelope. Thus, in summary, the two lowest energy absorption envelopes, in the spectrum of **2** are assigned, to be the $^1A_1 \rightarrow {}^1B_2$ and $^1A_1 \rightarrow {}^1A_1$ transitions, by virtue of the correlation between the calculated and experimental data.

The calculated results show that the $^1A_1 \rightarrow {}^1B_2$ transition energy becomes lower, when the polarity of the surrounding solvent increases. This is supported, by a small bathochromic shift, observed for the lowest energy absorption band, when the spectra in toluene and CH_3CN are compared (2.90 eV in toluene *vs.* 2.87 eV in acetonitrile). This energetic shift supports that **2** is more dipolar in the $^1B_2$ states, when compared to the ground states (*vide supra*). In summary, the calculated results are comparable to experimental data, and can therefore by used, as a handy tool to investigate, how substituents affect the $^1A_1 \rightarrow {}^1B_2$ transition of **2**, which is the purpose of the next section.

8.4 The Impact of Substituents on the Absorption Properties

This section concerns an investigation, of disubstituted derivatives of **2**. The purpose is to deduce, how substituents affect the $^1A_1 \rightarrow {}^1B_2$ transition energy. Only symmetrical disubstituted derivatives are considered, and substituent effects in the 1-, 4-, 5-, and 8-positions of **2**, are not considered to avoid the complicating influence of steric interactions. The derivatives of **2**, which were subject to computational investigation, are shown in Fig. 8.9. The nitro- and dimethylamino groups were chosen, to represent π-electron withdrawing and donating groups, respectively. For clarity, the computational results are discussed in two separate subsections, concerning the nitro- and dimethylamino group derivatives. The computational methods described in the previous section were also applied here.

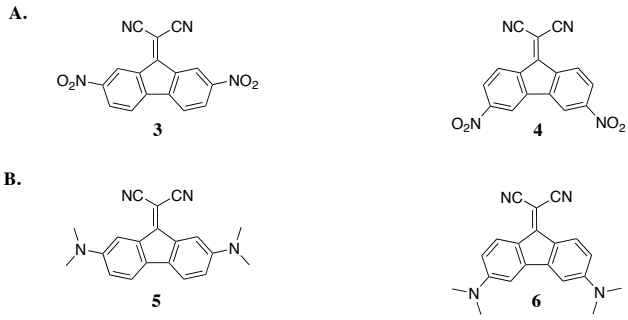

Figure 8.9: Substituted derivatives of **2**, which were subject to a computational investigation, of how substituents affect the $^1A_1 \rightarrow {}^1B_2$ transition energy of **2**. **A**. Compound **3** and **4** are substituted with the π-electron withdrawing nitro groups, in the 2- and 7-positions and 3- and 6-positions, respectively. **B**: Compound **5** and **6** are substituted with the π-electron donating dimethylamino groups, in the 2- and 7-positions and the 3- and 6-positions, respectively.

8.4.1 The Impact of the Nitro Groups

In this section, the computational results regarding the derivatives **3** and **4** are presented. The ground state structures of **3** and **4**, were optimized in vacuum, and in the presence of reaction fields, corresponding to toluene, CH_2Cl_2, and CH_3CN. In all environments, the compounds were calculated to be planar C_{2v} symmetric structures. The calculated bond lengths, for **3** and **4** in vacuum are shown in Fig. 8.10, on the following page.

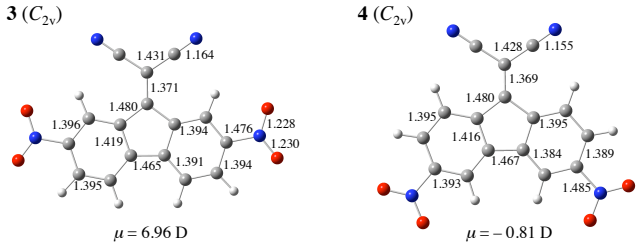

Figure 8.10: Calculated bond lengths (in Å) for the ground state structures of **3** and **4** (B3LYP/6-311G(d,p)). C−H bond lengths are not shown for clarity. The magnitudes of the dipole moments (in D) are also given for each compound. A positive value indicates that the dipole moment is directed from a negative charge at the exocyclic region to a positive charge in the fluorene moiety, and *vice versa* for a negative value.

The calculated bond lengths, in the "**2** moiety", of **3** and **4** are fairly similar, to those calculated for **2**. It is therefore argued, that the ground state structures, of these compounds, can be interpreted, as the resonance structures shown in Fig. 8.11, similarly to **2**. The calculated magnitudes of the dipole moment of **3** (6.96 D), is comparable to the magnitude calculated for **2** (6.71 D). On the other hand, the dipole moment, of **4**, is calculated to have opposite direction, and to have a much smaller magnitude, in comparison to **2** and **3**. This can be explained, by the presence of π-electron withdrawing and σ-inductive effects, from the nitro groups, which are opposite, and stronger than the π-electron withdrawing and σ-inductive effects from the dicyanomethylene group, for this compound.

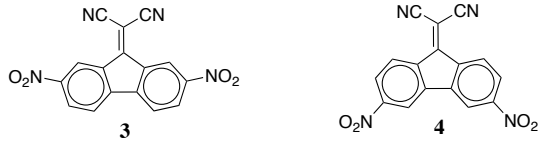

Figure 8.11: Important resonance structures for the description of **3** and **4** in the ground states, based on the calculated bond lengths in Fig. 8.10.

The calculated structures of **3** and **4**, were used to calculate the $S_0 \rightarrow S_1$ and $S_0 \rightarrow S_2$ transitions, in four different environments, and the results are listed in Table 8.3 for **3** and in Table 8.4 for **4**. The orbitals calculated to be mainly involved, in these excitations, are depicted in Fig. 8.12. The orbitals correlate with the π-orbitals and π^*-orbitals of **2** (Fig. 8.5). It is therefore meaningful to compare the transitions, for the nitro group containing derivatives, and the parent compound.

Table 8.3: Calculated lowest two vertical excitation energies (ΔE_{cal}, in eV), and the corresponding oscillator strengths (f) for **3**. The character of the transition (Character) is listed, with the weighting of the electron configuration given percentage in parentheses. The orbitals involved in the calculated transitions are depicted in Fig. 8.12.

Compound	Environment[a]	Transition (Character)[c]	ΔE_{cal} (eV)[b]	f ($\times 10^3$)[b]
3 (C_{2v})	Vacuum	$S_0(^1A_1) \rightarrow S_1(^1B_2)$ ($\pi_{\mathbf{3}} \rightarrow \pi^*_{\mathbf{3}}$, 96 %)	3.25	20.0
		$S_0(^1A_1) \rightarrow S_2(^1B_2)$ ($n \rightarrow \pi^*$)[d]	3.89	0
	Toluene	$S_0(^1A_1) \rightarrow S_1(^1B_2)$ ($\pi_{\mathbf{3}} \rightarrow \pi^*_{\mathbf{3}}$, 96 %)	3.19	30.2
		$S_0(^1A_1) \rightarrow S_2(^1A_1)$ ($\pi_{\mathbf{3}}$' $\rightarrow \pi^*_{\mathbf{3}}$, 97 %)	3.68	514.5
	CH_2Cl_2	$S_0(^1A_1) \rightarrow S_1(^1B_2)$ ($\pi_{\mathbf{3}} \rightarrow \pi^*_{\mathbf{3}}$, 96 %)	3.15	30.5
		$S_0(^1A_1) \rightarrow S_2(^1A_1)$ ($\pi_{\mathbf{3}}$' $\rightarrow \pi^*_{\mathbf{3}}$, 97 %)	3.63	504.3
	CH_3CN	$S_0(^1A_1) \rightarrow S_1(^1B_2)$ ($\pi_{\mathbf{3}} \rightarrow \pi^*_{\mathbf{3}}$, 96 %)	3.14	29.5
		$S_0(^1A_1) \rightarrow S_2(^1A_1)$ ($\pi_{\mathbf{3}}$' $\rightarrow \pi^*_{\mathbf{3}}$, 97 %)	3.61	475.9

[a] Calculations involving solvation have been performed by inclusion of the PCM model. [b] TD-M062X/6-311+G(2d,p)//B3LYP/6-311G(d,p). [c] The contribution percentages are calculated, as two times the square of the value of the largest expansion coefficient for the excited state Kohn-Sham solution. [d] This excitation involves three different excitations of $n \rightarrow \pi^*$ character, contributing with 40, 31, and 11 %. The orbitals are not shown, as they are not important in the context of the chapter.

Table 8.4: Calculated lowest two vertical excitation energies (ΔE_{cal}, in eV), and the corresponding oscillator strengths (f) for **4**. The character of the transition (Character) is listed, with the weighting of the electron configuration given in percentage in parentheses. The orbitals involved in the calculated transitions are depicted in Fig. 8.12.

Compound	Environment[a]	Transition (Character)[c]	ΔE_{cal} (eV)[b]	f ($\times 10^3$)[b]
4 (C_{2v})	Vacuum	$S_0(^1A_1) \rightarrow S_1(^1B_2)$ ($\pi_{\mathbf{4}} \rightarrow \pi^*_{\mathbf{4}}$, 97 %)	3.01	0
		$S_0(^1A_1) \rightarrow S_2(^1A_1)$ ($\pi_{\mathbf{4}}$' $\rightarrow \pi^*_{\mathbf{4}}$, 96 %)	3.81	487.5
	Toluene	$S_0(^1A_1) \rightarrow S_1(^1B_2)$ ($\pi_{\mathbf{4}} \rightarrow \pi^*_{\mathbf{4}}$, 97 %)	2.95	0.1
		$S_0(^1A_1) \rightarrow S_2(^1A_1)$ ($\pi_{\mathbf{4}}$' $\rightarrow \pi^*_{\mathbf{4}}$, 97 %)	3.68	634.3
	CH_2Cl_2	$S_0(^1A_1) \rightarrow S_1(^1B_2)$ ($\pi_{\mathbf{4}} \rightarrow \pi^*_{\mathbf{4}}$, 97 %)	2.91	0
		$S_0(^1A_1) \rightarrow S_2(^1A_1)$ ($\pi_{\mathbf{4}}$' $\rightarrow \pi^*_{\mathbf{4}}$, 96 %)	3.68	614.1
	CH_3CN	$S_0(^1A_1) \rightarrow S_1(^1B_2)$ ($\pi_{\mathbf{4}} \rightarrow \pi^*_{\mathbf{4}}$, 97 %)	2.90	0
		$S_0(^1A_1) \rightarrow S_2(^1A_1)$ ($\pi_{\mathbf{4}}$' $\rightarrow \pi^*_{\mathbf{4}}$, 96 %)	3.69	591.8

[a] Calculations involving solvation have been performed by inclusion of the PCM model. [b] TD-M062X/6-311+G(2d,p)//B3LYP/6-311G(d,p). [c] The contribution percentages are calculated, as two times the square of the value of the largest expansion coefficient for the excited state Kohn-Sham solution.

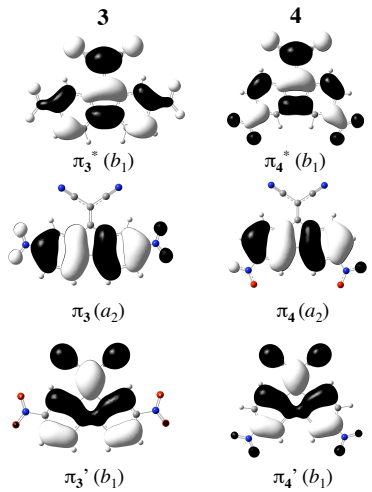

Figure 8.12: Orbitals involved in the calculated transitions for **3** and **4** (TD-M062X/6-311+G(2d,p)//B3LYP/6-311G(d,p)). Orbital symmetries are given in parentheses. The compounds are calculated within the C_{2v} point group.

In similarity to **2**, the $S_0 \rightarrow S_1$ transitions, for **3** and **4**, are $^1A_1 \rightarrow {}^1B_2$ transitions, while the $S_0 \rightarrow S_2$ transitions are $^1A_1 \rightarrow {}^1A_1$ transitions. With regard to the $^1A_1 \rightarrow {}^1B_2$ transition energies, they are calculated to decrease, as the polarity of the surrounding medium is increased. When the environment is changed from gas phase to CH_3CN, the $^1A_1 \rightarrow {}^1B_2$ transition energies decrease by 0.11 eV, for both **3** and **4**. Thus, the dipolarity of the two compounds, also becomes larger in the FC $^1B_2$ state, in comparison to the ground state. However, it must be remembered, that **3** and **4** have opposite dipolarity in their ground states. Therefore the electron density is shifted differently, when they are excited to the $^1B_2$ state. Inspection of the π- and π^*-orbitals, in Fig. 8.12, for **3** and **4** can be used to reveal, how the π-electron density in these compounds is reorganized, when excited to the $^1B_2$ state. For both compounds, the π-electron density is reorganized within the fluorene moiety, and is enhanced in the exocyclic region, and at the nitro groups. This electron density reorganization, will effectively enhance the dipolarity of **3**, in the $^1B_2$ state, which is in accordance, with the calculated bathochromic shift of the $^1A_1 \rightarrow {}^1B_2$ transition energy. In **4**, the π-electron reorganization is guided in opposite directions. In order for this to be consistent, with the calculated bathochromic shift of the $^1A_1 \rightarrow {}^1B_2$ transition, the electron density must be reorganized, predominantly towards the nitro groups in the FC $^1B_2$ state, in order to obtain a higher dipolarity in this state, when comparing to the ground state. Based on the inspection of the π-orbitals, it is proposed that the resonance structure representations, shown for **3** and **4**, in Fig. 8.13 are important, for the description of the two compounds in the FC $^1B_2$ state.

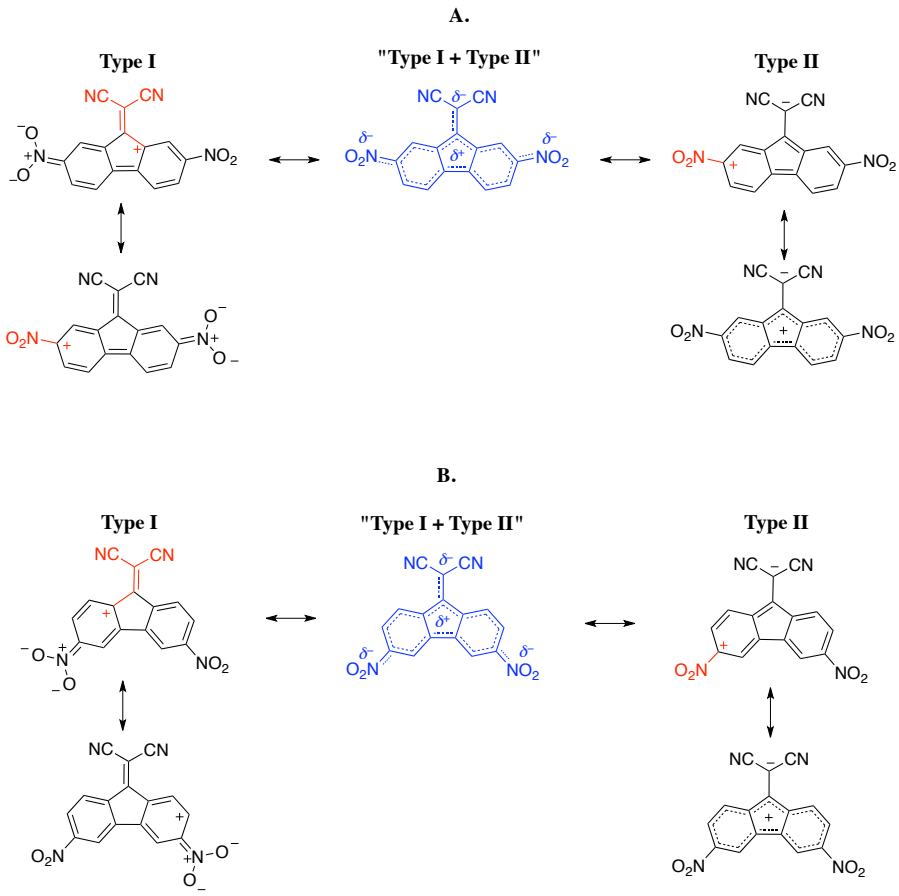

Figure 8.13: Different resonance structure representations, which are significantly contributing to the description of the **3** (Part **A**) and **4** (Part **B**).

The resonance structures, shown in blue should be regarded, as a combination of the resonance structures, which are donated **Type I** and **Type II** resonance structures, in Fig. 8.13. The **Type I** resonance structures, illustrates the aspects associated with reorganization of π-electron density, between the fluorene moiety and the nitro groups. The **Type II** resonance structures, illustrates the aspects associated with reorganization of π-electron density, between the fluorene moiety and the exocyclic dicyanomethylene group. These resonance structure interpretations can be used to rationalize, how the nitro groups affect the $^1A_1 \rightarrow {}^1B_2$ transition energies, in comparison to **2**.

The $^1A_1 \rightarrow {}^1B_2$ transition energies for, **3** and **4**, are calculated to be larger in comparison, to **2**. In the gas phase the energies are 3.01 eV and 3.25 eV, for **3** and **4**, respectively, which should be compared to 2.96 eV for **2**. In the excited state of **3** (**A**, in Fig. 8.13), both the **Type I** and **Type II** resonance structure representations, can be argued to be important, as they will both effectively contribute, to an enhanced dipolarity of **3** in the FC $^1B_2$ state, in comparison to the ground state. For **3**, both the **Type I** and **Type II** resonance structures are connected with unfavorable electron interactions between the substituents, which are marked in red, in Fig. 8.13. Thus, in the FC $^1B_2$ state of **3**, the adoption of the dipolar π-electron density distribution, are less favorable in comparison to **2**, and consequently the $^1A_1 \rightarrow {}^1B_2$ transition energy for **3**, is higher than for **2**.

Interestingly, the $^1A_1 \rightarrow {}^1B_2$ transition energy of **4** is closer to the corresponding energy of **2**. This can also be rationalized, by inspection of the resonance structures in **B**, Fig. 8.13. The **Type I** resonance structures, for **4**, are only associated, with the unfavorable interaction, between the nitro groups and the dicyanomethylene group, and not between the two nitro groups, as in the case for the **Type I** resonance structures for **3**. For **4**, the unfavorable interaction, between the nitro groups, is present in the **Type II** resonance forms of **4**. However, in the FC $^1B_2$ state of **4**, the **Type I** resonance structure has predominant influence, in comparison to the **Type II** resonance structure, as the calculated bathochromic shift, indicate that **4** has enhanced dipolarity upon excitation. From this, it can be argued, that the nitro groups affect the $^1A_1 \rightarrow {}^1B_2$ transition energy, when positioned in the 2- and 7-positions.

8.4.2 The Impact of the Dimethylamino Groups

The ground state structure of **5**, was calculated to be C_2 symmetric, with the dimethylamino groups being slightly pyramidal. In contrast, the structure **6**, was optimized to a C_{2v} symmetric minimum structure, suggesting that the dimethylamino groups are planar. This indicates, that the N atoms, in the 2,7-dimethylamino substituted compounds have more sp^3 hybridized character, compared to the 3,6-disubstituted compounds, which are sp^2 hybridized. The calculated bond lengths, for the dimethylamino substituted derivates of **2** are shown in Fig. 8.14, on the following page. The calculated bond lengths, follow the same trends calculated for **2** in the ground state. However, the bond length alternation in the benzene rings, of these compounds, are more pronounced, in comparison to **2** and the nitro group substituted derivatives. This suggests, that the dimethylamino groups disturb the π-electron density in the benzene rings to a larger extent in the ground state, in comparison to the nitro groups. From the trends in the bond lengths, in Fig. 8.14, it is proposed that these compounds can also be viewed, as the resonance structures shown in Fig. 8.7.

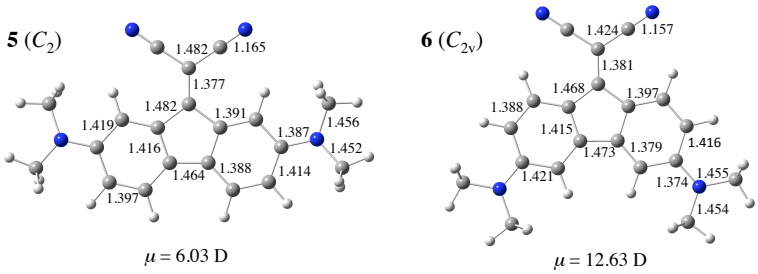

Figure 8.14: Calculated bond lengths for the ground state structures of **5** and **6** (B3LYP/6-311G(d,p)). C−H bond lengths are not given for clarity. The magnitude of the dipole moments are given for each compound.

The dipole moment of **6** was calculated to be 12.63 D, which is nearly twice the magnitude calculated for **2**. In contrast, **5** was calculated to possess a dipole moment of 6.03 D, which is more comparable to **2**, in the ground state. The larger dipolarity of **6**, in the ground state can be explained, as an effect of the dimethylamino groups, being in *para*-positions to the dicyanomethylene group. This allows cooperative interaction, between the two groups, through the benzene moiety, as shown in Fig. 8.15.

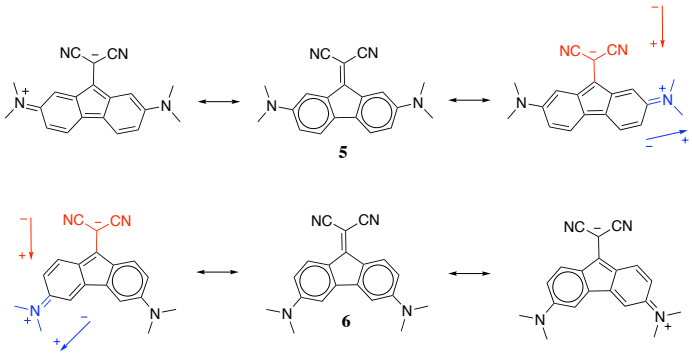

Figure 8.15: Illustration of the the dipolar resonance structures for **5** and **6**, which contribute to the larger dipolarity of **6**, compared to **2** and **5**. The local bond dipoles are illustrated, in red for the C−C(CN)$_2$ bond, and in blue for the C–N(CH$_3$)$_2$ bond.

This interaction effectively enhances, the dipolarity of **6**, compared to **2**. As illustrated in Fig. 8.15, this interaction can also be argued, to be present in **5**. However, for **5**, this interaction affects the dipolarity of the compound less, as the local bond dipoles, shown in red and blue in Fig. 8.15, have opposite directions in contrast to **6**, where they possess the same direction. The calculated excitation energies are listed in Table 8.5 and Table 8.6 for **5** and **6**, respectively, on the following two pages.
The orbitals involved in these transitions are shown in Fig. 8.16. The lowest energy transitions of **5** and **6** were calculated to be $^1A \rightarrow {}^1B$ and $^1A_1 \rightarrow {}^1B_2$ transitions both of $\pi \rightarrow \pi^*$ character. Although, the π- and π^*-orbitals involved in the $^1A \rightarrow {}^1B$ transition for **6**, in Fig. 8.16, correlate with those of **2**, it should be noted that the nodal planes, of the $\pi_{\mathbf{6}}$ orbital, are differently located, when compared to those of the $\pi_{\mathbf{2}}$ orbital. This may question the similarity between the $\pi_{\mathbf{6}}$ and the $\pi_{\mathbf{2}}$ orbitals, and thus, the similarity between the $^1A_1 \rightarrow {}^1B_2$ transitions for **2** and **6**. However, positions of nodal planes, in the molecular orbitals, changes when substituents are introduced,[160] but in my personal opinion, this difference is rather large, and comparisons between the $^1A_1 \rightarrow {}^1B_2$ transitions, for **2** and **6** should be done with caution.

Table 8.5: Calculated lowest two vertical excitation energies (ΔE_{cal}, in eV), and the corresponding oscillator strengths (f) for **5**. The character of the transitions (Character) are listed, with the weighting of the electron configuration given in percentage, in parentheses. The orbitals involved in the calculated transitions are shown in Fig. 8.16.

Compound	Environment[a]	Transition (Character)[c]	ΔE_{cal} (eV)[b]	f ($\times 10^3$)[b]
5 (C_2)	Vacuum	$S_0(^1A) \rightarrow S_1(^1B)$ ($\pi_5 \rightarrow \pi_5^*$, 98 %)	1.85	8.9
		$S_0(^1A) \rightarrow S_2(^1A)$ (π_5" $\rightarrow \pi_5^*$, 92 %)	3.35	5.8
	Toluene	$S_0(^1A) \rightarrow S_1(^1B)$ ($\pi_5 \rightarrow \pi_5^*$, 98 %)	1.73	10.8
		$S_0(^1A) \rightarrow S_2(^1A)$ (π_5" $\rightarrow \pi_5^*$, 94 %)	3.22	14.2
	CH_2Cl_2	$S_0(^1A) \rightarrow S_1(^1B)$ ($\pi_5 \rightarrow \pi_5^*$, 98 %)	1.65	9.8
		$S_0(^1A) \rightarrow S_2(^1A)$ (π_5" $\rightarrow \pi_5^*$, 95 %)	3.13	15.1
	CH_3CN	$S_0(^1A) \rightarrow S_1(^1B)$ ($\pi_5 \rightarrow \pi_5^*$, 98 %)	1.63	9.2
		$S_0(^1A) \rightarrow S_2(^1A)$ (π_5" $\rightarrow \pi_5^*$, 95 %)	3.11	14.4

[a] Calculations involving solvation have been performed using the PCM model [b] TD-M062X/6-311+G(2d,p)//B3LYP/6-311G(d,p). [c] The contribution percentages are calculated, as two times the square of the value of the largest expansion coefficient for the excited state Kohn-Sham solution.

Table 8.6: Calculated lowest two vertical excitation energies (ΔE_{cal}, in eV), and the corresponding oscillator strengths (f) for **6**. The character of the transitions (Character) are listed, with the weighting of the electron configuration given in percent, in parentheses. The orbitals involved in the calculated transitions are shown in Fig. 8.16.

Compound	Environment[a]	Transition (Character)[c]	ΔE_{cal} (eV)[b]	f ($\times 10^3$)[b]
6 (C_{2v})	Vacuum	$S_0(^1A_1) \rightarrow S_1(^1B_2)$ ($\pi_{\mathbf{6}} \rightarrow \pi^*_{\mathbf{6}}$, 93 %)	2.68	95.8
		$S_0(^1A_1) \rightarrow S_2(^1A_1)$ ($\pi_{\mathbf{6}}$' $\rightarrow \pi^*_{\mathbf{6}}$, 98 %)	3.41	701.1
	Toluene	$S_0(^1A_1) \rightarrow S_1(^1B_2)$ ($\pi_{\mathbf{6}} \rightarrow \pi^*_{\mathbf{6}}$, 94 %)	2.51	160.9
		$S_0(^1A_1) \rightarrow S_2(^1A_1)$ ($\pi_{\mathbf{6}}$' $\rightarrow \pi^*_{\mathbf{6}}$, 98 %)	3.18	894.4
	CH_2Cl_2	$S_0(^1A_1) \rightarrow S_1(^1B_2)$ ($\pi_{\mathbf{6}} \rightarrow \pi^*_{\mathbf{6}}$, 94 %)	2.41	181.1
		$S_0(^1A_1) \rightarrow S_2(^1A_1)$ $\pi_{\mathbf{6}}$' $\rightarrow \pi^*_{\mathbf{6}}$, 98 %)	3.14	880
	CH_3CN	$S_0(^1A_1) \rightarrow S_1(^1B_2)$ $\pi_{\mathbf{6}} \rightarrow \pi^*_{\mathbf{6}}$, 94 %)	2.38	183.4
		$S_0(^1A_1) \rightarrow S_2(^1A_1)$ $\pi_{\mathbf{6}}$' $\rightarrow \pi^*_{\mathbf{6}}$, 98 %)	3.14	857.3

[a] Calculations involving solvation have been performed using the PCM model. [b] TD-M062X/6-311+G(2d,p)//B3LYP/6-311G(d,p) [c] The contribution percentages are calculated, as two times the square of the value of the largest expansion coefficient for the excited state Kohn-Sham solution.

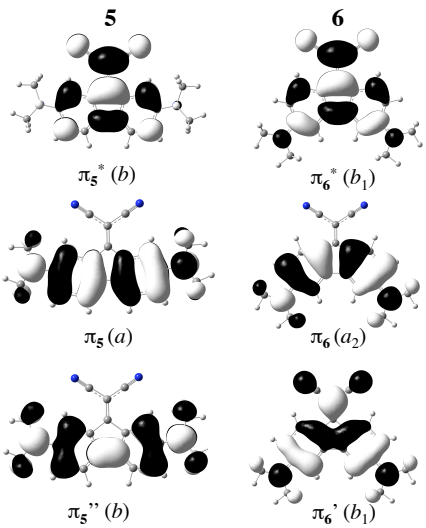

Figure 8.16: Orbitals involved in the two lowest calculated energy transitions for **5** and **6** (TD-M062X/6-311+G(2d,p)//B3LYP/6-311G(d,p)). Orbital symmetries are given in parentheses. The compound **5** is calculated within the C_2 point group, and **6** within the C_{2v} point group.

Interestingly, the ^1A ($^1A_1$) $\rightarrow$ ^1B ($^1B_2$) transitions energies for **5** (**6**) are calculated, to be significantly lower, than the $^1A_1 \rightarrow {}^1B_2$ transition energy of **2**, in all the investigated environments. In analogy, to what was calculated, for the dinitro-substituted derivatives, substitution of **2** in the 2- and 7-positions in comparison to substitution in the 3- and 6-positions, tend to have the largest effect on the $^1A_1 \rightarrow {}^1B_2$ energy, when compared to **2**.

Inspection of the π- and π^*-orbitals in Fig. 8.16 reveals the similarity between the π- and π^*-orbitals for **5**, **6**, and **2**. It is therefore argued that the π-electron density is also reorganized within the ring, and is enhanced in the exocyclic dicyanomethylene region, when **5** and **6** are excited to their ^1B ($^1B_2$) states. Moreover, for **5**, the $\pi_{\mathbf{5}}$-orbital possess significant lobes, at the dimethylamino groups, but these lobes are much smaller in the $\pi^*_{\mathbf{5}}$-orbital. Thus, the π-electron density is effectively reduced, at the dimethylamino groups, when **5** is excited to the ^1B state. In collection, the π-electron density can be considered as being effectively reorganized from the fluorene moiety and the dimethylamino groups to the exocyclic dicyanomethylene group. For **6**, the lobes at the dimethylamino groups are present, in both the $\pi_{\mathbf{6}}$-orbital and the $\pi^*_{\mathbf{6}}$-orbital, and it is therefore argued, that the relocation of π-electron density from the dimethylamino group, to the exocyclic dicyanomethylene group is less pronounced, when **6** is excited to the $^1B_2$ state.

In Fig. 8.17, the important resonance structures are shown, for the description of the π-electron density distribution in the FC ^1B state of **5**, and the FC $^1B_2$ state of **6**, based on the inspection of the π-orbitals in Fig. 8.16. These resonance structures are associated with favorable interactions between the dimethylamino groups, and the dicyanomethylene groups in both **5** and **6**. Thus, this explains why the $S_0 \rightarrow S_1$ excitation energies for **5** and **6** are lower, in comparison to the corresponding $^1A_1 \rightarrow {}^1B_2$ transition energy of **2**. According to this, the dipolarity of **5** and **6** should be larger in the FC ^1B and $^1B_2$ states, respectively. Indeed, this can be argued to be the case, as the transitions energies are lowered by 0.22 eV and 0.30 eV for **5** and **6**, respectively, when going from vacuum to a CH_3CN environment.

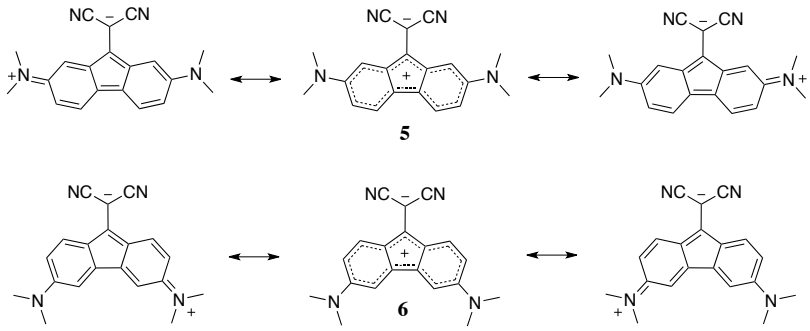

Figure 8.17: Important resonance structures for the description of the π-electron density distribution on the FC ^1B state of **5**, and the FC $^1B_2$ state of **6**.

In summary, the results of the computational investigation show, that incorporation of substituents, indeed affects the $^1A_1 \rightarrow {}^1B_2$ transition energy of **2**. The presence, of the π-electron withdrawing nitro-groups in the 2- and 7-positions, and the 3- and 6-positions of **2**, tend to increase the $^1A_1 \rightarrow {}^1B_2$ transition energy, in comparison to **2**. On the other hand, incorporation of π-electron donating dimethylamino groups, in the 2- and 7-positions and in the 3- and 6-positions of **2** is calculated to lower the $^1A_1 \rightarrow {}^1B_2$ transition energies significantly. These substituent effects illustrate that dibenzofused derivatives of pentafulvene can also be controlled in a systematic fashion, by utilizing the knowledge on how π-electrons prefer to be delocalized in the excited states. In order to investigate whether the concept applies for the compounds in reality, the 2,7-disubstituted derivatives were investigated experimentally. Presently, the 3,7-disubstituted derivatives have not been prepared, and can therefore not be investigated experimentally.

8.5 The Absorption Spectra of the 2,7-Disubstituted Compounds

The 2,7-disubstituted compounds, **3** and **5**, were prepared by PhD student Christian Dahlstrand from Uppsala University. The absorption spectra of **3** and **5**, were recorded in toluene, CH_2Cl_2, and CH_3CN, and are shown in Fig. 8.18. The absorption spectra, of **2**, are shown again in Fig. 8.18, for comparison.

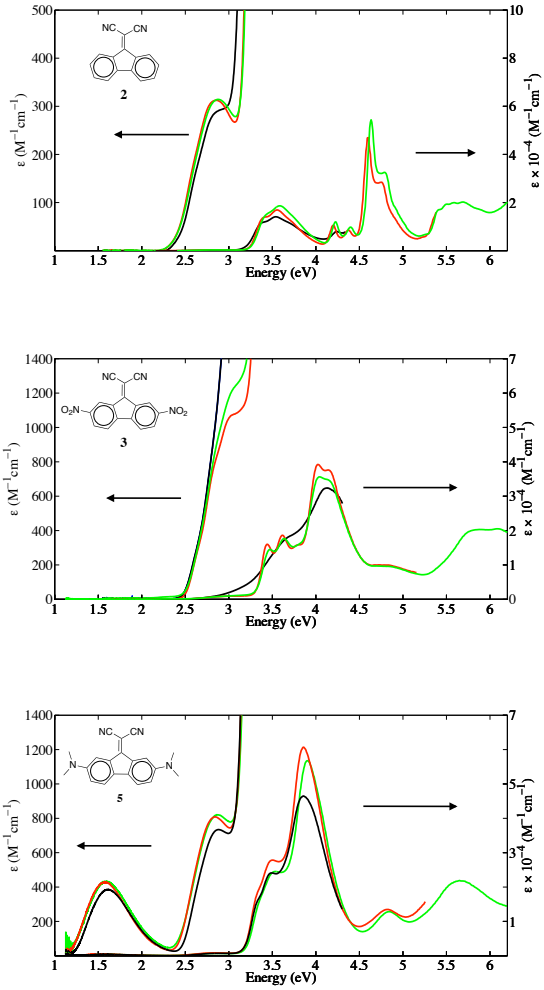

Figure 8.18: Absorption spectra of **2** (top), **3** (middle), and **5** (bottom), in toluene (black lines), CH_2Cl_2 (red lines), and CH_3CN (green lines) solutions.

The absorption spectra for **3** and **5** are qualitatively similar, in the different solvents, except for **3** in toluene, which is broader and more featureless, compared to the spectra of **3** in CH_2Cl_2 and CH_3CN. In the spectrum of **3**, the lowest energy absorption envelope starts to appear at approximately 2.50 eV. This absorption envelope appears as a shoulder to the remaining spectrum. In toluene, this transition is completely covered by the remaining spectrum. The intensity of this transition appears, in the spectrum of **3**, to be nearly four times more intense, than the lowest energy transition in the spectrum of **2**. From the shape of the shoulder, this transition is estimated, to be located at approximately 3.10 eV and 3.09 eV in CH_2Cl_2 and CH_3CN, respectively.

The second lowest energy absorption envelope for **3**, is very similar in intensity, to the second lowest energy absorption envelope of **2**. It consists of two bumps separated by 0.17 eV (1400 cm^{-1}), in both CH_2Cl_2 and CH_3CN. This absorption envelope is most intense at 3.64 and 3.62 eV in CH_2Cl_2 and CH_3CN, respectively. A small bump is also observed at approximately 3.70 eV, in the absorption spectrum of **3** in toluene.

The calculated energies for the $^1A_1 \rightarrow {}^1B_2$ and $^1A_1 \rightarrow {}^1A_1$ transitions of **3**, presented in the previous section, are very close to the experimentally determined values mentioned above. Thus, from comparison of the calculated and experimental results, the $S_0 \rightarrow S_1$ transition for **3** is assigned to the $^1A_1 \rightarrow {}^1B_2$ transition, and the $S_0 \rightarrow S_2$ transition is assigned to be the $^1A_1 \rightarrow {}^1A_1$ transition.

The absorption spectrum of **5** starts to appear at 1.15 eV. The lowest energy absorption envelope has a maximum intensity, at 1.61, 1.58, and 1.59 eV, in toluene, CH_2Cl_2, and CH_3CN, respectively. The calculated energies for the $^1A \rightarrow {}^1B$ tranistion (1.73, 1.65, and 1.63 eV, in toluene, CH_2Cl_2, and CH_3CN, respectively) are close to the experimental energies. No other transitions are calculated to appear in the energy region of the absorption spectrum, where the lowest energy absorption envelope is observed. Thus, the lowest energy absorption envelope is assigned to be the $^1A \rightarrow {}^1B$ transition. The calculated small oscillator strength is also supported, by the low intensity of this absorption band. The second lowest energy absorption envelope in the absorption spectrum of **5** is, in contrast to **2** and **3**, present as a low intensity absorption envelope, which appears as a shoulder to the remaining spectrum. This absorption envelope has a maximum intensity, at 2.88, 2.85, and 2.87 eV, in toluene, CH_2Cl_2, and CH_3CN, respectively. In comparison, the calculated energies, for the $S_0 \rightarrow S_2$ transition are slightly higher, than the observed experimental values. However, the calculated oscillator strengths, for the $S_0 \rightarrow S_2$ transition supports, that this transition is slightly more intense, than the lowest energy transition, which is observed experimentally. Thus, the result are consistent, with the assignment of the $S_0 \rightarrow S_2$ transition as the $^1A \rightarrow {}^1A$ transition, which involves promotion from the $\pi_{\mathbf{5}}$" to the $\pi^*_{\mathbf{5}}$ orbital (Fig. 8.16).

In summary, there is very good correlations, between the calculated results and the experimental results obtained from absorption spectroscopy. The experimental results, verify that the $^1A_1 \rightarrow {}^1B_2$ transition energy of **2** is controllable, by the strategic positioning of substituents, in a similar way as the pentafulvenes. However, the 3,6-disubstituted compounds remain to be experimentally investigated, in order to elucidate how the absorption properties of **2** are influenced, by substituents in these positions.

However, it has to be mentioned, that the model presented above has been strongly criticized and is claimed to be wrong by others. This criticism is justified by inspection of the absorption spectra. The critique regards the assignment of the lowest energy absorption envelopes in the absorption spectra for **2**, **3**, and **5**. As previously described, the lowest energy absorption bands in the spectra of **2**, **3**, and **5** were assigned to be correlating $\pi \rightarrow \pi^*$ transitions, as shown in **Model I** in Fig. 8.19. However, as the gray dotted line reveal in **Model II**, in Fig. 8.19, an absorption envelope similar to the lowest energy absorption envelope of **2** is present at nearly the same energy in the three spectra. It can therefore be argued that the absorption envelopes, which are dissected by the dotted gray line, are correlating $\pi \rightarrow \pi^*$ transitions, which are uninfluenced by the presence of substituents. The lowest energy absorption envelope in **Model II** is assigned to be "a new $\pi \rightarrow \pi^*$ transition", that does not correlate, with the lowest energy absorption envelope of **2** and **3**. In addition, it was proposed that the low energy absorption band, could be due to aggregation of **5**. The latter is not the case, as the relative intensity between the lowest energy absorption envelope, and the other absorption bands in the absorption spectrum of **5** remains constant at different concentrations. In terms of "$\pi \rightarrow \pi^*$" transitions, the assignment of the transitions are reasonable in both **Model I** and **Model II**, but **Model II** may appear as the most reliable. However, the calculated results support the assignment of the transitions in **Model I**, as they suggest that the lowest energy absorption envelope in the spectrum of **5** corresponds to the transition, which correlate with to the lowest energy transition in **3** and **2**. The second lowest absorption envelope is, according the calculated results, indeed a $\pi \rightarrow \pi^*$ transition, but this transition does not correlate to the lowest energy transition in **3** and **2**. Thus, **Model II** is not supported by the computational results.

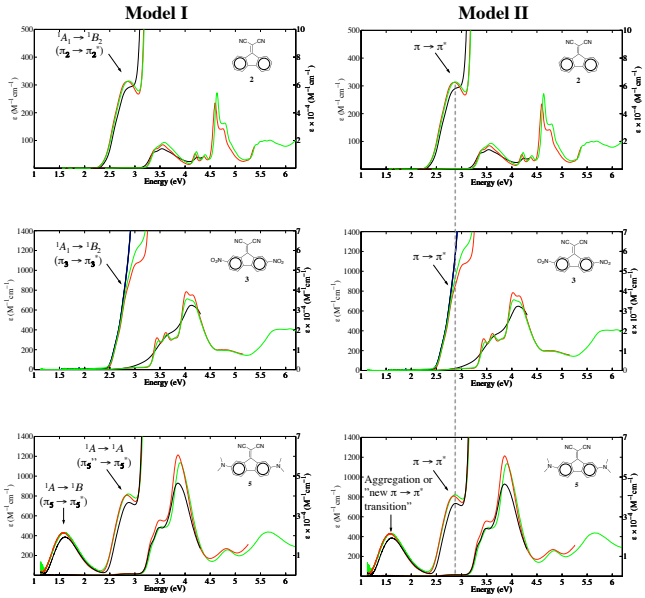

Figure 8.19: Presentation of two explanatory models. **Model I** is presented in this chapter, and the alternative interpretation of the spectra is presented in **Model II**.

8.6 Modification of the Exocyclic Substituent

The low energy absorbing compound **5**, was prepared by reacting 2,7-bis(dimethylamino)-9*H*-fluorenone, (**7**) with malononitrile, in a solvent-free Knoevenagel condensation reaction, analogues to the procedure described by Wang and Cheng.[175] The reaction is shown in Fig. 8.20.

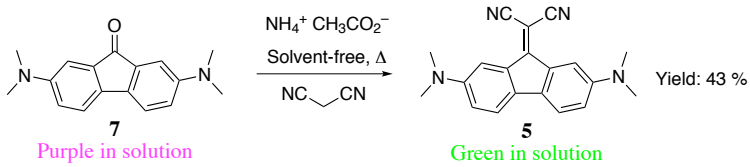

7
Purple in solution

5
Green in solution

Figure 8.20: Synthetic scheme for preparation of **5**, from Knoevenagel condensation between malononitrile and **7**. The synthesis was performed by Christian Dahlstrand from Uppsala University.

It was noticed, that **7** is purple in solution, and this encouraged us, to investigate this compound experimentally, as well as computationally. The absorption spectrum of **7** (presented later), appears to be very similar, to that of **5**. Interestingly, the computational results suggest (discussed later) that the lowest energy absorption band, can be assigned to a $^1A \rightarrow {}^1B$ transition, which involves orbitals that are very similar to those involved in the $^1A \rightarrow {}^1B$ transition of **5**. Triggered by this similarity, the absorption properties of **7**, 9*H*-fluorenone (**8**), and 2,7-dinitro-9*H*-fluorenone (**9**), shown in Fig. 8.21, were also investigated. The compounds **8** and **9** were both purchased from Sigma-Aldrich. **8** was recrystallized twice from absolute ethanol. **9** was recrystallized from glacial acetic acid, as described by Bennett *et al.*[177]

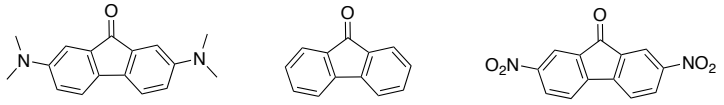

7 **8** **9**

Figure 8.21: The three compounds, which were subject for the investigation presented in this section.

The absorption spectra of the three fluorenone derivatives were recorded in toluene, CH_2Cl_2, and CH_3CN solutions. The spectra are presented in Fig. 8.22. As mentioned, the spectrum of **7** is very similar to that of **5**, in Fig. 8.18. Moreover, the similarities between the spectra of **8** and **2**, and between **9** and **3** are also evident.

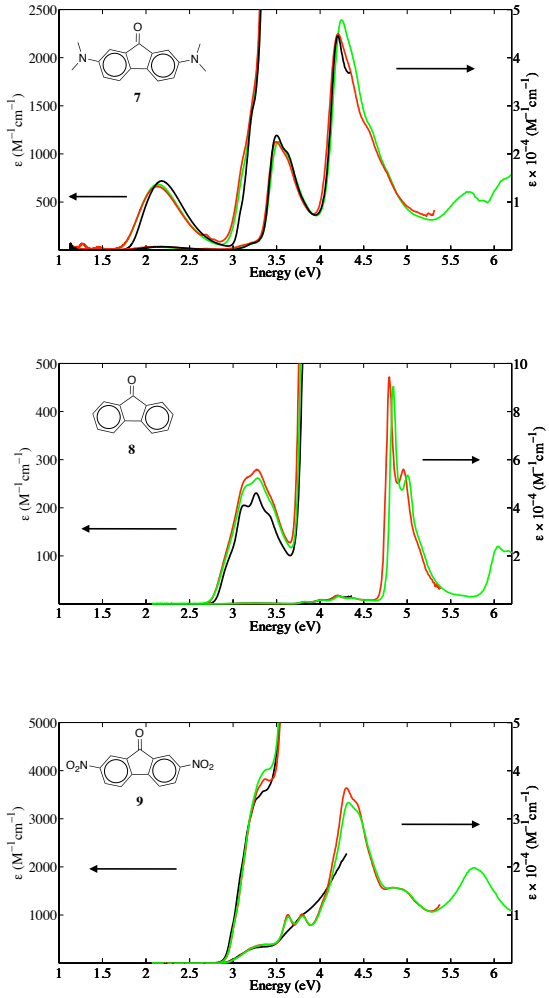

Figure 8.22: Absorption spectra of **7** (top), **8** (middle), and **9** (bottom), in toluene (black lines), CH_2Cl_2 (red lines), and CH_3CN (green lines) solutions. Note the different scalings of the vertical axis.

In order to further investigate the relation between the 'carbonyl compounds' (**7**, **8**, and **9**) and the 'dicyanomethylene compounds' (**2**, **3**, and **5**), the vertical excitation energies were also calculated for the carbonyl compounds, in order to assign the lowest energy transitions in their absorption spectra. The structural optimization of **7**, **8**, and **9** resulted in structural parameters, that were similar to structural aspects of **5**, **2**, and **3**. Therefore, the ground state structures of **7**, **8**, and **9**, can be interpreted, in a fashion similar to the corresponding dicyanomethylene compounds.

For the carbonyl compounds, the vertical excitation energies were only calculated, in vacuum and a CH_3CN environment. The results of the calculations are presented on the following three pages, in Table 8.7 for **7**, in Table 8.8 for **8**, and in Table 8.9 for **9**. The orbitals involved in the calculated excitations are depicted in Fig. 8.23.

Table 8.7: Calculated lowest two vertical excitation energies (ΔE_{cal}, in eV) and the corresponding oscillator strengths (f) for **7**. The character of the transitions (Character) are listed in parentheses, with the weighting of the electron configuration, given in percent. The orbitals involved in the calculated transitions are shown in Fig. 8.23.

Compound	Environment[a]	Transition (Character)[c]	ΔE_{cal} (eV)[b]	f ($\times 10^3$)[b]
7 (C_2)	Vacuum	$S_0(^1A) \rightarrow S_1(^1B)$ ($\pi_{\mathbf{7}} \rightarrow \pi^*_{\mathbf{7}}$, 97 %)	2.63	19.3
		$S_0(^1A) \rightarrow S_2(^1A)$ ($n_{\mathbf{7}} \rightarrow \pi^*_{\mathbf{7}}$, 90 %)	3.29	0
	CH_3CN	$S_0(^1A) \rightarrow S_1(^1B)$ ($\pi_{\mathbf{7}} \rightarrow \pi^*_{\mathbf{7}}$, 97 %)	2.35 (2.13)[d]	22.0
		$S_0(^1A) \rightarrow S_2(^1A)$ ($n_{\mathbf{7}} \rightarrow \pi^*_{\mathbf{7}}$, 90 %)	3.39	0

[a] Calculations involving solvation have been performed by inclusion of the PCM model. [b] TD-M062X/6-311+G(2d,p)//B3LYP/6-311G(d,p). [c] The contribution percentages are calculated, as two times the square of the value of the largest expansion coefficient for the excited state Kohn-Sham solution. [d] Value in parentheses is determined from the maximum intensity of the lowest energy absorption envelope.

Table 8.8: Calculated lowest two vertical excitation energies (ΔE_{cal}, in eV), and the corresponding oscillator strengths (f) for **8**. The character of the transitions (Character) are listed in parentheses, with the weighting of the electron configuration, given in percent. The orbitals involved in the calculated transitions are shown in Fig. 8.23.

Compound	Environment[a]	Transition (Character)[c]	ΔE_{cal} (eV)[b]	f ($\times 10^3$)[b]
8 (C_{2v})	Vacuum	$S_0(^1A_1) \rightarrow S_1(^1A_2)$ ($n_{\mathbf{8}} \rightarrow \pi^*_{\mathbf{8}}$, 89 %)	3.24	0
		$S_0(^1A_1) \rightarrow S_2(^1B_2)$ ($\pi_{\mathbf{8}} \rightarrow \pi^*_{\mathbf{8}}$, 97 %)	3.56 (3.40)[d]	4.0
	CH_3CN	$S_0(^1A_1) \rightarrow S_1(^1A_2)$ ($n_{\mathbf{8}} \rightarrow \pi^*_{\mathbf{8}}$, 90 %)	3.36	0.0
		$S_0(^1A_1) \rightarrow S_2(^1B_2)$ ($\pi_{\mathbf{8}} \rightarrow \pi^*_{\mathbf{8}}$, 97 %)	3.40 (3.28)[d]	3.4

[a] Calculations involving solvation have been performed by inclusion of the PCM model. [b] TD-M062X/6-311+G(2d,p)//B3LYP/6-311G(d,p). [c] The contribution percentages are calculated, as two times the square of the value of the largest expansion coefficient for the excited state Kohn-Sham solution. [d] Values in parentheses are determined from the maximum intensity of the lowest energy absorption envelope.

Table 8.9: Calculated lowest two vertical excitation energies (ΔE_{cal}, in eV), and the corresponding oscillator strengths (f) for **9**. The character of the transitions (Character) are listed in parentheses, with the weighting of the electron configuration, given in percent. The orbitals involved in the calculated transitions are shown in Fig. 8.23.

Compound	Environment[a]	Transition (Character)[c]	ΔE_{cal} (eV)[b]	f ($\times 10^3$)[b]
9 (C_{2v})	Vacuum	$S_0(^1A_1) \rightarrow S_1(^1A_2)$ ($n_{\mathbf{9}} \rightarrow \pi^*_{\mathbf{9}}$, 58 %)[d]	3.18	0
		$S_0(^1A_1) \rightarrow S_2\,^1B_2$ ($\pi_{\mathbf{9}} \rightarrow \pi^*_{\mathbf{9}}$, 86 %)[d]	3.70	91.3
	CH_3CN	$S_0(^1A_1) \rightarrow S_1(^1A_2)$ ($n_{\mathbf{9}} \rightarrow \pi^*_{\mathbf{9}}$, 47 %)[d]	3.30 (3.38)[e]	0
		$S_0(^1A_1) \rightarrow S_2(^1B_2)$ ($\pi_{\mathbf{9}} \rightarrow \pi^*_{\mathbf{9}}$, 84 %)[d]	3.58	156.3

[a] Calculations involving solvation have been performed by inclusion of the PCM model. [b] TD-M062X/6-311+G(2d,p)//B3LYP/6-311G(d,p). [c] The contribution percentages are calculated, as two times the square of the value of the largest expansion coefficient for the excited state Kohn-Sham solution. [d] The excitation involves contributions, from other excitations of the same character (> 10 %). [e] Value in parentheses is determined from the maximum intensity of the lowest energy absorption envelope.

In short, the calculated results indicate that the lowest energy absorption envelope, in the spectrum of **7**, can be assigned to the $^1A \rightarrow {}^1B$ transition, which correlates with the $S_0(^1A) \rightarrow S_1(^1B)$ transition for **5**.

The spectrum for **8**, is consistent with previously reported spectra.[178–184] The calculated results, suggest that the $S_0(^1A_1) \rightarrow S_1(^1A_2)$ and $S_0(^1A_1) \rightarrow S_2(^1B_2)$ transitions are located underneath the lowest energy absorption envelope, in the experimental spectrum. This is consistent with experimental results, which verifies that this absorption envelope covers a $\pi \rightarrow \pi^*$ transition, to a state of $^1B_2$ symmetry,[178,179,181–186] and a much lower intensity $n \rightarrow \pi^*$ transition, which accounts for the weak vibrational structure of the absorption band.[180] In consistency with earlier investigations,[178,179,181–186] the absorption maximum of the lowest absorption envelope of **8**, is assigned to be representative for the experimental energy of the $^1A_1 \rightarrow {}^1B_2$ transition. The similarities between the $^1A_1 \rightarrow {}^1B_2$ transitions for **8** and **2**, is clear from the correlation of the π- and π^*-orbitals, shown in Fig. 8.23 and Fig. 8.5.

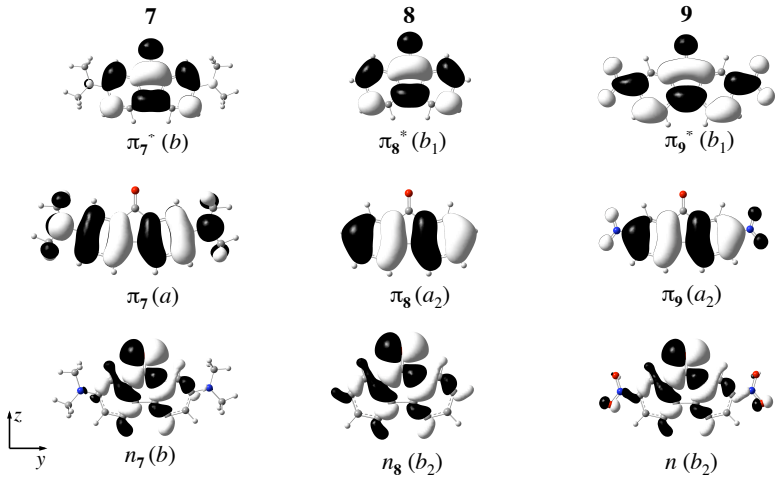

Figure 8.23: Orbitals involved in the two lowest calculated extatations, for the compounds **7**, **8**, and **9** (TD-M062X/6-311+G(2d,p)//B3LYP/6-311G(d,p)). The compounds **8** and **9** were calculated to belong within the C_{2v} point group, and **7** within the C_2 point group.

With regard to **9**, the calculated results predict the $S_0 \rightarrow S_1$ transition to be a $^1A_1 \rightarrow {}^1A_2$ transition of $n \rightarrow \pi^*$ character. The lowest absorption envelope in the spectrum of **9**, appears as a shoulder to the remaining spectrum. The envelope has an intensity maximum, located at an energy, which is very close to the calculated $^1A_1 \rightarrow {}^1A_2$ transition energy. Moreover, this intensity maximum of the shoulder, exhibits a small hypsochromic shift, when solvent polarity is increased (3.33, 3.37, and 3.38 eV in toluene, dichloromethane, and acetonitrile). Such a solvatochromic behavior is characteristic for $n \rightarrow \pi^*$ transitions,[187] and this shoulder is therefore assigned to be the $^1A_1 \rightarrow {}^1A_2$ transition. The presence of the calculated $S_0(^1A_1) \rightarrow S_2(^1B_2)$ cannot be verified through inspection of the absorption spectrum, but if it is present, it will be located at energies higher than 3.33 eV in the absorption spectra.

A particular interesting thing to notice, is that the $^1A_1 \rightarrow {}^1B_2$ ($^1A \rightarrow {}^1B$) transition energies are in general higher for the three carbonyl compounds, when **7** is compared with **5**, and when **2** is compared with **8**. This trend is found between both the calculated and experimental $^1A_1 \rightarrow {}^1B_2$ ($^1A \rightarrow {}^1B$) transition energies. When the calculated $^1A_1 \rightarrow {}^1B_2$ transition energies are compared for **3** and **9**, the same trend is found. Due to the correlation between the π-orbitals in Fig. 8.5 and Fig. 8.23, it is assumed, that the carbonyl compounds, are also influenced, by a similar dipolar π-electron density distribution in the FC $^1B_2$ state, as the dicyanomethylene compounds. The latter trend can be explained, by noting that the dicyanomethylene group is a better π-electron withdrawing group, in comparison to the carbonyl group.

Thus, the dicyanomethylene compounds can stabilize the more polarized π-electron density distribution in the $^1B_2$ state to a larger extent, when compared to the fluorenone derivatives. Consequently, the $^1A_1 \rightarrow {}^1B_2$ ($^1A \rightarrow {}^1B$) transition energies are lower for the dicyanomethylene compounds. Thus, the above discussion illustrates, that the $^1A_1 \rightarrow {}^1B_2$ transition energy can also be tuned if the π-electron withdrawing, abilities of the exocyclic position is varied through substitution.

In this context it is worth mentioning the recent results reported by Sato *et al.*, which illustrates how excitation energies can be varied, in compounds that are closely related to **2** and **8**.[188] Sato *et al.* reported, that the lowest energy absorption of 2,7-bis-(5-bromo-4-decylthiophen-2-yl)-9*H*-fluorenone (**TFO**, in Fig. 8.24) is systematically shifted to lower energies, when the carbonyl group is exchanged with groups, possessing better π-electron withdrawing abilities.[188] Their results indicate, that the tunable lowest energy transition, clearly correlates with the $^1A_1 \rightarrow {}^1B_2$ transition of **2** and **8**.

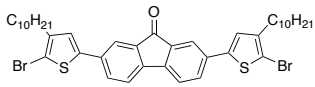

TFO

Figure 8.24: Illustration of 2,7-bis-(5-bromo-4-decylthiophen-2-yl)-9*H*-fluorenone, (**TFO**), which was subject to investigation in the work of Sato *et al.*[188]

On a final note, it should be mentioned, that Christian Dahlstrand from Uppsala University, recently succceded in the synthesis of the novel compounds 2,7-bis(dihexylamino)-9*H*-fluorenone (**10**, in Fig. 8.25) and 2-(2,7-bis(dihexylamino)-9*H*-fluoren-9-ylidene)malononitrile (**11**, in Fig. 8.25).

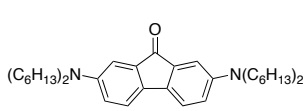

10

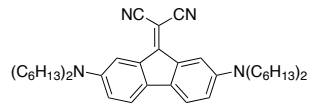

11

Figure 8.25: Illustration of the recently synthesized compounds **10** and **11**.

The absorption spectra of **10** and **11** are shown in Fig. 8.26, and are qualitative similar to those of **7** and **5**. However, the absorption bands that correspond to the $S_0 \rightarrow S_1$ transition, are shifted to 2.03 and 1.47 eV for **10** and **11**, respectively. These are bathochromic shifts of 0.10 eV and 0.12 eV, when compared to **7** and **5**, respectively. Thus, the dihexylamino groups appear to be more π-electron donating, in comparison the the dimethylamino groups. Additionally, **10** and **11** appear to possess greater solubility in a larger variety of solvents, when compared to **7** and **5**.

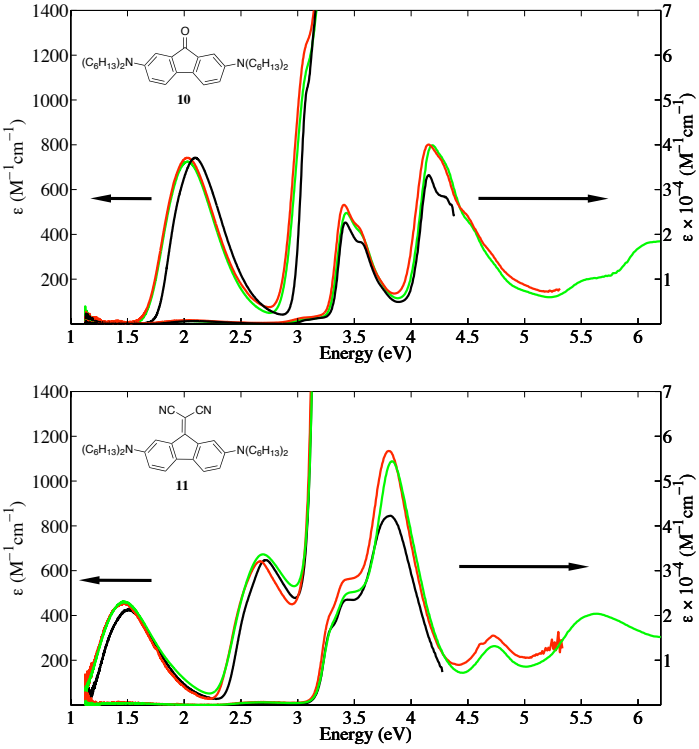

Figure 8.26: Absorption spectra of **10** (top) and **11** (bottom) in toluene (black lines), CH_2Cl_2 (red lines), and CH_3CN (green lines) solutions. Note the different scalings of the vertical axis.

It is convenient to close this section of, with a visual illustration of the consequences of the concept of substituent controlled manipulation of excited state energies. This is shown in Fig. 8.27, where the picture illustrates, how the understanding of how π-electrons prefer to be delocalized in the ground and excited states, allows for design of compounds, with a variety of optical properties. This definitely deserves further investigations in the future.

An interesting aspect to investigate is how the emissive properties of **2** and **8** are affected by the presence of the substituents, which is the focus of the following section.

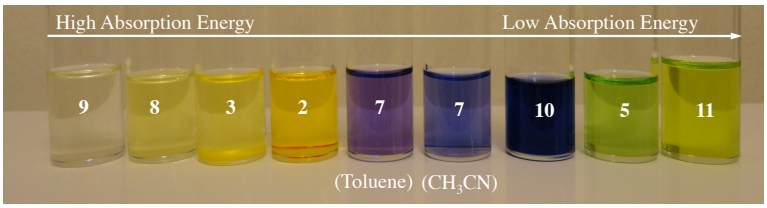

Figure 8.27: Solutions of the compounds **2**, **3**, **5**, **7**, **8**, **9**, **10**, and **11**, which illustrate their different absorption properties - properties which are a result of substituent controlled manipulation of excited state energies.

8.7 The Control of Emission Properties

The emission properties of the dicyanomethylene compounds, **2**, **3**, **5**, and **11**, together with the carbonyl compounds **7**, **8**, **9**, and **10** were investigated experimentally at ambient temperature, in toluene, CH_2Cl_2, and CH_3CN solutions. The recorded emission spectra are shown in Fig. 8.28 and Fig. 8.29, for the dicyanomethylene and carbonyl compounds, respectively, on the following two pages. Table 8.10 presents the experimentally determined emission energies (ΔE_{em}), the corresponding quantum yields Φ_{em}, and the energies for the 0-0 transitions ($\Delta E_{0\text{-}0}$), between the emissive state and the ground state.

The compounds **5**, **10** and **11**, were found to be non-emissive at these conditions. Measurements on these compounds at lower temperature, are in progress. Compound **7** is very weakly emissive in toluene and CH_3CN, while no emission could be detected in CH_2Cl_2 solution. Thus, determination of quantum yields for this compound was not performed, due to the poor signal-to-noise ratio in the recorded emission spectra. Compound **9** appear to be a photoactive compound, and new species are formed upon irradiation by the intense excitation source in the emission spectrophotometer. This revealed itself, through changes in the absorption spectrum, recorded after the measurement of emission spectra, and through the development of an emission band, at approximately 2.25 eV upon elongated irradiation. Therefore no experimental data are given for this compound. In Table 8.10 the calculated emission energies in vacuum and CH_3CN environment, are also listed for the compounds **2**, **3**, **5**, **7**, and **8**. These will be explained in the following.

The experimental details regarding the emission measurements can be found in the Appendix.

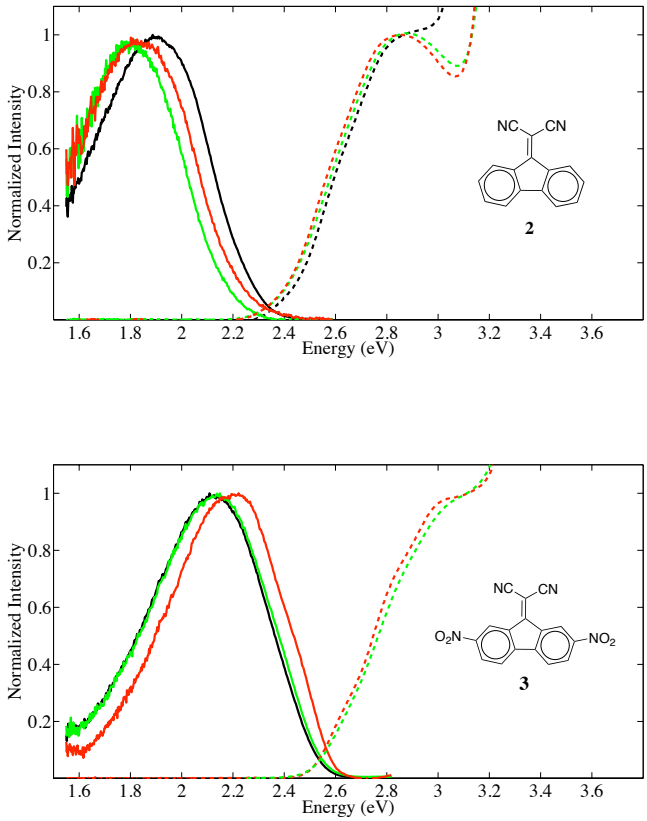

Figure 8.28: Normalized emission spectra of **2** (full lines, top) and **3** (full lines, bottom) in toluene (black), CH_2Cl_2 (red) and CH_3CN (green) solutions. The absorption spectra are presented with dotted lines, and are normalized with respect to the lowest energy absorption envelope. The emission spectra for **3**, recorded in toluene and CH_3CN solutions for **2** overlap with each other. The emission spectra were recorded with excitation, at 375 nm (3.31 eV) for both compounds. The presented emission spectra (I_{em}) have been corrected from wavelength (λ) to energy (E) by $I_{em}(\lambda) = \lambda^2 I_{em}(E)$.

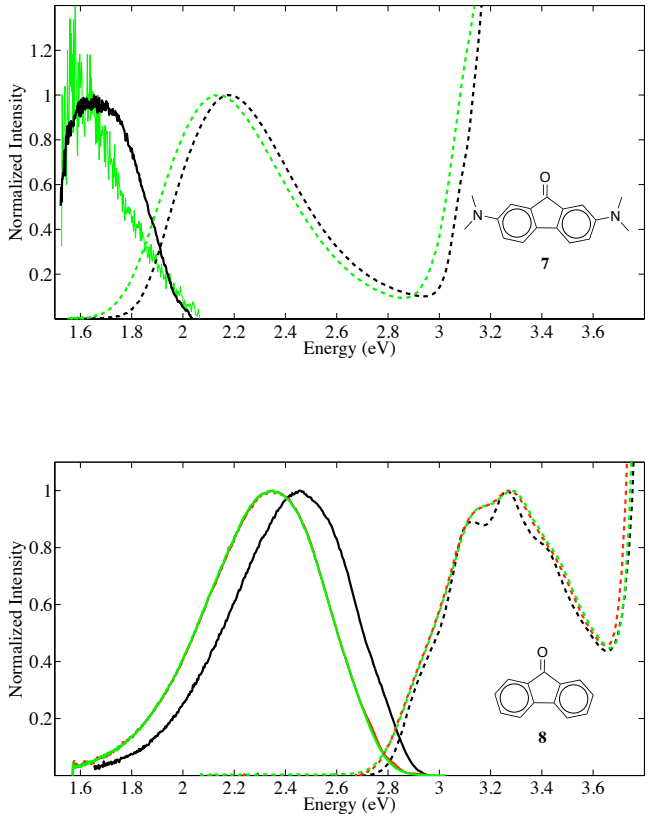

Figure 8.29: Normalized emission spectra of **7** (full lines, top) and **8** (full lines, bottom) in toluene (black), CH_2Cl_2 (red) and CH_3CN (green) solutions. The absorption spectra are presented with dotted lines, and are normalized with respect to the lowest energy absorption envelope. No emission from **7** was observed in CH_2Cl_2. The emission spectrum of **7** in CH_3CN is noisy at the emission maximum and have therefore been normalized with respect to what appears as the "center" of the noise. The absorption and emission spectra of **8** recorded CH_2Cl_2 and CH_3CN solutions, are identical and therefore overlap. The emission spectra were recorded with excitation, at 490 nm (2.53 eV) and 400 nm (3.10 eV) for **2** and **8**, respectively. The presented emission spectra (I_{em}) have been corrected from wavelength (λ) to energy (E) by $I_{em}(\lambda) = \lambda^2 I_{em}(E)$.

Table 8.10: Emission maxima, (ΔE_{em}, in eV) and the corresponding quantum yields (Φ_{em}), and 0-0 transition energies ($\Delta E_{0\text{-}0}$, in eV), for the compounds **2**, **3**, **5**, **7**, and **8**.

Compound	Environment	ΔE_{em} (eV)[a]	Φ_{em} ($\times 10^3$)	$\Delta E_{0\text{-}0}$ (eV)[b]
2	Vacuum[c]	*2.14*	-	*2.61*
	Toluene	1.90	0.26	2.35
	CH_2Cl_2	1.84	0.17	2.32
	CH_3CN[d]	1.80, *1.84*	0.09	2.29, *2.27*
3	Vacuum[c]	*2.38*	-	*2.90*
	Toluene	2.13	3.2	-
	CH_2Cl_2	2.22	1.5	2.56
	CH_3CN[d]	2.14 *2.20*	1.9	2.54 *2.68*
5	Vacuum[c]	*1.22*	-	*1.56*
	Toluene	-	-	-
	CH_2Cl_2	-	-	-
	CH_3CN[d]	*0.80*	-	*1.14*
7	Vacuum[c]	*1.95*	-	*2.31*
	Toluene	1.65	-	1.91
	CH_2Cl_2	-	-	
	CH_3CN[d]	1.57, *1.50*	-	1.8, *1.87*
8	Vacuum[c]	*2.67*	-	*3.17*
	Toluene	2.46	9.8	2.84
	CH_2Cl_2	2.35	18	2.78
	CH_3CN[d]	2.35, *2.40*	23	2.78, *2.90*

[a] Determined from the maxima of the energy corrected emission spectra. [b] Determined from the intersection between the normalized energy corrected emission spectrum, and the absorption spectrum normalized with respect to the lowest energy absorption envelope.[160] [c] Values in *italics* are energies calculated, at the (TD)-M062X/6-311+G(2d,p)//(TD)-B3LYP/6-311G(d,p) level. [d] Values in *italics* are energies calculated, at the PCM/(TD)-M062X/6-311+G(2d,p)//PCM/(TD)-B3LYP/6-311G(d,p), with state specific equilibrium solvation of the $^1B_2$ state optimized structures. See text for details.

At this point, it is unknown, if the emission for the various compounds originate from the states, which correlate with the $^1B_2$ state of **2**. In order to investigate whether this is the case, the emission energies from these states were calculated for the compounds **2**, **3**, **5**, **7**, and **8**. The emission energies were calculated in vacuum, and in CH_3CN environment, in order to compare with the experimental results in Table 8.10.

In vacuum, the calculations were performed as follows. The five compounds were structurally optimized along the excited energy state potential energy surfaces, which correlate with the $^1B_2$ state of **2**. The structural optimizations were performed at the TD-B3LYP/6-311G(d,p) level, as previously described for **2**. The vertical excitation energies for the ground state of the $^1B_2$ (^1B) excited state optimized structures, were then calculated at the TD-M062X/6-311+G(2d,p) level. For all five compounds, the results of the latter calculations suggested that the $^1B_2$ (^1B) state, is the lowest excited state. Thus, according to the results from the calculations, the emission will originate from the $^1B_2$ (^1B) state for each compound in vacuum, if Kasha's rule is assumed to be obeyed.[189] The emission energy from this state, will be the latter calculated transition energies.

The calculations of emission energies of the compounds in a CH_3CN environment are less straight-forward. For this purpose Fig. 8.30, in the following page, is helpful in the description of the steps. Fig. 8.30 illustrates the concept for **2**, but the strategy is equivalent for the other compounds. First, **2** is optimized to the lowest energy conformation in the $^1B_2$ excited state (red **2** in Fig. 8.30), with inclusion of a PCM solvation model, to simulate the CH_3CN environment for **2** in the $^1B_2$ state. When the equilibrium conformation of **2** in the $^1B_2$ state is located, the vertical excitation energy to the $^1B_2$ state is calculated, from the ground state of this conformation, at the TD-M062X/6-311+G(2d,p) level, using state specific equilibrium solvation.[190,191] This yields the energy for **2** in the $^1B_2$ state, with excited state solvation (red brackets around red **2**). The ground state energy of the $^1B_2$ state equilibrium conformation, is then calculated, at the M062X/6-311+G(2d,p) level, with the PCM solvation data, from the latter state specific equilibrium solvation calculation. This yields the energy, which corresponds to the blue colored **2** in the red excited state solvation brackets. The energy difference between the last two calculated energies, then correspond to the calculated emission energy of **2** from the $^1B_2$ state in acetonitrile.

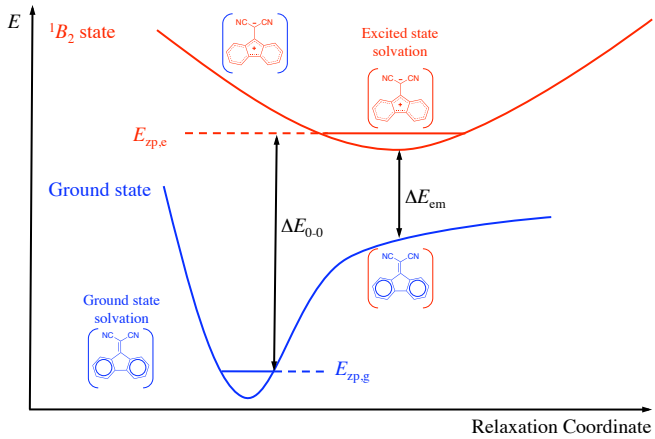

Figure 8.30: Illustration of the different aspects of the absorption and emission processes for **2**. The resonance structures represent the π-electron density distribution of **2** in the two states.

The 0-0 transition energies correspond to the energy difference, between the energy of the ground state equilibrium conformation, calculated at the M062X/6-311+G(2d,p)//B3LYP/6-311G(d,p) level (with or without PCM solvation), and the energy of the $^1B_2$ state equilibrium conformation obtained as described above. To this energy difference is added the difference in zero-point energy in the ground state ($E_{zp,g}$, in Fig. 8.30) and the $^1B_2$ state ($E_{zp,e}$, in Fig. 8.30), calculated at the (TD)-B3LYP/6-311G(d,p) level. For each of the compounds this contribution is less than 0.1 eV, and therefore only accounts for a small contribution to the 0-0 transition energy.

Before discussing the data in Table 8.10, it is appropriate to comment on the structural aspect of the $^1B_2$ (^1B) state equilibrium structures, from which the emission is calculated to originate from. In short, the $^1B_2$ (^1B) states of **3**, **5**, **7**, and **8** exhibit the same structural in differences in their fluorene moeity, as those described for **2**, *i.e.* the most prominent bond length differences are found in the five-membered ring moiety. Moreover, the dipole moments for each of these compounds are calculated to be larger in the $^1B_2$ (^1B) state, in comparison to the ground state. This underlines that the dipolar $4n\pi$-electron density distribution, which was argued to be important in the description of the π-electron density distribution in the FC $^1B_2$ (^1B) states, is also important for each of the compounds, in their lowest energy conformation in the $^1B_2$ (^1B) states. The $^1B_2$ (^1B) state equilibrium conformation of the compounds can therefore be interpreted as shown in Fig. 8.31.

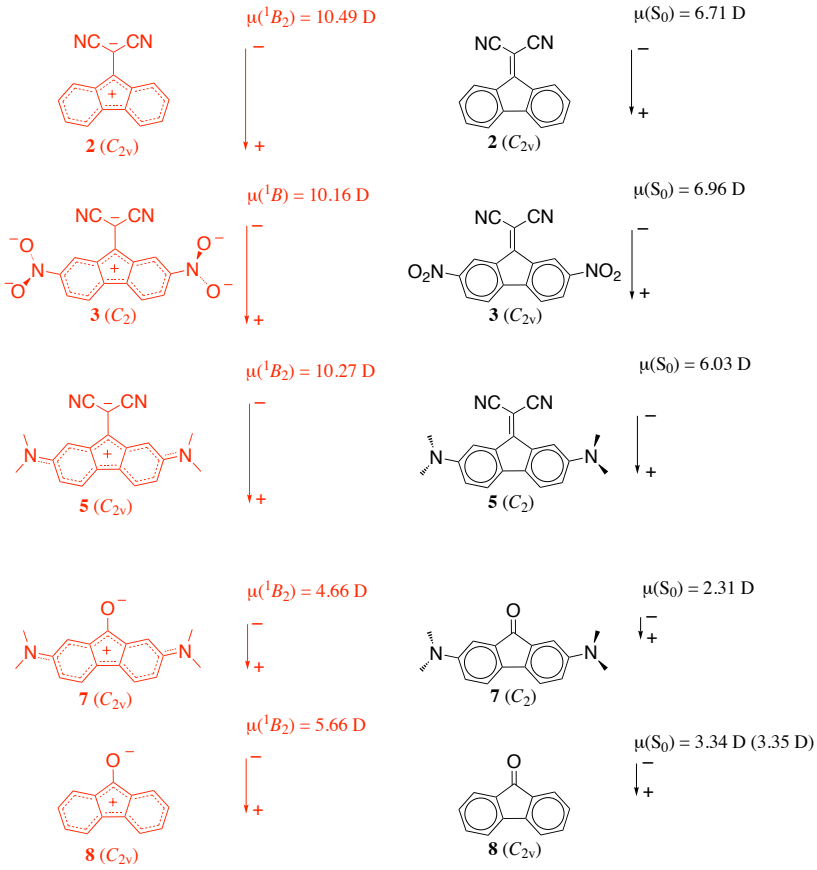

Figure 8.31: The results of the calculated ground state and $^1B_2$ (^1B) state equilibrium structures and dipole moments, suggest that the various compounds can be interpreted as the resonance structure representations, shown in black for the ground state structures and in red for the $^1B_2$ (^1B) state structures, for each compound. Point group symmetries are given in parenthesis, and the dipole moments are calculated at the TD-B3LYP/6-311G(d,p) and B3LYP/6-311G(d,p) level for the excited and ground state equilibrium conformations, respectively.

Some interesting aspects to notice are, that **3** is calculated to adopt a C_2 symmetric conformation in the ^1B state, with nitro groups twisted 19.40° out of the molecular plane. This will result in poorer π-electron orbital overlap, between the fluorene moiety and the nitro groups, when compared to the planar ground state conformation. This is interpreted as a consequence of the unfavorable interaction, between the π-electron withdrawing nitro groups and the electron deficient fluorene moiety. The molecule can reduce this unfavorable interaction by twisting the nitro groups as calculated.

The structures of **5** and **7** adopt C_{2v} symmetric equilibrium conformations in their $^1B_2$ states, and the C−N(CH_3)$_2$ bond lengths are shortened by 0.02 Å. This indicates that the π-electron interaction between the dimethylamino groups and the fluorene moiety is more pronounced in the $^1B_2$ state, in comparison to the ground state. From this result, it appears most likely that the emission energy from $^1B_2$ (^1B) state is controlled by the influence of substituents.

The calculated emission energies and the 0-0 transition energies in CH_3CN are in very good agreement with the available experimental data. Thus, it is therefore reasonable to assign the emission to originate from the $^1B_2$ ($^1B_2$) states of the compounds. This is in accordance with several results of luminescence spectroscopic measurements, which reveal that the emission from **8** originates from a $^1B_2$ excited state.[179–181,184,185] The calculated result for **5** serves as one explanation for why no emission is observed for this compound. An emission energy of 0.80 eV, is to low to be detected by the photomultiplier tubes in the spectrophotometer used, which can only detect photons, with energies higher than 1.30 eV.

Interestingly, the calculated emission energies in vacuum follow the pattern: ΔE_{em}(**8**) > ΔE_{em}(**3**) > ΔE_{em}(**2**) > ΔE_{em}(**7**) > ΔE_{em}(**5**). Most importantly, this pattern persists between the experimental results. This verifies, that the substituents can also be used for tuning emission energies in a systematic manner for **2** and **8**, by utilizing the knowledge of how π-electrons prefer to be delocalized in the excited states. The $\Delta E_{0\text{-}0}$ values follow the same pattern as described above. This is a manipulation pattern, which is consistent with how substituents affect the ΔE_{ST} of pentafulvene, and illustrate the close similarity between the excited states of pentafulvene and the fulvenic molecules investigated in this chapter.

In summary, it was illustrated both computationally and experimentally that substitution of **2** and **8** affect the $^1B_2$ state excited state energies in a predicable manner. The substituent controlled manipulation of the absorption-, emission-, and 0-0 transition energies are illustrated in the collective Fig. 8.32.

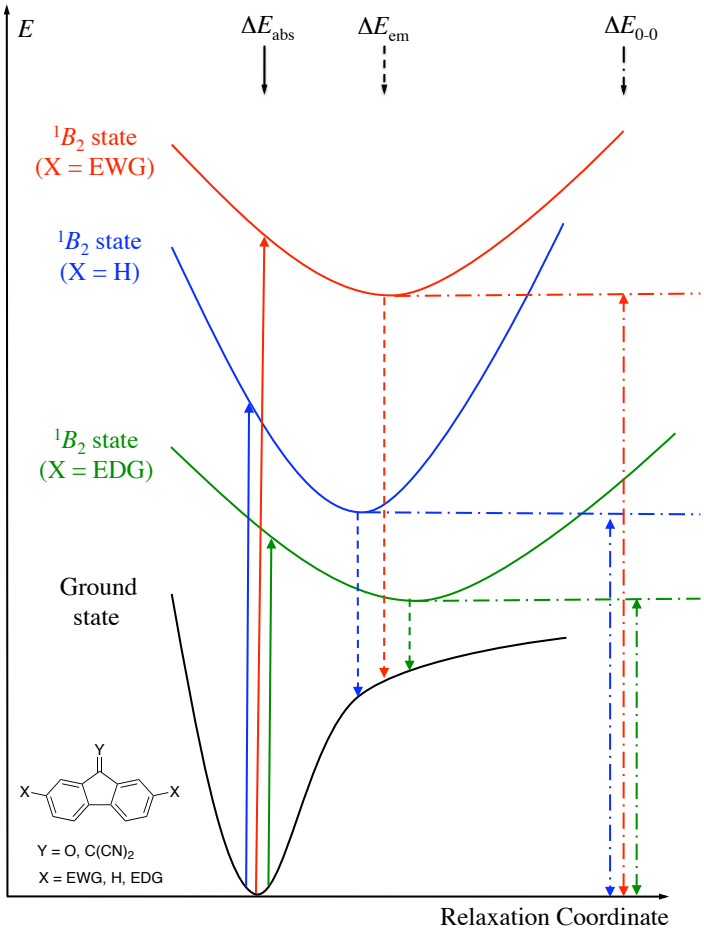

Figure 8.32: Illustration of how the substituents (X) affect the absorption- (ΔE_{abs}), emission- (ΔE_{em}), and 0-0 transition energies ($\Delta E_{0\text{-}0}$) in derivatives of **2** (Y = $C(CN)_2$) and **8** (Y = O). Electron withdrawing- and electron donating substituents are abbreviated EWG and EDG, respectively. For clarity, in this Figure the $\Delta E_{0\text{-}0}$ does not include the zero-point vibrational energies of the ground- and $^1B_2$ state.

For future investigations, the compounds **13**-**17** are interesting in the context of substituent controlled manipulation of excited state energies. Although, these compounds are so far hypothetical, their synthesis are plausible in theory, and should be attempted. This series of compounds represent a set, where the π-electron donation from the substituents to the fluorene moeity, is gradually increased. Thus, if the idea in Fig. 8.32 is applicable, the $^1B_2$ excited state energies of the compounds, should exhibit a systemic bathochromic shift from **13** to **17**. If the model in Fig. 8.32 is not supported, it has to be revised, or discarded in the "worst case scenario".

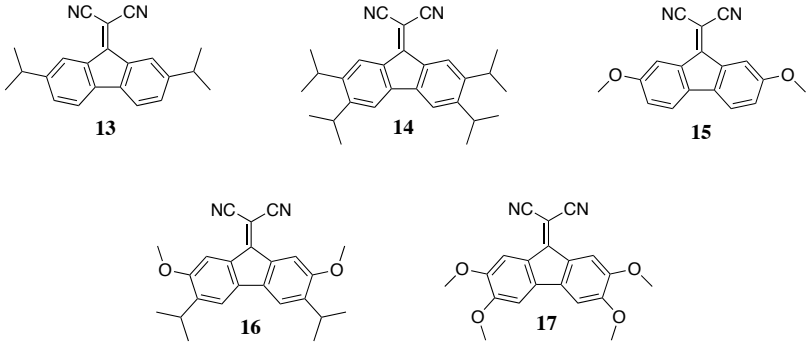

Figure 8.33: Target molecules for future research.

Chapter 9

Final remarks

In my personal opinion, it is unfortunate that the energetic aspects, associated with excited state π-electron delocalization, has not drawn more significant attention in organic photochemistry. Although photochemistry textbooks describe the photochemical behavior of molecules, which contains cyclic arrays of π-electrons, this behavior is rarely set in relation to the energetic aspects associated with π-electron delocalization in the excited states. This thesis demonstrates that a range of photochemical and photophysical observations can be rationalized, using the knowledge π-electron interactions in cyclic arrays, in both the ground state and excited states.

Recently, we have submitted a comprehensive review, which gathers the research reports that have in one way or another dealt with cyclic delocalization of π-electrons in the excited states.[15] This review illustrates the systematic trends associated to cyclic delocalization of π-electrons in excited state cyclic polyenic systems. Hopefully, this will convince chemists that the understanding, and application of excited state π-electron delocalization has been a neglected area in organic chemistry, which deserves more attention in the future.

Fortunately, there has been a considerable number of research reports recently, which focus on this topic.[25,192–199] Especially, the optical and electrochemical properties of pentafulvene derivatives, and compounds in close relation to **2** and **8** in Chapter 8, has drawn considerable attention.[166,170,188,188,193,200–205] This illustrates that scientist are opening up their eyes for the wonders of the excited state π-electron delocalization.

Appendix

Appendix

Spectroscopic Methods

Absorption Spectroscopy

The absorption spectra presented in this thesis were recorded by using a Cary 50 Bio spectrophotometer (Varian Inc.) in a 1 cm quartz cuvette (Hellma) using the pure solvent as a baseline. All solvents, except dichloromethane and acetonitrile were purchased from LabScan and were of HPLC grade. Dichloromethane and acetonitrile were purchased from Sigma-Aldrich and were of spectroscopic grade. All solvents were used as received.

In this thesis, the absorption spectra are presented as the molar absorption spectra. They were determined, as the average of three molar absorption spectra recorded with three different concentrations (1-10 μM) of the compound, using a scan rate of 200 nm per minute and an excitation slit width of 0.5 nm. The molar absorption spectra of the low intensity regions in the spectra, were determined as the average of four molar absorption spectra recorded, at four different concentrations (0.1-1 mM) of the compound, using a scan rate 200 nm per minute and an excitation slit width of 0.5 nm.

Emission Spectroscopy

The emission spectra presented in this thesis were recorded on a Jobin Yvon Horiba Fluorolog spectrophotometer with monochromator slit widths at the excitation and emission sites of 5 and 7 nm, respectively. Compounds **2**, **3**, were excited at 375 nm, and **8** at 400 nm in all solvents. In these measurements a longpass filter (> 400 nm) was inserted in front of the monochromater at the emission site. **7** was excited at 490 nm, using excitation and emission slit widths of 13 nm. No bandpass filter was used in the measurement of this compound. The presented emission spectra are average spectra of three, recorded at three different concentrations of the compounds. Each spectrum has been corrected for the emission spectra of the solvents used, recorded at the same conditions.

Quantum yields were calculated with respect to a reference with known quantum yield (Φ_R) calculated from:[162]

$$\Phi = \Phi_R \frac{I}{I_R} \frac{A_R}{A} \frac{n^2}{n_R^2} \tag{9.1}$$

Where I_R and I are the values of the energy domain integrated emission spectrum for the reference and the compound in question, respectively. The parameters A_R and A are the values of absorption, at the excitation wavelength used of the reference compound and the compound in question, respectively. The constants n and n_R are the refractive indexes of the solvents, in which the spectra of the reference compound and the compound in question are measured, respectively. In the measurement of quantum yields, A and A_R were kept less than 0.1, at the excitation wavelengths to ensure linearity between the emission and absorption intensities. For **2** and **3**, and **8** the quantum yield of **8** in acetonitrile solution was used as reference (Φ = 0.023).[206]

The detection range of the photomultiplier tube used were limited to an upper wavelength of 800 nm. To simulate the remaining part of the emission spectra for **2** outside the detection range, the emission spectra were fitted to a sum of Gaussian functions such that $R^2 > 0.99$. The analytical expressions for the spectra were then integrated in the energy domain, and used for the determination of the quantum yields. The quantum yields given as the average of values obtained with three different concentrations of the compounds.

Excitation spectra were recorded at the maximum intensity of the emission spectra for the compounds. The excitation spectra were similar to the absorption spectra of the compounds, suggesting that the observed emission, does not originate from impurities. Furthermore, no concentration dependent features were observed in the emission spectra, indicating that no intermolecular interactions, such as exciplex formations, give rise to the observed emission.

References

[1] Clayden, J.; Greeves, N.; Warren, S.; Wothers, P. *Organic Chemistry*; Oxford University Press, 2001.

[2] Reppe, W.; Schlichting, O.; Klager, K.; Toepel, T. *Ann.* **1948**, *560*, 1–92.

[3] Allinger, N. L.; Miller, M. A.; Tushaus, L. A. *J. Org. Chem.* **1963**, *28*, 2555–2557.

[4] Dewar, M. *Tetrahedron Suppl.* **1966**, *22, 8*, 75–92.

[5] Minkin, V. I.; Glukhovtsev, M. N.; Simkin, B. Y. *Aromaticity and Antiaromaticity*; John Wiley and Sons, 1994.

[6] Schleyer, P. v. R.; Jiao, H. *Pure Appl. Chem.* **1996**, *68*, 209–218.

[7] Krygowski, T.; Cyrañski, M.; Czarnocki, Z.; Häfelinger, G.; Katritzky, A. R. *Tetrahedron* **2000**, *56*, 1783–1796.

[8] Schleyer, P. v. R. *Chem. Rev.* **2001**, *101*, 1115–1118.

[9] Schleyer, P. v. R. *Chem. Rev.* **2005**, *105*, 3433–3435.

[10] Carey, F. A.; Sundberg, R. J. *Advanced Organic Chemistry, Part A: Structure and Mechanisms*, 5th ed.; Springer, 2007.

[11] Carey, F. A.; Sundberg, R. J. *Advanced Organic Chemistry, Part B: Reaction and Synthesis*, 5th ed.; Springer, 2007.

[12] Smith, M. B.; March, J. In *March's Advanced Organic Chemistry: Reactions, Mechanisms, and Structure*, 6th ed.; Thomas, S., Amos, R., Eds.; John Wiley and Sons, 2007.

[13] Feixas, F.; Matito, E.; Solá, M.; Poater, J. *J. Phys. Chem. A* **2008**, *112*, 13231–13238, PMID: 18834099.

[14] Baird, N. C. *J. Am. Chem. Soc.* **1972**, *94*, 4941–4948.

[15] Rosenberg, M.; Dahlstrand, C.; Kilså, K.; Ottosson, H. *Submitted to Chem. Rev.* **2012**,

[16] Hückel, E. *Z. Phys.* **1931**, *70*, 204–286.

[17] Hückel, E. *Z. Phys.* **1931**, *72*, 310–337.

[18] Hückel, E. *Z. Phys.* **1932**, *76*, 628–648.

[19] Hückel, E. *Z. Elektrochem.* **1937**, *43*, 752–788.

[20] Atkins, P. W.; Friedman, R. S. *Molecular Quantum Mechanics*, 4th ed.; Oxford University Press, 2005.

[21] Dewar, M. J. S. *J. Am. Chem. Soc.* **1952**, *74*, 3341–3345.

[22] Lin, C. Y.; Krantz, A. *J. Chem. Soc., Chem. Commun.* **1972**, 1111–1112.

[23] Chapman, O. L.; McIntosh, C. L.; Pacansky, J. *J. Am. Chem. Soc.* **1973**, *95*, 614–617.

[24] Maier, G. *Angew. Chem., Int. Ed.* **1988**, *27*, 309–332.

[25] Karadakov, P. B. *J. Phys. Chem. A* **2008**, *112*, 7303–7309.

[26] Olah, G. A.; Staral, J. S. *J. Am. Chem. Soc.* **1976**, *98*, 6290–6304.

[27] Katz, T. J. *J. Am. Chem. Soc.* **1960**, *82*, 3784–3785.

[28] Katz, T. J. *J. Am. Chem. Soc.* **1960**, *82*, 3785–3786.

[29] Bartmess, J. E.; Scott, J. A.; McIver, R. T. *J. Am. Chem. Soc.* **1979**, *101*, 6046–6056.

[30] Rosenberg, M.; Ottosson, H.; Kilså, K. *J. Org. Chem.* **2010**, *75*, 2189–2196.

[31] von E. Doering, W.; Knox, L. H. *J. Am. Chem. Soc.* **1954**, *76*, 3203–3206.

[32] Masamune, S.; Souto-Bachiller, F. A.; Machiguchi, T.; Bertie, J. E. *J. Am. Chem. Soc.* **1978**, *100*, 4889–4891.

[33] Bally, T.; Masamune, S. *Tetrahedron* **1980**, *36*, 343–370.

[34] Balkova, A.; Bartlett, R. J. *J. Chem. Phys.* **1994**, *101*, 8972–8987.

[35] Bastiansen, O.; Hedberg, L.; Hedberg, K. *J. Chem. Phys.* **1957**, *27*, 1311–1317.

[36] Andrés, J. L.; Castaño, O.; Morreale, A.; Palmeiro, R.; Gomperts, R. *J. Chem. Phys.* **1998**, *108*, 203–207.

[37] Thiele, J. *Chem. Ber.* **1900**, *33*, 666–673.

[38] Bordwell, F. G.; Drucker, G. E.; Fried, H. E. *J. Org. Chem.* **1981**, *46*, 632–635.

[39] Breslow, R.; Chu, W. *J. Am. Chem. Soc.* **1973**, *95*, 411–418.

[40] Dauben, H. J.; Rifi, M. R. *J. Am. Chem. Soc.* **1963**, *85*, 3041–3042.

[41] von E. Doering, W.; Gaspar, P. P. *J. Am. Chem. Soc.* **1963**, *85*, 3043–3043.

[42] Breslow, R. *Acc. Chem. Res.* **1973**, *6*, 393–398.

[43] Wiberg, K. B. *Chem. Rev.* **2001**, *101*, 1317–1332.

[44] Krygowski, T. M.; Cyrañski, M. K. *Chem. Rev.* **2001**, *101*, 1385–1420.

[45] Chen, Z.; Wannere, C. S.; Corminboeuf, C.; Puchta, R.; Schleyer, P. v. R. *Chem. Rev.* **2005**, *105*, 3842–3888.

[46] Cyrañski, M. K. *Chem. Rev.* **2005**, *105*, 3773–3811.

[47] Poater, J.; Duran, M.; Solá, M.; Silvi, B. *Chem. Rev.* **2005**, *105*, 3911–3947.

[48] Krygowski, T.; Cyrañski, M.; Czarnocki, Z.; Häfelinger, G.; Katritzky, A. R. *Tetrahedron* **2000**, *56*, 1783–1796.

[49] Baird, N. C.; West, R. M. *J. Am. Chem. Soc.* **1971**, *93*, 4427–4432.

[50] Gellini, C.; Salvi, P. R. *Symmetry* **2010**, *2*, 1846–1924.

[51] Levchenko, S. V.; Krylov, A. I. *J. Chem. Phys.* **2004**, *120*, 175–185.

[52] Eckert-Maksic, M.; Vazdar, M.; Barbatti, M.; Lischka, H.; Maksic, Z. B. *J. Chem. Phys.* **2006**, *125*, 064310.

[53] Garavelli, M.; Bernardi, F.; Cembran, A.; Castaño, O.; Frutos, L. M.; Merchán, M.; Olivucci, M. *J. Am. Chem. Soc.* **2002**, *124*, 13770–13789.

[54] Frutos, L.-M.; Castaño, O.; Merchán, M. *J. Phys. Chem. A* **2003**, *107*, 5472–5478.

[55] Jug, K.; Malar, E. *J. Mol. Struct. (THEOCHEM)* **1987**, *153*, 221–226.

[56] Gogonea, V.; Schleyer, P. v. R.; Schreiner, P. R. *Angew. Chem., Int. Ed.* **1998**, *37*, 1945–1948.

[57] Klärner, F.-G. *Angew. Chem., Int. Ed.* **2001**, *40*, 3977–3981.

[58] Villaume, S.; Fogarty, H. A.; Ottosson, H. *ChemPhysChem* **2008**, *9*, 257–264.

[59] Nishinaga, T.; Ohmae, T.; Iyoda, M. *Symmetry* **2010**, *2*, 76–97.

[60] Wenthold, P. G.; Hrovat, D. A.; Borden, W. T.; Lineberger, W. C. *Science* **1996**, *272*, 1456–1459.

[61] Saunders, M.; Berger, R.; Jaffe, A.; McBride, J. M.; O'Neill, J.; Breslow, R.; Hoffmann, J. M.; Perchonock, C.; Wasserman, E. *J. Am. Chem. Soc.* **1973**, *95*, 3017–3018.

[62] Wörner, H. J.; Merkt, F. *Angew. Chem., Int. Ed.* **2006**, *45*, 293–296.

[63] Wörner, H. J.; Merkt, F. *J. Chem. Phys.* **2007**, *127*, 034303.

[64] Wörner, H.; Merkt, F. *Angew. Chem., Int. Ed.* **2009**, *48*, 6404–6424.

[65] Callomon, J. H.; Dunn, T. M.; Mills, I. M. *Phil. Trans. R. Soc. Lond. A* **1966**, *259*, 499–532.

[66] Meisl, M.; Janoschek, R. *J. Chem. Soc., Chem. Commun.* **1986**, 1066–1067.

[67] Palmer, I. J.; Ragazos, I. N.; Bernardi, F.; Olivucci, M.; Robb, M. A. *J. Am. Chem. Soc.* **1993**, *115*, 673–682.

[68] Haas, Y.; Zilberg, S. *J. Am. Chem. Soc.* **1995**, *117*, 5387–5388.

[69] Shaik, S.; Shurki, A.; Danovich, D.; Hiberty, P. C. *J. Am. Chem. Soc.* **1996**, *118*, 666–671.

[70] Yoshihiro, O. *Chem. Phys. Lett.* **1988**, *145*, 541–544.

[71] Buma, W. J.; Van der Waals, J. H.; Van Hemert, M. C. *J. Am. Chem. Soc.* **1989**, *111*, 86–87.

[72] Buma, W. J.; van der Waals, J. H.; van Hemert, M. C. *J. Chem. Phys.* **1990**, *93*, 3733–3745.

[73] de Groot, M.; van der Waals, J. *Mol. Phys.* **1963**, *6*, 545–562.

[74] de Groot, M.; Hesselmann, I.; van der Waals, J. *Mol. Phys.* **1967**, *13*, 583–586.

[75] de Groot, M.; Hesselmann, I.; van der Waals, J. *Mol. Phys.* **1969**, *16*, 45–60.

[76] Wan, P.; Krogh, E. *J. Chem. Soc., Chem. Commun.* **1985**, 1207–1208.

[77] Wan, P.; Krogh, E. *J. Am. Chem. Soc.* **1989**, *111*, 4887–4895.

[78] Wan, P.; Krogh, E.; Chak, B. *J. Am. Chem. Soc.* **1988**, *110*, 4073–4074.

[79] McAuley, I.; Krogh, E.; Wan, P. *J. Am. Chem. Soc.* **1988**, *110*, 600–602.

[80] Krogh, E.; Wan, P. *Can. J. Chem.* **1990**, *68*, 1725–1731.

[81] Wan, P.; Budac, D.; Krogh, E. *J. Chem. Soc., Chem. Commun.* **1990**, 255–257.

[82] Wan, P.; Budac, D.; Earle, M.; Shukla, D. *J. Am. Chem. Soc.* **1990**, *112*, 8048–8054.

[83] Krogh, E.; Wan, P. *J. Am. Chem. Soc.* **1992**, *114*, 705–712.

[84] Budac, D.; Wan, P. *J. Org. Chem.* **1992**, *57*, 887–894.

[85] Wan, P.; Shukla, D. *Chem. Rev.* **1993**, *93*, 571–584.

[86] Budac, D.; Wan, P. *J. Photochem. Photobiol., A* **1996**, *98*, 27–37.

[87] Budac, D.; Wan, P. *Can. J. Chem.* **1996**, *74*, 1447–1464.

[88] Brousmiche, D.; Shukla, D.; Wan, P. *Chem. Commun.* **1997**, 709–710.

[89] Shukla, D.; Wan, P. *J. Photochem. Photobiol., A* **1998**, *113*, 53–64.

[90] Shukla, D.; Lukeman, M.; Shi, Y.; Wan, P. *J. Photochem. Photobiol., A* **2002**, *154*, 93–105.

[91] Mecklenburg, S. L.; Hilinski, E. F. *J. Am. Chem. Soc.* **1989**, *111*, 5471–5472.

[92] Gaillard, E.; Fox, M. A.; Wan, P. *J. Am. Chem. Soc.* **1989**, *111*, 2180–2186.

[93] McClelland, R. A.; Mathivanan, N.; Steenken, S. *J. Am. Chem. Soc.* **1990**, *112*, 4857–4861.

[94] Brauman, J. I.; Schwartz, J.; Van Tamelen, E. E. *J. Am. Chem. Soc.* **1968**, *90*, 5328–5329.

[95] Schwartz, J. *J. Chem. Soc. D* **1969**, 833–834.

[96] van Tamelen, E. E.; Brauman, J. I.; Ellis, L. E. *J. Am. Chem. Soc.* **1967**, *89*, 5073–5074.

[97] Hunter, E. P. L.; Lias, S. G. *J. Phys. Chem. Ref. Data* **1998**, *27*, 413.

[98] Goebbert, D. J.; Wenthold, P. G. *Int. J. Mass Spectrom.* **2006**, *257*, 1–11.

[99] Taft, R. W.; Bordwell, F. G. *Acc. Chem. Res.* **1988**, *21*, 463–469.

[100] Furuyama, S.; Golden, D. M.; Benson, S. W. *J. Chem. Thermodyn.* **1970**, *2*, 161–169.

[101] Roth, W. R.; Böhm, M.; Lennartz, H.-W.; Vogel, E. *Angew. Chem.* **1983**, *95*, 1011–1012.

[102] Roux, M. V.; Temprado, M.; Chickos, J. S.; Nagano, Y. *J. Phys. Chem. Ref. Data* **2008**, *37*, 1855–1996.

[103] Rakus, K.; Verevkin, S. P.; Schützer, J.; Beckhaus, H.-D.; Rüchardt, C. *Chem. Ber.* **1994**, *127*, 1095–1103.

[104] Birks, J. B. *Photophysics of Aromatic Molecules*; Wiley Interscience, 1970.

[105] Frueholz, R. P.; Kuppermann, A. *J. Chem. Phys.* **1978**, *69*, 3614–3621.

[106] von E. Doering, W.; Wiley, D. *Tetrahedron* **1960**, *11*, 183–198.

[107] Billups, W. E.; Lin, L. J.; Casserly, E. W. *J. Am. Chem. Soc.* **1984**, *106*, 3698–3699.

[108] Staley, S. W.; Norden, T. D. *J. Am. Chem. Soc.* **1984**, *106*, 3699–3700.

[109] Norden, T. D.; Staley, S. W.; Taylor, W. H.; Harmony, M. D. *J. Am. Chem. Soc.* **1986**, *108*, 7912–7918.

[110] Baron, P.; Brown, R.; Burden, F.; Domaille, P.; Kent, J. *J. Mol. Spectrosc.* **1972**, *43*, 401–410.

[111] Bauder, A.; Keller, C.; Neuenschwander, M. *J. Mol. Spectrosc.* **1976**, *63*, 281–287.

[112] Hollenstein, R.; von Philipsborn, W.; Vögeli, R.; Neuenschwander, M. *Helv. Chim. Acta* **1973**, *56*, 847–860.

[113] Hollenstein, R.; Mooser, A.; Neuenschwander, M.; von Philipsborn, W. *Angew. Chem.* **1974**, *86*, 595–596.

[114] Domaille, P.; Kent, J.; O'Dwyer, M. *Aust. J. Chem.* **1974**, *27*, 2463–2466.

[115] Scott, A. P.; Agranat, I.; Biedermann, P. U.; Riggs, N. V.; Radom, L. *J. Org. Chem.* **1997**, *62*, 2026–2038.

[116] Möllerstedt, H.; Piqueras, M. C.; Crespo, R.; Ottosson, H. *J. Am. Chem. Soc.* **2004**, *126*, 13938–13939.

[117] Benson, R. C.; Flygare, W. H.; Oda, M.; Breslow, R. *J. Am. Chem. Soc.* **1973**, *95*, 2772–2777.

[118] Crabtree, J. H.; Bertelli, D. J. *J. Am. Chem. Soc.* **1967**, *89*, 5384–5389.

[119] Serrano-Andres, L.; Pou-Amerigo, R.; Fulscher, M. P.; Borin, A. C. *J. Chem. Phys.* **2002**, *117*, 1649–1659.

[120] Ottosson, H.; Kilså, K.; Chajara, K.; Piqueras, M. C.; Crespo, R.; Kato, H.; Muthas, D. *Chem.–Eur. J.* **2007**, *13*, 6998–7005.

[121] Yamakawa, M.; Watanabe, H.; Mukai, T.; Nozoe, T.; Kubo, M. *J. Am. Chem. Soc.* **1960**, *82*, 5665–5667.

[122] Nozoe, T.; Mukai, T.; Osaka, K.; Shishido, N. *Bull. Chem. Soc. Jpn.* **1961**, *34*, 1384–1390.

[123] Ammon, H. L. *J. Am. Chem. Soc.* **1973**, *95*, 7093–7101.

[124] Breslow, R.; Pecararo, J.; Sugirnoto, T. *Org. Synth.* **1977**, *57*, 41.

[125] Takahashi, K.; Namekata, N.; Takase, K.; Takeuchi, A. *Tetrahedron Lett.* **1987**, *28*, 5683–5686.

[126] Weber, H.-M.; Maas, G. *Synthesis* **1988**, *8*, 604–608.

[127] Dahnke, K. R.; Paquette, L. A. *Org. Synth.* **1993**, *71*, 181.

[128] Bauer, W.; Daub, J.; Hasenhündl, A.; Rapp, K. M.; Schmidt, P. *Tetrahedron Lett.* **1981**, *22*, 2977 – 2980.

[129] Daub, J.; Hasenhündl, A.; Rapp, K. M. *Chem. Ber.* **1982**, *115*, 2643–2651.

[130] Bauer, W.; Betz, I.; Daub, J.; Jakob, L.; Pickl, W.; Rapp, K. M. *Chem. Ber.* **1983**, *116*, 1154–1173.

[131] Wheland, G. W.; Mann, D. E. *J. Chem. Phys.* **1949**, *17*, 264–268.

[132] Day, J. H. *Chem. Rev.* **1953**, *53*, 167–189.

[133] Ogliaruso, M. A.; Romanelli, M. G.; Becker, E. I. *Chem. Rev.* **1965**, *65*, 261–367.

[134] Bergmann, E. D. *Chem. Rev.* **1968**, *68*, 41–84.

[135] Chapman, O. L.; McIntosh, C. L. *J. Chem. Soc. D* **1971**, 770–771.

[136] Ammon, H. L.; Plastas, L. A. *J. Chem. Soc. D* **1971**, 356–357.

[137] Ammon, H. L.; Wheeler, G. L. *J. Chem. Soc. D* **1971**, 1032–1034.

[138] Peterson, M. L.; Strnad, J. T.; Markotan, T. P.; Morales, C. A.; Scaltrito, D. V.; Staley, S. W. *J. Org. Chem.* **1999**, *64*, 9067–9076.

[139] Stepien, B. T.; Cyranski, M. K.; Krygowski, T. M. *Chem. Phys. Lett.* **2001**, *350*, 537–542.

[140] Stepien, B. T.; Krygowski, T. M.; Cyranski, M. K. *J. Org. Chem.* **2002**, *67*, 5987–5992.

[141] Nakajima, T.; Katagiri, S. *Bull. Chem. Soc. Jpn.* **1962**, *35*, 910–916.

[142] Inuzuka, K.; Yokota, T. *J. Chem. Phys.* **1966**, *44*, 911–915.

[143] Nakajima, T.; Kohda, S.; Tajiri, A.; Karasawa, S. *Tetrahedron* **1967**, *23*, 2189–2194.

[144] Dreyer, J.; Klessinger, M. *J. Chem. Phys.* **1994**, *101*, 10655–10665.

[145] Asmis, K. R.; Allan, M.; Schafer, O.; Fülscher, M. *J. Phys. Chem. A* **1997**, *101*, 2089–2095.

[146] Galasso, V. *Chem. Phys.* **1993**, *171*, 171–178.

[147] Bearpark, M. J.; Bernardi, F.; Olivucci, M.; Robb, M. A.; Smith, B. R. *J. Am. Chem. Soc.* **1996**, *118*, 5254–5260.

[148] Alfalah, S.; Belz, S.; Deeb, O.; Leibscher, M.; Manz, J.; Zilberg, S. *J. Chem. Phys.* **2009**, *130*, 124318.

[149] Mendive-Tapia, D.; Lasorne, B.; Worth, G. A.; Bearpark, M. J.; Robb, M. A. *Phys. Chem. Chem. Phys.* **2010**, *12*, 15725–15733.

[150] Kent, J. E.; Harman, P. J.; O'Dwyer, M. F. *J. Phys. Chem.* **1981**, *85*, 2726–2730.

[151] Dahlstrand, C.; Ottosson, H. *In preparation*

[152] Rosenberg, M.; Ottosson, H.; Kilså, K. *Phys. Chem. Chem. Phys.* **2011**, *13*, 12912–12919.

[153] Frisch, M. J. et al. Gaussian 03, Revision E. 01. Gaussian, Inc., 2004; Gaussian Inc. Wallingford CT.

[154] Connors, R. E.; Lacroix, M.; Chen, B. *J. Mol. Struct.* **2009**, *935*, 13–18.

[155] Mennucci, B.; Tomasi, J. *J. Chem. Phys.* **1997**, *106*, 5151–5158.

[156] Cances, E.; Mennucci, B.; Tomasi, J. *J. Chem. Phys.* **1997**, *107*, 3032–3041.

[157] Cossi, M.; Barone, V.; Mennucci, B.; Tomasi, J. *Chem. Phys. Lett.* **1998**, *286*, 253–260.

[158] Suppan, P. *J. Photochem. Photobiol., A* **1990**, *50*, 293–330.

[159] Suppan, P. *Chemistry and Light*; Royal Society of Chemistry, 1994.

[160] Klessinger, M.; Michl, J. *Excited States and Photochemistry of Organic Molecules*; VCH Publishers, Inc., 1995.

[161] Onsager, L. *J. Am. Chem. Soc.* **1936**, *58*, 1486–1493.

[162] Lakowitz, J. R. *Principles of Fluorescence Spectroscopy*; Springer, 2006.

[163] Reichardt, C. *Chem. Rev.* **1994**, *94*, 2319–2358.

[164] Reichardt, C. *Solvents and Solvent Effects in Organic Chemistry*; Wiley-VCH, 2003.

[165] Frisch, Æ.; Frisch, M. J. *Gaussian 03 User's Reference*; Gaussian Inc.: Wallington, 2003.

[166] Andrew, T. L.; Cox, J. R.; Swager, T. M. *Org. Lett.* **2010**, *12*, 5302–5305.

[167] Potter, R. G.; Hughes, T. S. *J. Org. Chem.* **2008**, *73*, 2995–3004.

[168] Romer, R., Duane *Synthesis* **2011**, *2011*, 2721–2723.

[169] Katritzky, A. R.; Fan, W.-Q.; Liang, D.-S.; Li, Q.-L. *J. Heterocycl. Chem.* **1989**, *26*, 1541–1545.

[170] Jayamurugan, G.; Gisselbrecht, J.-P.; Boudon, C.; Schoenebeck, F.; Schweizer, W. B.; Bernet, B.; Diederich, F. *Chem. Commun.* **2011**, *47*, 4520–4522.

[171] Jayamurugan, G.; Gisselbrecht, J.-P.; Boudon, C.; Schoenebeck, F.; Schweizer, W. B.; Bernet, B.; Diederich, F. *ChemInform* **2011**, *42*.

[172] Frisch, M. J. et al. Gaussian 09 Revision A.1. 2009; Gaussian Inc. Wallingford CT.

[173] Zhao, Y.; Truhlar, D. G. *Theor. Chem. Acc.* **2007**, *120*, 215–241.

[174] Jacquemin, D.; Perpète, E. A.; Ciofini, I.; Adamo, C. *J. Chem. Theory Comput.* **2010**, *6*, 1532–1537.

[175] Wang, G.-W.; Cheng, B. *ARKIVOC* **2004**, *9*, 4–8.

[176] Mukherjee, T. K. *J. Phys. Chem.* **1969**, *73*, 4381–4382.

[177] Bennett, C. W.; Jewsbury, W. G.; Dupuis, J. P. *J. Am. Chem. Soc.* **1946**, *68*, 2489–2490.

[178] Kuboyama, A. *Bull. Chem. Soc. Jpn* **1964**, *37*, 1540–1544.

[179] Yoshihara, K.; Kearns, D. R. *J. Chem. Phys.* **1966**, *45*, 1991–1999.

[180] Liptay, W.; Weisenberger, H.; Tiemann, F.; Eberlein, W.; Konopka, G. *Z. Naturforsch.* **1968**, *23a*, 377–393.

[181] Dehler, J.; Fritz, K. *Tetrahedron Lett.* **1969**, *10*, 2157–2160.

[182] Singer, L. A. *Tetrahedron Lett.* **1969**, *10*, 923–926.

[183] Marchetti, A. P. *Mol. Cryst. Liquid Cryst.* **1972**, *16*, 127–135.

[184] Zwarich, R.; Bree, A. *J. Mol. Spectrosc.* **1974**, *52*, 329–343.

[185] Dörr, V. F.; Dehler, J. *Tetrahedron Lett.* **1965**, *6*, 189–194.

[186] Yamaguchi, H.; Ninomiya, K.; Ogata, M. *Chem. Phys. Lett.* **1980**, *75*, 593–595.

[187] Brealey, G. J.; Kasha, M. *J. Am. Chem. Soc.* **1955**, *77*, 4462–4468.

[188] Sato, S.; Hashimoto, K.; Tajima, K. *Synth. Met.* **2011**, *161*, 1289–1298.

[189] Kasha, M. *Discuss. Faraday Soc.* **1950**, *9*, 14–19.

[190] Improta, R.; Barone, V.; Scalmani, G.; Frisch, M. J. *J. Chem. Phys.* **2006**, *125*, 054103.

[191] Improta, R.; Scalmani, G.; Frisch, M. J.; Barone, V. *J. Chem. Phys.* **2007**, *127*, 074504.

[192] Karadakov, P. B. *J. Phys. Chem. A* **2008**, *112*, 12707–12713.

[193] Dahlstrand, C.; Yamazaki, K.; Kilså, K.; Ottosson, H. *J. Org. Chem.* **2010**, *75*, 8060–8068.

[194] Feixas, F.; Vandenbussche, J.; Bultinck, P.; Matito, E.; Sola, M. *Phys. Chem. Chem. Phys.* **2011**, *13*, 20690–20703.

[195] Poater, J.; Sola, M. *Chem. Commun.* **2011**, *47*, 11647–11649.

[196] Fuentealba, P.; C. Santos, J. *Curr. Org. Chem.* **2011**, *15*, 3619–3626.

[197] Ishida, M.; Shin, J.-Y.; Lim, J. M.; Lee, B. S.; Yoon, M.-C.; Koide, T.; Sessler, J. L.; Osuka, A.; Kim, D. *J. Am. Chem. Soc.* **2011**, *133*, 15533–15544.

[198] Ulusoy, I. S.; Nest, M. *J. Am. Chem. Soc.* **2011**, *133*, 20230–20236.

[199] Esselman, B. J.; McMahon, R. J. *J. Phys. Chem. A* **2012**, *116*, 483–490.

[200] Zhang, Y.; Pan, Q.-J.; Guo, Y.-R.; Fu, H.-G.; Zhang, H.-X. *J. Mol. Struct. (THEOCHEM)* **2009**, *907*, 41–45.

[201] Estrada, L. A.; Neckers, D. C. *J. Org. Chem.* **2009**, *74*, 8484–8487.

[202] Wang, X.-Z.; Wang, Q.; Yan, L.; Wong, W.-Y.; Cheung, K.-Y.; Ng, A.; Djurfá, A. B.; Chan, W.-K. *Macromol. Rapid Commun.* **2010**, *31*, 861–867.

[203] Estrada, L. A.; Cai, X.; Neckers, D. C. *J. Phys. Chem. A* **2011**, *115*, 2184–2195.

[204] Estrada, L. A.; Yarnell, J. E.; Neckers, D. C. *J. Phys. Chem. A* **2011**, *115*, 6366–6375.

[205] Liao, Y.; Yang, G.-C.; Feng, J.-K.; Shi, L.-L.; Yang,; YangYang, L.; Ren, A.-M. *J. Phys. Chem. A* **2006**, *110*, 13036–13044.

[206] Yatsuhashi, T.; Nakajima, Y.; Shimada, T.; Inoue, H. *J. Phys. Chem. A* **1998**, *102*, 3018–3024.